UNIVERSITY OF MIAMI
COLLEGE of ENGINEERING

Politecnico di Torino

Polytechnic of Turin and University of Miami

Master's Degree Programme in
CIVIL ENGINEERING

Master Thesis

Scale-dependent maximum reinforcement percentage in GFRP-RC beams: A Fracture Mechanics application

Supervisors:
Prof. Alberto Carpinteri
Prof. Antonio Nanni
Co- Supervisors:
Prof. Federico Accornero
Ing. Renato Cafarelli

Candidate:
Gianfrancesco Gallina
289181

Academic year 2022/2023

Table of contents

List of figures

List of tables

List of graphs

ABSTRACT

Glass Fiber Reinforced Polymer (GFRP) Reinforced Concrete (RC) can be defined as an advanced cementitious material, where the secondary reinforcing phase consists in corrosion-resistant GFRP rebars. New eco-sustainable materials, through innovative engineering approaches based on environmental sustainability, increase the service life and the safety of structures. For this next-generation structural material, experimental flexural tests highlight how the post-cracking response is strongly affected by the amount of GFRP together with the structural size-scale. In the present thesis, the Cohesive/Overlapping Crack Model is adopted to describe the transition between cracking and crushing failures occurring in GFRP-RC beams by increasing the beam depth and/or the reinforcement percentage. Within this Nonlinear Fracture Mechanics model, the tensile and compression ultimate behaviours of the concrete matrix are modelled through two different process zones that advance independently of each other. Moreover, this model is able to capture local mechanical instabilities in the structural behaviour: tensile snap-back and snap-through, which are due to concrete cracking and reinforcement bridging action, and compression snap-back generated by the unstable growth of the crushing zone. In such a context, the application of the Cohesive/Overlapping Crack Model demonstrates that the ductility, which is represented by the plastic rotation capacity of the GFRP-RC element subjected to bending, is a function of reinforcement percentage, beam depth, and bond strength between concrete and GFRP bars. In this way, a rational and quantitative definition of over-reinforcement is provided as a GFRP

percentage depending on the beam depth. The over-reinforcement upper limit is strongly influenced by the bond strength between the two materials. An inverse proportion between bond strength and over-reinforcement limit percentage is evident. An identification procedure for the nominal values of $G_F, G_C,$ and τ is defined in an innovative way. The identification procedure develops in three different subsequent steps. The first step represents the identification of the fracture energy G_F at the first cracking point. The second step represents the identification of the crushing energy G_C at t the crushing point. The third and last step represents the identification of the bond strength τ at the starting point of the pseudo-plastic plateau. The currently used pull-out and beam-bond tests do not guarantee the superposition of experimental and theoretical diagrams. Analogously, the current recommended tests to measure the fracture mechanics parameters of the cementitious matrix, G_F and G_c, do not allow the same superposition. In the experiments, two different size-scales and two different bond strengths are investigated through the Cohesive/Overlapping Crack Model. The parameter identification rules the experimental and numerical procedures. At the end of the identification procedure, an excellent agreement emerges between experimental and numerical load versus deflection diagrams.

Keywords: *Fracture Mechanics, Cohesive/Overlapping Crack Model, GFRP-RC beams, Maximum reinforcement percentage, Scale effects*

CHAPTER 1:

INTRODUCTION

Corrosion of internal reinforcing steel is one of the chief causes of failure of concrete structures. Inevitably concrete will crack, creating a direct avenue for chlorides to begin oxidizing the steel rebar. The oxidizing process on the steel bar it is possible because the iron binds with oxygen and/or with the water:

$$4F_e + 3O_2 \rightarrow 2F_{e2}O_3$$

Eq 1

$$2F_e + 3H_2O \rightarrow F_{e2}O_3 + 3H_2$$

Eq 2

The mechanism of rust formation involves chemical reactions with carbon dioxide, moisture, air oxygen and sulfur dioxide and the process take place faster when the surface is exposed to air, and if the surface is rough, or if the artifact is subjected to mechanical tensile stress.

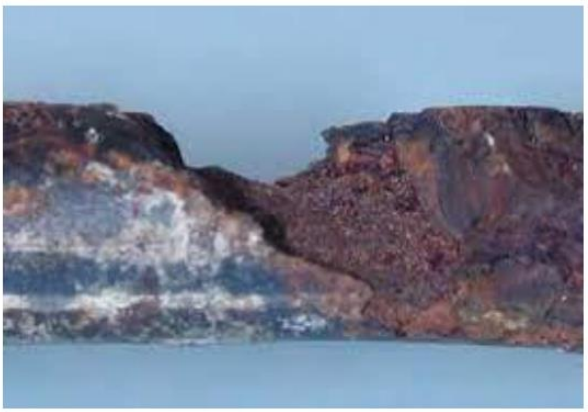

Figure 1: Steel bar corrosion

Fiber Reinforced Polymers (FRP's) are a proven and successful alternative reinforcing that will give structures a longer service life. A complete spectrum of authoritative consensus design guides, test methods, material and construction standards, product procurement specifications and qualification procedures allow at the designer to implement FRP's safely and economically in many different types of structures. Considering the concrete exposed to: De-Icing Chlorides, Marine Chlorides or High Voltages and Electromagnetic field, the durability of the element and consequently of the structures decrease considerably. The corrosion of the steel decreases not only the cross section of the bar but taking into account that the corrosion process is in volume increase, if the bars are inside the concrete, the concrete cover will be degraded up to complete separation from the structure.

Figure 2: Chloride corrosion steel bars

Is it possible to prevent this process in the concrete structure? It is possible to reduce and delay this phenomenon with the GFRP bars that come to our aid to solve this problem.

1.1: What is GFRP

Fiber composites are an excellence alternative which have been successfully used since the 1980's in various industries (e.g. automotive, aircraft ships and construction). One of the most prominent among composites is Glass Fiber Reinforced Plastics (GFRP). GFRP is an acronym for Glass Fiber Reinforced Polymer, a polymer rod reinforced with glass fiber. It is a variant of FRP, a composite material that has been used for structural applications since at least the late 1990s. GFRP are destined to be used in many applications in modern construction industry and remedy a magnitude of previously unsolvable problems. One of its most interesting applications is its use as concrete reinforcement after extensive development and certified testing.

GFRP Rebar is:

1) Corrosion resistant: thereby the amount of concrete cover can be reduced to a minimum and extending the life of the construction element considerably;
2) Cost-efficient: reducing the maintenance process in such a case GFRP bar results less expensive than steel bar solution;
3) Resistant: being resistant to corrosive environments significantly extends the overall lifespan;

4) Sustainable: because fewer materials are required, the lifespan of structures are extended with less environmental impact;
5) Corrosion resistant: thereby no rusting occurs as a result of carbonation of the concrete;
6) Corrosion-free: which extends the intervals between renovations and minimizes maintenance costs:
7) Not a conductor: therefore, the rebar does not conduct any electrical current and is transparent to magnetic fields and radio waves.

Therefore, a new standard of sustainability is achieved. GFRP bars create a reinforcement technology, which combines modern construction with a clear economic value. The mechanic characteristic of GFRP bar is define below:

1) Density: GFRP bars are approximately one fourth the weight of steel rebar. For the diameter equal to 22mm the unit weight on length is equal to 0.8096 k_g/m;
2) Ultimately tensile strength: [500; 1600] MPa;
3) Ultimate strain (for Aslan) equal to 1,49%;
4) Tensile modulus of elasticity; [40: 76] GPa;
5) Coefficient of Thermal Expansion: $33{,}7 \cdot 10^{-6/℃}$;
6) Transverse Shear Stress: 152 MPa;
7) Glass Fiber Content by Weight: 70% minimum per ASTM D2584;
8) Lap Splice Length: approximately equal to 40 bar diameters;
9) Constitutive low characterized by linear elastic behavior until rapture.

Figure 3: GFRP bars

And for the bond strength? The GFRP bars are product with different cover. This issue is one of the most important for this new material because the cover typologies influence the bond strength between the concrete and the rebar.

1.2: Bond strength

Good performance of FRP reinforced concrete requires adequate interfacial bond between bars and concrete, due to the tensile stress transfer from concrete matrix to reinforcement. Bond-slip interaction between the FRP bar and surrounding concrete is ensured by the stress propagation which depends on bar's geometry, mechanical interaction, chemical adhesion, and frictional forces as well as the compressive strength of concrete. The following parameters have the main effect on the bond behavior of the FRP reinforcement to concrete: the nominal diameter of bars, concrete cover, the type of FRP bar, its surface preparation, bond length, and concrete strength. The review

of the existing research on the FRP-to-concrete bond behavior has shown that, contrary to conventional steel bars, a GFRP bar has no standardization for surface preparation.

Table 1: Investigated parameters in existing beam bond tests.

Reference	Nominal diameter	Embedment length	Concrete cover	Rebar surface treatment	Failure mode type
H. Mazaheripour, J.A.O. Barros [6]	✓	✓	✓	✓	✓
Tighiouart B, Benmokrane B [7]	✓	✓		✓	✓
Pecce M, Manfredi G [8]		✓			✓

Variable surface characteristics based on: a sand-coated, ribbed surface with rope winding, a helically wrapped surface, an indented and wrapped GFRP bar, strongly affect the bond behavior between GFRP and concrete.

Figure 4: Sand coated, sand-helical wrapping, helical wrapping

There is a lot of research on bond behavior of FRP reinforcement to concrete based mainly on: the direct pull-out test, the beam test, the splice test and the ring pullout test. The setups of direct and ring pullout test do not correspond to the real bond conditions existing in a reinforced concrete

element. Hence, only the beam test and splice test can reflect an approximative evaluation of the reinforcement bond behavior. The best method to determine the bond behavior seems to be the bending method, because it considers the actual operating conditions of a structural element.

Table 2: Existing bond test models.

			Investigated parameters		
Type of research	ϕ [mm]	L_b	FRP type	a/c [mm]	various surface
Pull out test	8,9,10,12,13,16,19,20	4ϕ,5ϕ,10ϕ	GFRP,CFRP	75, 100	✓
Beam test	8,12,16,20	5ϕ,6ϕ,10ϕ,16ϕ,20ϕ	GFRP	15, 30	✓

1.3: Bond test

Existing method and application.

Pull-out test (ASTM D7913/D7913M − 14 (2020))

The pull-out test is not very representative of the actual bar-concrete bending adhesion because, the confinement of the jaws on the concrete specimen creates a state of compression tension that confines the concrete and thus, increases the adhesion with the bar.

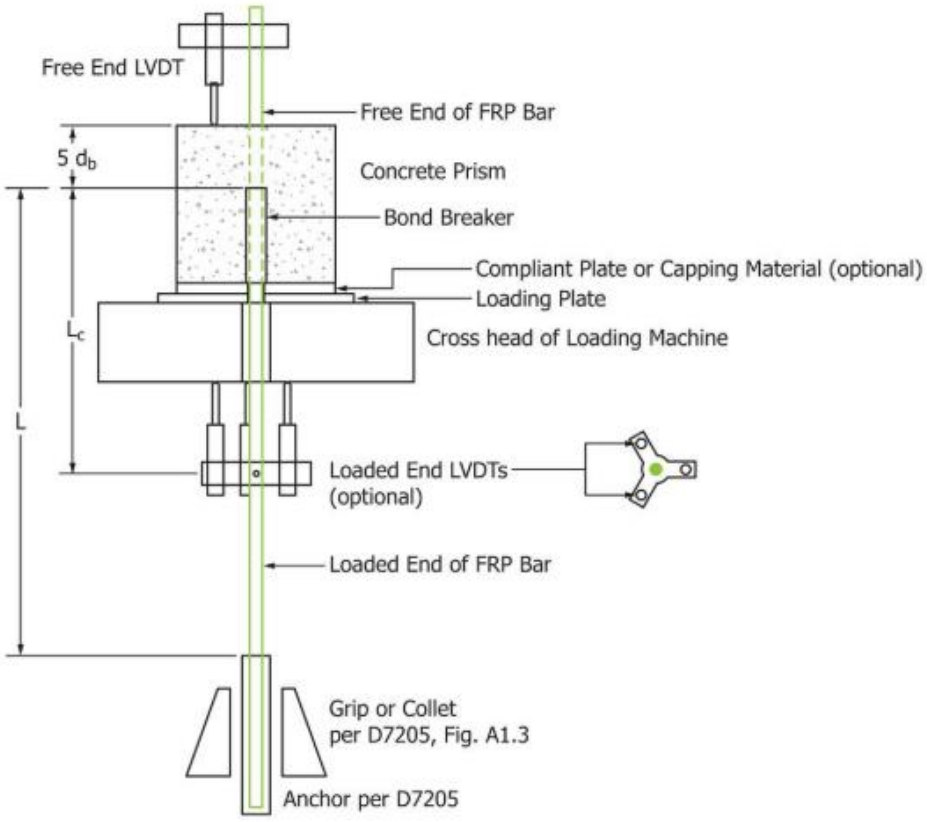

Figure 5: Pull-out test

This test method covers the determination of the bond strength of fiber-reinforced polymer (FRP) composite bars used as reinforcing bars. FRP bars are cast in concrete prisms in one of two orientations and the concrete is allowed to cure for 28 days. Cured specimens are placed in a test fixture consisting of a compression platen at one end. The loaded-end of the bar is gripped in a tension anchor and loaded in tension until failure. The average bond stress is calculated as the maximum force observed during the test divided by the surface area of the bar bonded to the concrete prism. The behavior of the bond between concrete and FRP reinforcing bars is an important performance aspect that has been used in material specifications and design standards.

The test method serves as a means for uniformly preparing specimens and testing FRP bar-to-concrete bond, and for providing a standard method to calculate, evaluate and report bond strength. Measuring bond strength by pullout testing is intended for use in laboratory tests in which the principal variable is the size or type of FRP bars. The results from the procedures presented are limited to the material and test factors.

- Gripping: The method of gripping has been known to cause premature tensile failures in bars. Anchors, if used, should be designed in such a way that the required tensile capacity can be achieved without slip throughout the length of the anchor during the test.
- Concrete Cover Splitting: The concrete prism may split during the test, an indication that the force in the bar is too high for the given specimen configuration. It may be necessary to decrease the bonded length or increase the prism size for bars with unusually high bond strength. A prism dimension of 300 mm is suggested in situations where prism splitting occurs.
- Bar Surface Characteristics: The average bond strength is related to the surface characteristics of the bar. Modifications to this texture are likely to affect bond strength and any such modifications made during specimen preparation should be reported. If the bar has a representative length that is greater than the bonded length, the bond strength may vary depending on the location of the bonded section in relation to the representative length.

- Concrete Prism Flatness: Flatness of the bearing surface of the concrete prism where it meets the steel loading plate should be ensured. Non-flat surfaces or lack of perpendicularity between the concrete surface and the FRP bar may lead to premature fracture of the concrete prism due to stress concentrations and may increase the displacement readings at the loaded-end of the bars due to deformation of the concrete prism.
- Measurement of Cross-Sectional Area: The nominal cross-sectional area of the bar is measured by immersing a prescribed length of the specimen in water to determine its buoyant weight per Test Methods D792 and D7205/D7205M.

The average bond stress shall be calculated according to Eq 3 and reported with a precision to three significant digits for each force reading taken during the test.

$$\tau = \frac{F}{C_b l}$$

Eq 3

where:

- τ = average bond stress, [MPa];
- F = tensile force,[N];
- C_b = effective circumference of FRP bar, calculated as 3.1416 d_b, where d_b is the effective bar diameter of the bar, calculated according to Test Method D7205/ D7205M, Section 11.2.5.1 [mm];

- l = bonded length, [mm].

This test method should not be used to establish design bond values and development lengths for FRP bars embedded in concrete, as it does not represent the state of bond stress observed in concrete flexural members reinforced with FRP bars.

Beam bond test

The beam test specimens suggested by RILEM recommendation RC6 part 1 are more suitable to evaluate the bond strength of reinforcing bars subjected to bending. The specimen, consisting of two half-beams connected on top by a hinge and at the bottom by a reinforcing bar, is loaded on top introducing bending moments in the beam. Thus, a more realistic stress distribution inside and around the bar is created. The steel hinge was secured to the beam 14 days before testing by using a traditional mortar. The prescribed bond length is 10 times the bar diameter.

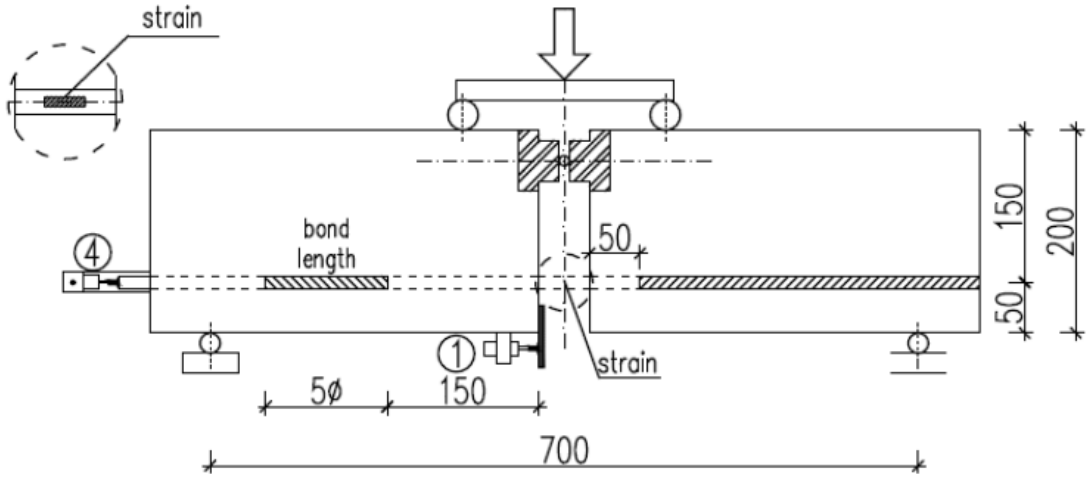

Figure 6: Beam bond test

The beam bond test does not add any stress tension and, for this reason, the value of the bond between the bar and the concrete is not altered by additional stresses. With this test it is possible to evaluate the value of the flexural bond stress closer to the real one. Anyway, the present literature has demonstrated that even if with the beam bond test the results are more precious than pull-test the real flexural bond stress value is overestimated.

Chapter 2:

Cohesive/Overlapping Crack Model (COCM)

2.1: Fractural mechanism

With the achievements made in recent decades in the study of the mechanics of materials has been highlighted as the classic concept of strength of the material, understood as force per unit of surface, is actually an obsolete concept and needs integration with additional parameters. The strength of the material must therefore be compared with another parameter, namely the toughness of the material. Only through the use of both descriptors it is possible to define: the size of the structure, the ductility and the fragility of the same. The structural response is then bound to a set of several factors considering 2 intrinsic characteristics of the material and a geometric characteristic. This new triplet of values is a minimum basis on which to base the study of structural response in the field of fracture mechanics. Anyway, in the history it always defines the ductile behavior and the brittle behavior based on the material. Let's go to look at this topic and at the weakness definition inside its. An element with a ductile behavior is an element able to carry largely value of the deformation before that it reaches the collapse. In other words, a ductile element is that element that gives us a providence before the collapse. Following this argument, the steel material is a ductile material, and it is possible to define in this way in any case.

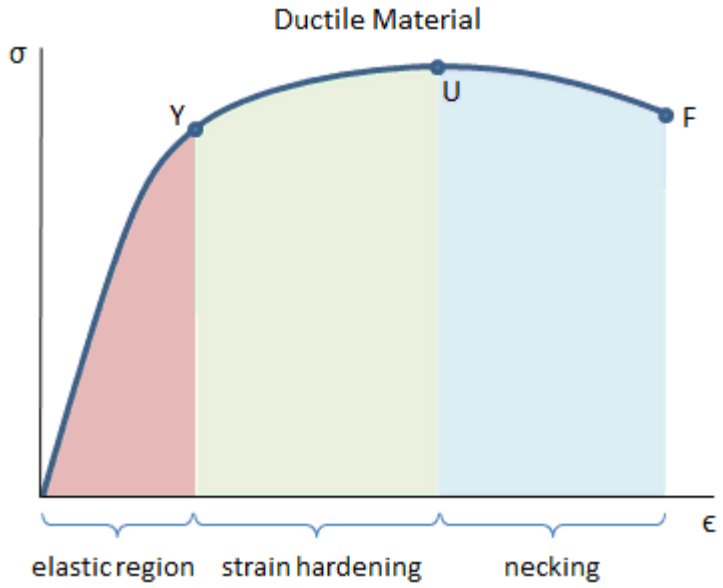

Figure 7: Constitutive law

Following this graph, the value of the ductility it is possible to define of the ratio between the collapse strain and the ultimate elastic strain:

$$\mu = \frac{\varepsilon_u}{\varepsilon_e}$$

Eq 4

On the other hands, the brittle behavior is the opposite of the behavior descript above. An element with a brittle behavior is an element that will collapse without big deformation and, moreover, considering the tension-strain constitutive law, the brittle collapse will be reached without any pseudo-horizontal curve. Following this definition, the concrete is defined of a brittle material in any case and in any application.

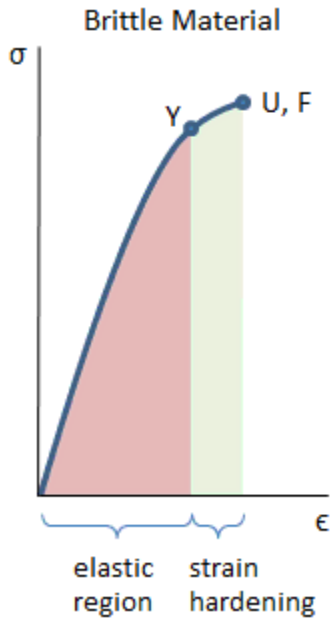

Figure 8: Brittle behavior

The weakness argument on these two definitions is carry out during the second word when the Liberty Ships collapsed suddenly in the port with stress state levels well below the ultimate stress level.

Figure 9: Liberty ship collapsed.

After the analysis of the fracture surfaces, it has been observed that in these cases the rupture starts from a defect or crack or crack of acute type with practically zero connection radius at the ends.

Under certain conditions, the crack, even if small, propagates with remarkable speeds sometimes until the complete collapse of the structure. This cause the break or rather the separation of the ships in two parts already in port where the level of the external stresses was minimal. The reason for the collapse is not the stress state but is dictated by another phenomenon. On the other hand, considering a brittle element as the glass if the scale will be reduced in laboratory scale it is possible to deform the glass as ductility element. It is possible to see that in the picture below that showing the large curvatures of the glass fiber:

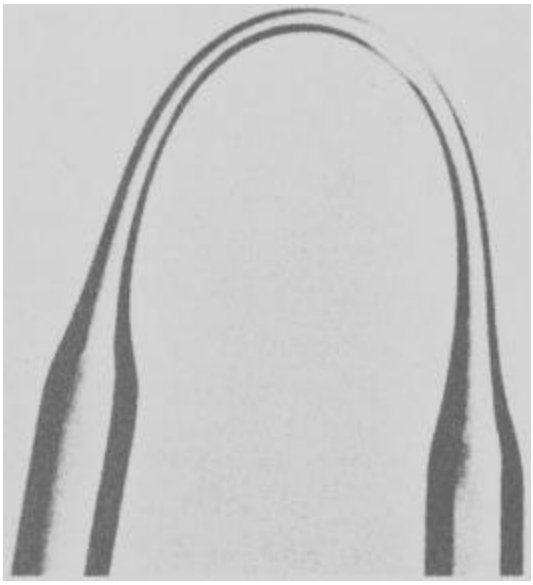

Figure 10: Glass laboratory ductility

This is possible because the glass filament at the micrometric scale is without any flaws and imperfections. Moreover, the glass filament shows a large resilience at this scale. Notes these

properties it is possible to use the glass filament as a reinforcement for other materials. For instance, GFRP bars are made with this concept.

The origins of fracture mechanics were in 1921 with Griffith's work, he moved from a tensional approach to an energetic approach that can better define the structural context. Griffith's experience is based on the study of a fragile material such as glass. Moreover, Griffith's theory is based on an energetic approach. In fact, it dealt with the problem of the stability of a crack in a fragile material through an energy-based approach, arriving at an energy balance expressed by the known critical condition:

$$\sigma_c\sqrt{a_c} = \sqrt{\frac{2TE}{\pi}}$$

Eq 5

From his studies, he introduced the concept of the factor of intensity of stress and thus arrived at the definition of the mechanics of the linear elastic fracture. In the light of such studies, it is therefore fundamental to express no longer the ductility of the material but the ductility of the element as a set of 2 intrinsic characteristics of the material and a geometric characteristic. This was the first time in which the ductility was treated not only as a material condition but with a combination between material condition and geometric quantities. In this way it is possible to define the ductile-fragile transition of a given element with given geometric properties and material characteristics. Considering now different specimens made with the same material but different scale.

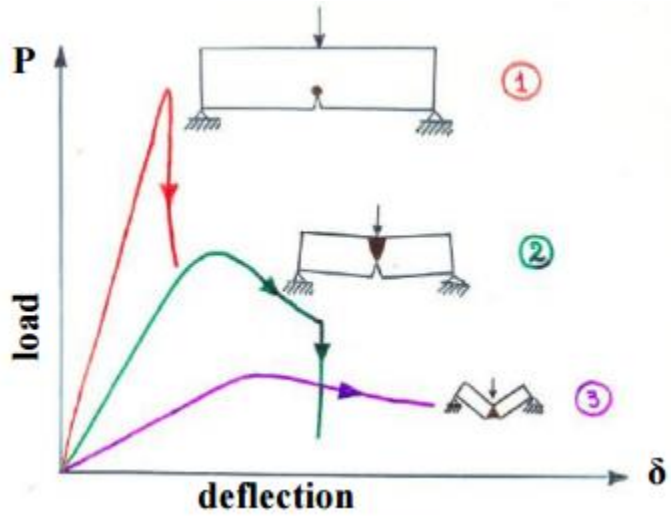

	Structural behaviour	Crack growth process
1	Brittle	Unstable
2	Ductile/Brittle	Stable/Unstable
3	Ductile	Stable

Figure 11: Brittle ductility transition

It is possible to note that:

1) The first element is representative of the largest scale. In this case, the value of the load increase and after the linear phase there is a drop off the load considerable. This behavior is defined like a brittle behavior of the element;
2) secondly, considering now the second element with an intermediate scale. In this case the element is able to lead a plastic path in which the value of the load increase until a

maximum value and after the peak value there is a softening decreasing of the load and an increase of the deflection. Finally, the element shows a brittle failure after a small plastic path;

3) last but not least, the third element characterized by the smallest scale show a totally ductile behavior. The value of the peak load is followed by a perfect softening behavior until the ductile collapse of the element. In this case, in the middle of the element it is possible to consider a plastic hinge.

As results of this remarkable instance, it is possible to establish that: the ductile and brittle behavior is more complex that a simple material characteristic. Therefore, the canonic and historic stress-strain constitutive law is no longer enough to define accurate the behavior of the element and the fundamental characteristics. It is mandatory to define a new material parameters able to describe the intrinsic and real material characteristic like the toughness of the material.

The fractural energy G_F is a parameter able to describe the toughness of the material.

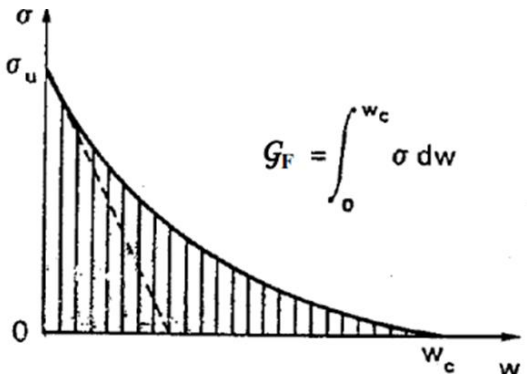

Figure 12: Tension-crack opening constitutive law

The formulation of the fractural energy in a nonlinear fractural mechanics is:

$$G_{IC} = \int_0^{wc} \sigma \, dw$$

Eq 6

Based on the constitutive law tension-crack opening, the area below the graph is defined as Fractural energy. This parameter is an intrinsic parameter of the material and able to define the behavior of it. It also possible to define the *ductile behavior* and the *brittle behavior*. According to different test results based on this issue, the dimension of the element is indirectly proportional with the ductile of the material. This means that, more the element will be small more the value of the ductility will be high. The transition ductile-brittle is studied in this experimental thesis in function of the reinforcement ratio, the scale and the bar cover.

2.2 Snap-back

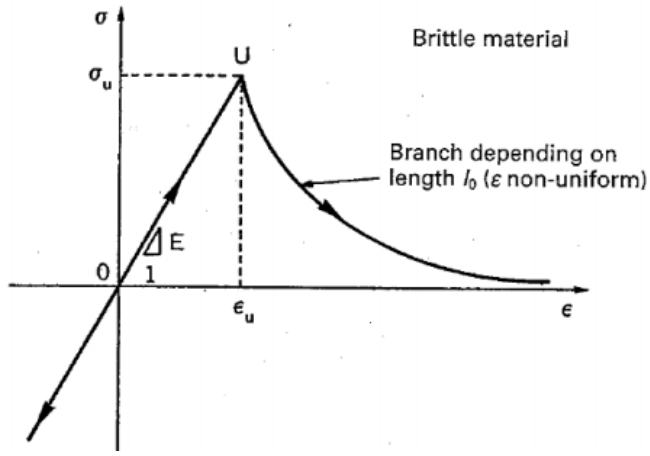

Figure 13: Brittle material

Considering a brittle material in which the tension and compression behavior is different as a concrete material. The behavior showed in the graph expresses an elastic behavior until the maximum tension σ_u and the strain ε_u this point is called *U* and expresses the localization strain. After this point has been reached, the softening branch will be showed in the graph. The softening branch

could have different slope in function of the length l_0. Moving now on the fractural energy and so the tension-crack opening graph, a not constant fractural energy is showed.

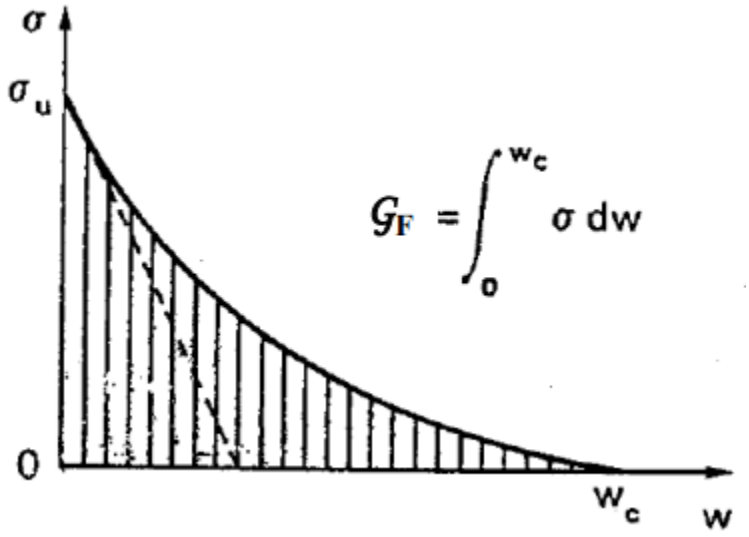

Figure 14: Fractural energy

The tension path showed in the graph expresses a peak stress value when the crack is closed and a softening branch in the tension with the crack opening until the ultimate value of the crack called *critical crack opening* w_c. Of the definition of the fractural energy in the $(F, \Delta l)$ graph, considering the constant value of G_F and different value of l_0, it is possible to understand the transition link with l_0 for reaching U.

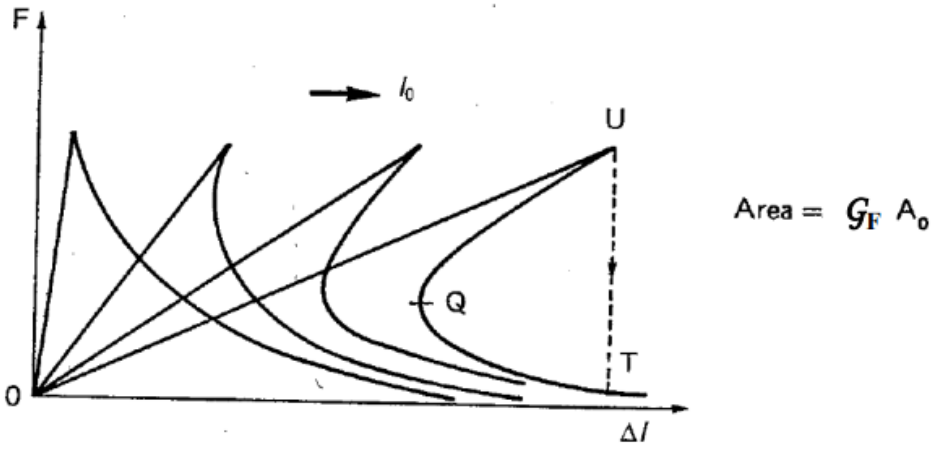

Figure 15: Transition behavior

The first two curves show a softening branch, on the other hand, for other increasing of the l_0 value the after peak branch became more slope and the snap back behavior need to be considered. In order to consider an analytical formulation of the snap back, the transition behavior will be analyzed in the tension-strain graph obtained by the previous one dividing the force F for the area A_0 and the length Δl for l_0.

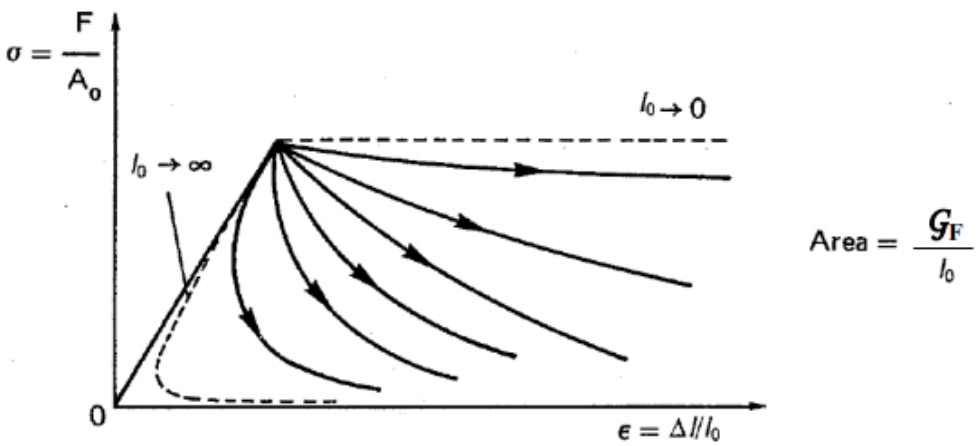

Figure 16: Transition behavior in tension-strain graph

The value of the area now is not constant, and it is function of the l_0. Considering the analytical formulation:

$$\varepsilon = \frac{\Delta l}{l_o} = \frac{\varepsilon_{el}\, l_0 + w}{l_o}$$

Eq 7

Where ε_{el} indicates the specific longitudinal dilation of the undamaged zone:

$$\varepsilon_{el} = \frac{\sigma}{e} \rightarrow \varepsilon = \frac{\sigma}{E} + \frac{1}{l_0} w(\sigma) \rightarrow \frac{d\varepsilon}{d\sigma} = \frac{1}{E} + \frac{1}{l_0}\frac{dw}{d\sigma}$$

Eq 8

Where:

- $\frac{dw}{d\sigma}$ is the cohesive law.

Softening with positive slope (snap-back) occurs when:

$$l_0 > E / \left|\frac{d\sigma}{dw}\right|_{max}$$

Eq 9

If the equation 10 is respected, the material behavior will be brittle for whatever material typologies because it is a brittle behavior correlated to the scale of the element. For a snap back behavior, after the peak is reached the drop off load will be immediately expresses a catastrophic phenomenon.

2.3 The cohesive model

Concrete in tension exhibits strain softening, a negative slope in the stress–deformation diagram, due to microcracking and localization of the deformation in a narrow band, where energy dissipation occurs. The behavior of the material outside this band is still linear and elastic. This phenomenon, observed experimentally by L'Hermite, Rusch and Hilsdorf, Hughes and Chapman, Evans and Marathe, among others, must be taken into account in order to provide a good explanation of the behavior of the material. From the Continuum Mechanics viewpoint, strain softening represents a violation of Drucker's Postulate, as was pointed out by Maier et al. These authors showed that, even in the absence of geometrical instability effects, the following phenomena may occur:

- loss of stability in the controlled load condition (snap-through);
- loss of stability in the controlled displacement condition (snap-back);
- bifurcation of the equilibrium path;
- loss of uniqueness of the solution in the incremental elastic-plastic response;
- dependence of the results on the type of mesh used in the numerical analysis.

A continuum described by strain-softening is also characterized by an imaginary wave speed or by the change of the equation of motion from hyperbolic to elliptic, as pointed out by Hadamard. This confirms the difficulties involved in this constitutive relationship, as compared to the classical strain-hardening one. The cohesive crack model is based on a softening stress–crack opening

displacement constitutive law. The cohesive crack model is able to describe materials that exhibit a strain-softening type behavior. The area under the closing stress vs. crack opening displacement curve represents the fracture energy G_f assumed as a material property. The cohesive crack model was initially proposed by Barenblatt and Dugdale. Subsequently, Dugdale's model was reconsidered by Bilby et al., Willis , Rice, and utilized by Wnuk, who referred to it as the final stretch criterion. Hillerborg et al. proposed the fictitious crack model in order to study crack propagation in concrete. The crack is assumed to propagate when the stress at the crack tip reaches the tensile strength σ_u. When the crack opens, the stress is not assumed to fall to zero at once, but to decrease with increasing crack width w. The amount of energy absorbed per unit crack area is the fractural energy G_f.

Recently, the former terminology of cohesive crack model has been reproposed by Carpinteri. Later on, in order to explain the size effects upon the parameters of the cohesive crack model, Carpinteri applied fractal geometry concepts and described the influence of the microstructural disorder typical of most of quasi-brittle materials. The fractal approach was further developed by Carpinteri et al. Recently, an improvement of the cohesive crack model, the so-called (scale-invariant) fractal cohesive crack model, has been proposed and applied to interpret the most extensive experimental tensile data from concrete specimens tested over a broad range of scales.

2.3.2 Basic concepts of the cohesive crack model

The basic assumption is the formation, as an extension of the real crack, of a fictitious crack, referred to as the process zone, where the material, albeit damaged, is still able to transfer stresses.

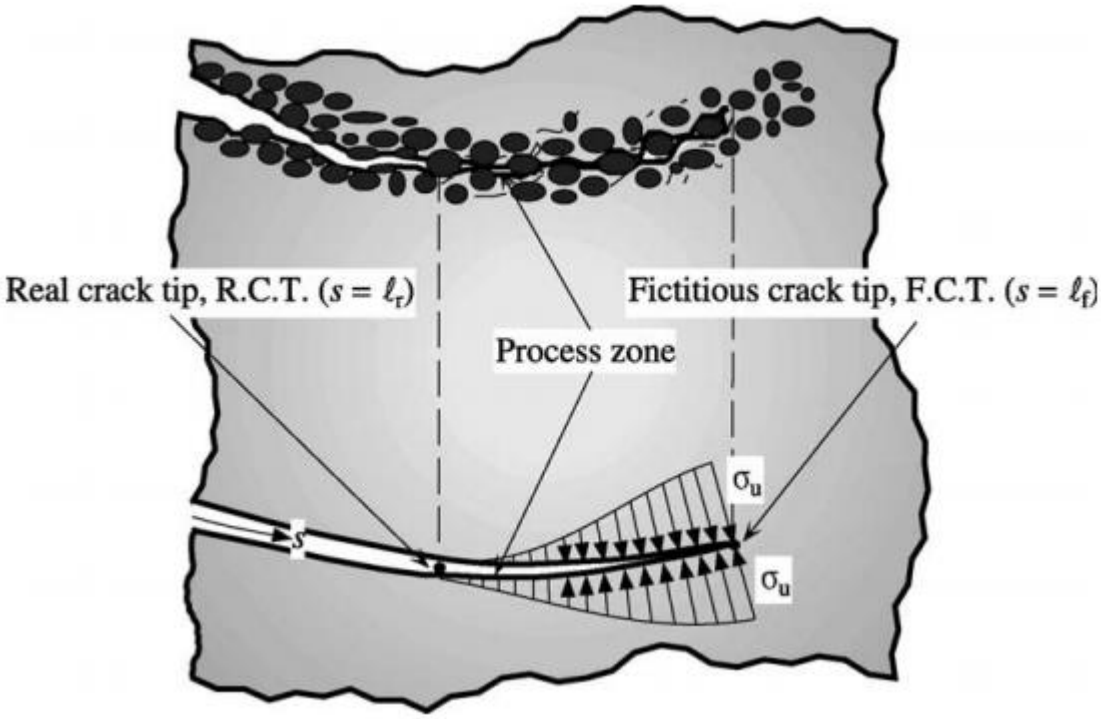

Figure 17: Process zone (without shearing stresses).

The point separating the stress-free area, the real crack, from the process zone, is called real crack tip, whilst the point separating the process zone from the uncracked material is referred to as fictitious crack tip. The process zone represents the area in which energy dissipation takes place: it begins to form when the principal tensile stress reaches the material ultimate tensile strength, σ_u, in the direction perpendicular to the direction of the principal tensile stress. In other words, within a cohesive crack, it is possible to recognize the fictitious crack tip, which is the point where the ultimate tensile strength, σ_t, is reached, and the real crack tip, which is the point where the critical crack opening, w_{crt} is gained. The region included within these two tips is the process zone where cohesive forces act, whereas the area below the $\sigma - w_t$ curve represents the fracture energy,

G_F. Furthermore, in the process zone, the stresses transferred by the material are decreasing functions of the displacement discontinuity, according to a proper cohesive law.

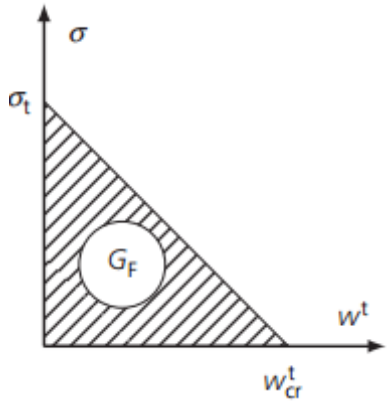

Figure 18: Cohesive law

The linear constitutive stress-crack opening law is represented by:

$$\sigma = \sigma_t \left(1 - \frac{w^t}{w_{ct}^t}\right)$$

Eq 10

Whilst in the uncracked zone the behavior of the material is linear-elastic:

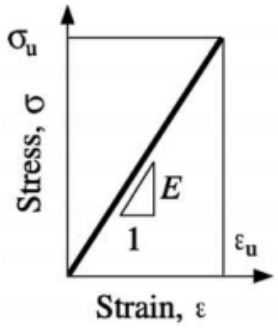

Figure 19: Linear-elastic constitutive law

The linear constitutive stress-strain law is represented by:

$$\sigma = E \cdot \varepsilon \qquad 0 \leq \sigma \leq \sigma_t$$

Eq 11

is adopted until the tensile strength, σ_t, is reached.

The cohesive model is possible to apply in the tension part in a beam. In light of these findings, two constitutive laws are the minimum base for describing the real behavior of the element in tension. The most common law, the linear elastic behavior will be used in the uncracked zone in which there are no damage, and this relation will work perfectly. On the other hand, when the crack zone is considered, the stress-strain relation is not able to consider this effect and the value of the tension drop off to zero. In order to avoid this and, in order to consider the energy exchange between the two side, the constitutive stress-open cracking law will be considered. The area below this graph is the fractural energy. The value of the stress will be decrease until the ultimate opening crack. This value w_t represents the limit for the energy exchange between the two surfaces. Anyway, if this is what happen in tension, it is also important wonder what happen in compression. In order to study the behavior in compression, a new model will be used, called Overlapping model.

2.4 Overlapping model

The compressive behavior of concrete materials has been studied by several researchers such as Carpinteri et al. (2001), Dahl and Brincker (1989), Hudson et al. (1971), Jansen and Shah (1997),

van Mier et al. (1997) and Vilet and Brincker (1996). A first model for the description of size effects on the compressive behavior of concrete was introduced by Hillerborg (1990), moving from a strain localization zone having a width equal to:

$$b = \eta x$$

Eq 12

Where:

- x is the position of the neutral axis;
- η is a coefficient that may be fixed equal to 0,8.

Within this zone, Hillerborg defines a softening law in compression and is able to calculate size-dependent moment–curvature diagrams for a beam subjected to bending. On the other hand, the overlapping crack model for concrete proposed by Carpinteri et al. (2009a, 2009b, 2010) is formally comparable to the cohesive crack model applied in tension. Within this model, the damage process takes place through a fictitious interpenetration (overlapping) zone, growing during the loading process.

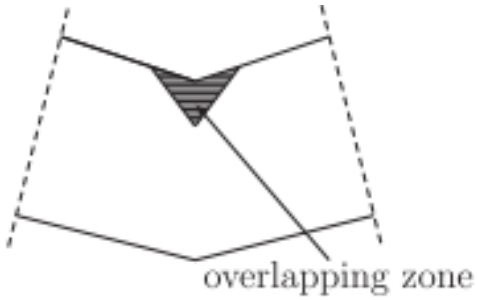

Figure 20: Overlapping zone

This damaged zone starts to develop when the compressive strength σ_c of concrete is reached at the beam extrados, and then an overlapping $\sigma - w_c$ law is adopted.

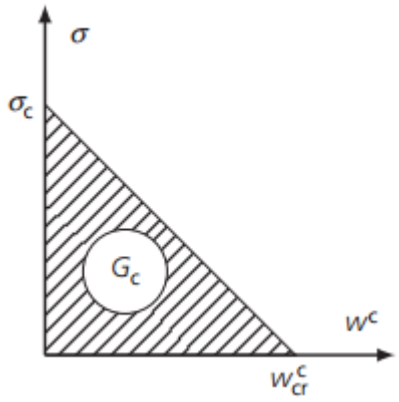

Figure 21: Overlapping constitutive law.

The linear constitutive stress-crack opening law is represented by:

$$\sigma = \sigma_c \left(1 - \frac{w^c}{w_{cr}^c}\right)$$

Eq 13

Outside the overlapping process zone, the material is assumed to be linear elastic, and a $\sigma - \varepsilon$ law is considered:

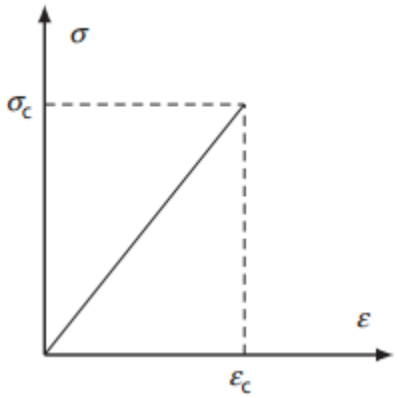

Figure 22: Linear constitutive stress-strain law

The linear constitutive stress-strain law is represented by:

$$\sigma = E \cdot \varepsilon \qquad 0 \leq \sigma \leq \sigma_c$$

Eq 14

The area subtended by the $\sigma - w_c$ curve defines the crushing energy, G_c. In this context, Ferrara and Gobbi (1995) studied the compressive behavior of concrete specimens varying both slenderness and scale. They tested three different specimen sizes, pointing out a remarkable variability in the post-peak regime of the structural behavior. This curve scattering suggests that, if a virtual concrete interpenetration, w_c, is taken into consideration, the post-peak branches lie within a narrow band. Hence, a $\sigma - w_c$ law may be assumed as a real constitutive law, and the crushing energy, G_c, constitutes an effective mechanical property that is independent of specimen geometry and size as suggested by Jansen and Shah (1997). Suzuki et al. (2008) proposed an evaluation of the crushing energy calibrated on compression tests carried out on plain and reinforced concrete specimens, taking into account the confinement effect provided by stirrups. On the other hand, using the formulation suggested by Model Code 2010 (fib, 2013) for the assessment of G_F, it is possible to compare the values assumed by G_c and G_F for several concrete grades, as reported in Table 3. It is possible to observe that G_c ranges between 30 and 55 N/mm, whereas G_F ranges between 0.133 and 0.163 N/mm. Hence, the crushing energy assumes a value which is larger than that of the fracture energy by two orders of magnitude. Meanwhile, it has been observed that the critical concrete overlapping $w_{cr}^{c} \approx 1\ mm$ is one order of magnitude larger than the critical crack opening w_{cr}^{t} (Carpinteri et al., 2007).

Table 3: Concrete stress and fractural energy

sc [MPa]	st [MPa]	G_F [N/mm]	G_c [N/mm]
20	2.210	0.133	30
30	2.896	0.141	30
40	3.509	0.147	30
60	4.598	0.156	47
80	5.570	0.163	55

Where:

- σ_c is the stress concrete compression;
- σ_t is the stress concrete tension evaluated like:

$$\sigma_t = 0.3 \cdot \sigma_c^{2/3} < C50$$

Eq 15

Where the formulation is given by: Model Code 2010 (fib, 2013).

- G_F the fractural energy in tension evaluated like:

$$G_F = 73/1000(\sigma_c + 8)^{0.18}$$

Eq 16

Where the formulation is given by: Akiyama et al. and Suzuki et al.

- G_C the fractural energy in compression evaluated like:

$$G_c = 80 - 50k_b$$

Eq 17

Where:

- $k_b = 40/\sigma_c < 1$

Eq 18

Where the formulation is given by: Akiyama et al. and Suzuki et al.

2.5: The Cohesive/Overlapping model

The mainly action to which the reinforced concrete beam are subjected is the flexural action. Flexural action is carried by the beam expresses two different zone: tension zone and compression zone. Considering the beam below description as a beam on two restrain point and one point load, looking at the deformation of the beam it is evidence that the above part of the beam is in compression and the below part is in tension. According to the Saint Venant theory, the flexural behavior is decomposed on the beam in two different forces of equal absolute value but with opposite mark and with a lever arm.

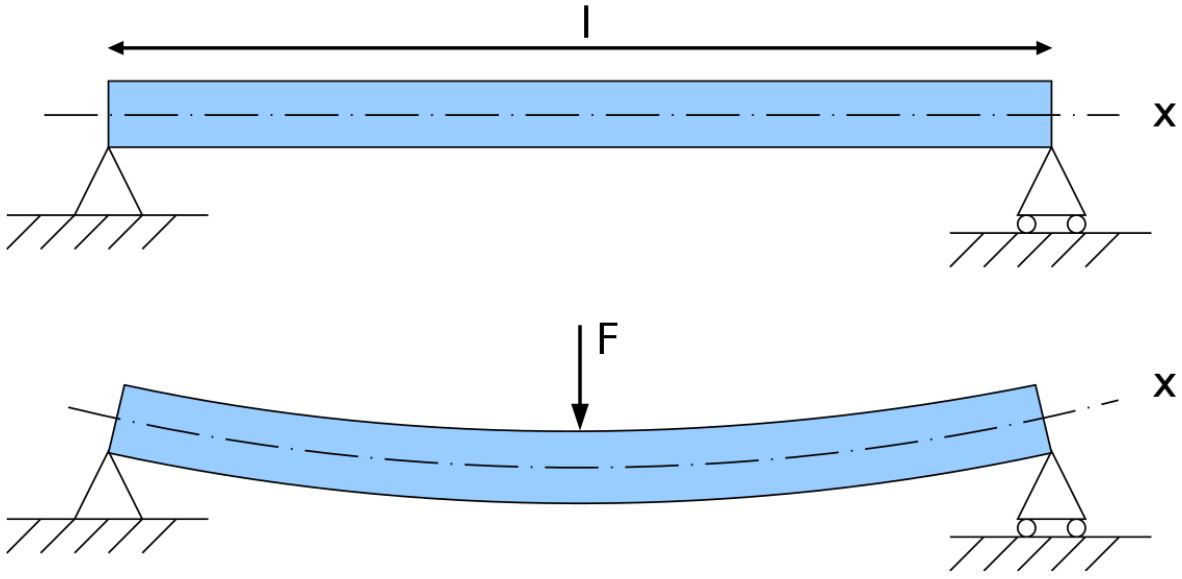

Figure 23: Three-point bending beam.

Considering the two different parts of the beam, the Cohesive/Overlapping model lead the study of the beam with two different law:

1) In tension, hence in the below part, the Cohesive model it is used;
2) In compression, hence in the bottom part, Overlapping model it is used.

Starting of the Cohesive model, in the previous chapter has been described the model in details anyway, for a quick summary the model is based on two different constitutive laws applied in along the fictitious crack considering elastic constitutive law before the crack opening and tension-crack opening constitutive law along the crack length. The last one is the constitutive law representative of the material, and the last part of the curve is composite by a softening decrease branch until the ultimate value of the crack opening w_{cr}^{t} that it is defined of a characteristic of the material.

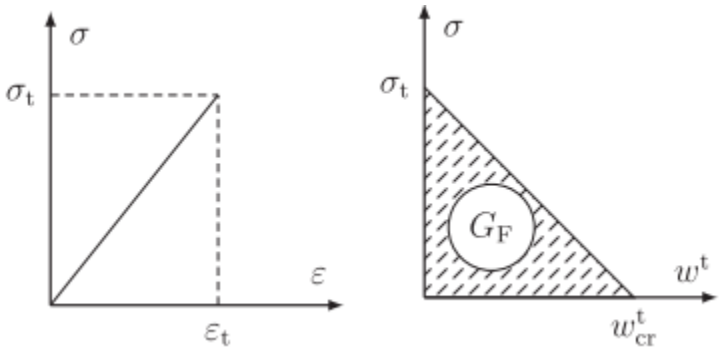

Figure 24: Cohesive crack model constitutive laws

Moving now on the Overlapping crack model, in order to use both the model on the same beam in order to keep the entirely information either the Overlapping model is based on the fictitious crack divided in two different length in which there are two different laws. The first length, in which the damage is not evolved, the linear elastic constitutive law is adopted. Moreover, where the damage zone is processes and the material start the crack in compression, the tension-crack constitutive

law is adopted. Either in this case, the final part of the constitutive law finish with a softening bracing until the critical value of the crack in compression w_{cr}^{t}.

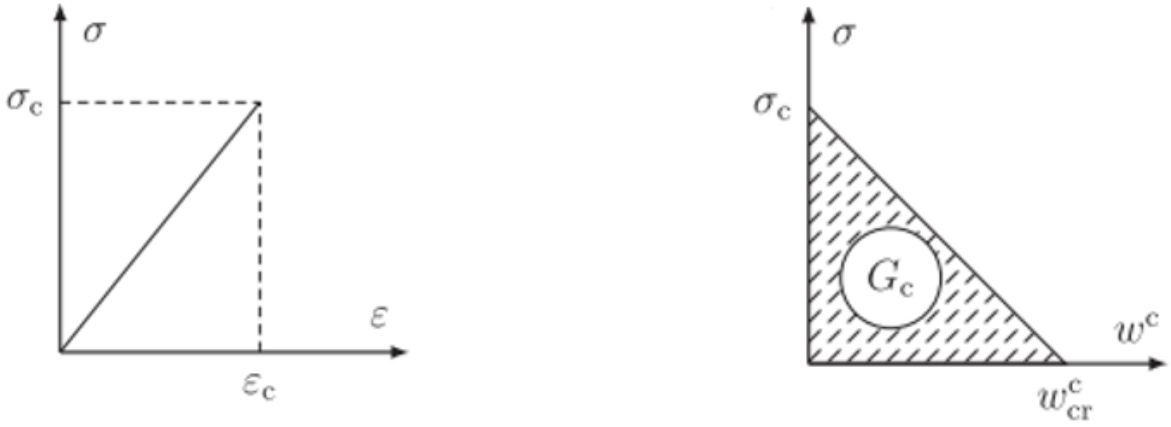

Figure 25: The cohesive laws

Both the model is summarized, anyway it is important to define some order of magnitude. The value of the ultimate tension stress is one order of magnitude lower than the compression stress; moreover, the value of the crack opening in tension is one order of magnitude lower than the crack opening in compression. For the definition of the fractural energy, after these considerations, it is obvious that the order of magnitude of the fractural energy in tension and in compression is different how it is possible to see in the Table 4.

Table 4: Concrete characteristics

sc [MPa]	st [MPa]	G_F [N/mm]	G_c [N/mm]	Ratio G_c/G_F
20	2.210	0.133	30	225.56
30	2.896	0.141	30	213.512
40	3.509	0.147	30	204.08
60	4.598	0.156	47	301.28
80	5.570	0.163	55	337.42

The Cohesive/Overlapping model definitely, considering two different crack zone independent to each other and able to propagate without any interference. For the cohesive zone, the crack propagation starts to the intrados and go through the extrados, on the other hand, for the overlapping zone, the crack propagation start to the extrados and go through the intrados.

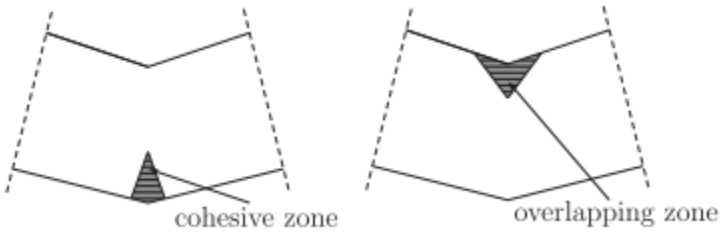

Figure 26: Processing zones

By means of this Nonlinear Fracture Mechanics Model, the RC beam cross-section is discretized into *n* different nodal points, being n = 161 in order to avoid numerical instabilities, as suggested by Carpinteri et al. For these nodes, the following equation applies:

$$\{w\} = [K_F]\{F\} + \{K_M\}M$$

Eq 19

Where:

- $\{w\}$ being the vector containing the crack opening/overlapping displacements;
- $[K_F]$ the matrix containing the coefficients of influence for the nodal displacements generated by the unit nodal forces;
- $\{K_M\}$ the vector containing the nodal displacements generated by a unit bending moment;
- $\{F\}$ the vector containing the forces applied;

- M the value of the applied bending moment.

The number of the unknowns in Eq 19 is equal to (2n + 1): n crack opening/overlapping displacements, n nodal forces, and the applied bending moment, M. In addition to Eq 20, the following conditions should be taken into account to describe the RC beam cross-section behavior:

$$F_i = 0 \; for \; i = 1, \dots, (j-1), i \neq r$$

Eq 20

$$F_i = F_t \left(1 - \frac{w_i}{W_{cr}^i}\right) for \; i = j, \dots, (m-1)$$

Eq 21

$$w_i = 0 \; for \; i = m, \dots, p$$

Eq 22

$$F_i = F_c \left(1 - \frac{w_i}{w_{cr}^c}\right) for \; i = (p+1), \dots, q$$

Eq 23

$$F_i = 0 \; for \; i = (q+1), \dots, n$$

Eq 24

$$F_i -= f(w_i) for \; i = r$$

Eq 25

Where:

- j being the real crack tip;

- m the fictitious crack tip;
- p the fictitious overlapping crack tip;
- q the real overlapping crack tip;
- r the node where the reinforcement layer is located.

Eq 25 correlates the crack opening at the level of reinforcement with the force exerted by the steel bar. This equation can be calibrated according to a bond-slip law proposed in Ruiz and Planas, Ruiz, Model Code 201039

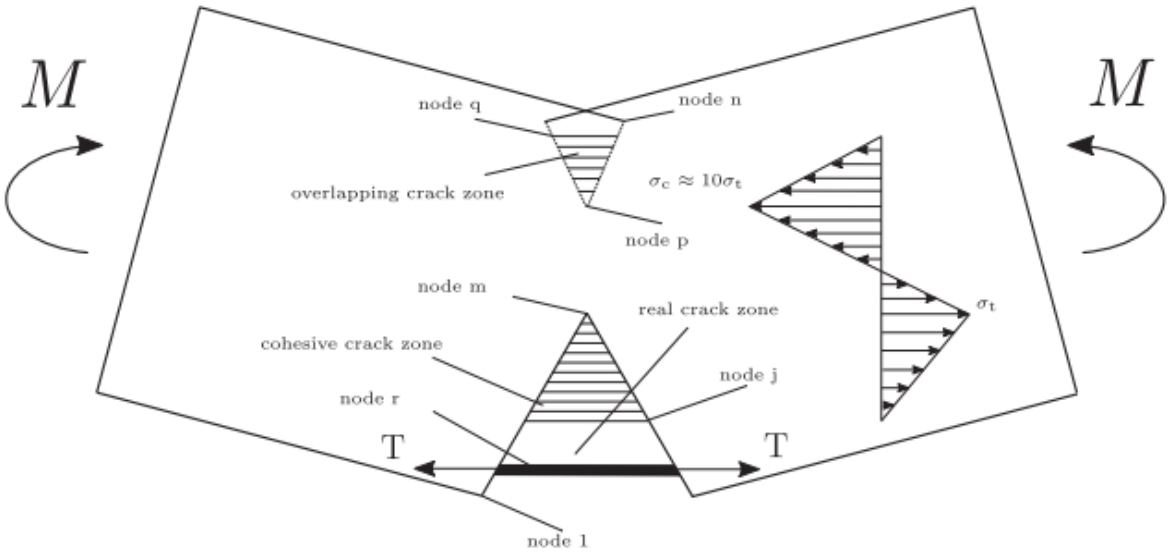

Figure 27: Cohesive/Overlapping model

Through the Cohesive/Overlapping model it is possible to follow the experimental results without losing any information. The importance of this model is given by the possibility of prediction the value of the experimental results with a elevate precision and, for this reason, it is possible to prediction the behavior and based a parametric analysis. The high corresponding between the

theory and the experimental results is given by the study of the two zones simultaneously. This process is possible thanks to Carpinteri that made the Overlapping crack model formally comparable to the Cohesive crack model applied in tension through the description of the real and fictitious crack in both the models.

The results obtained by the model is:

1) The bending moment and the rotation of the cross section;
2) The force applied on the beam and the deflection;
3) The bending moment and the crack opening;
4) The crack opening along the section.

The first graph that it is showed is the *Moment-Rotation*. In this graph the value of the bending moment is linked to the rotation of the cross section. The graph divided the cross-section behavior in different parts, and it is possible to summarize the:

1) Elastic linear branch;
2) Cracking moment M_{cr};
3) Pseudo-plastic plateau;
4) Concrete crushing.

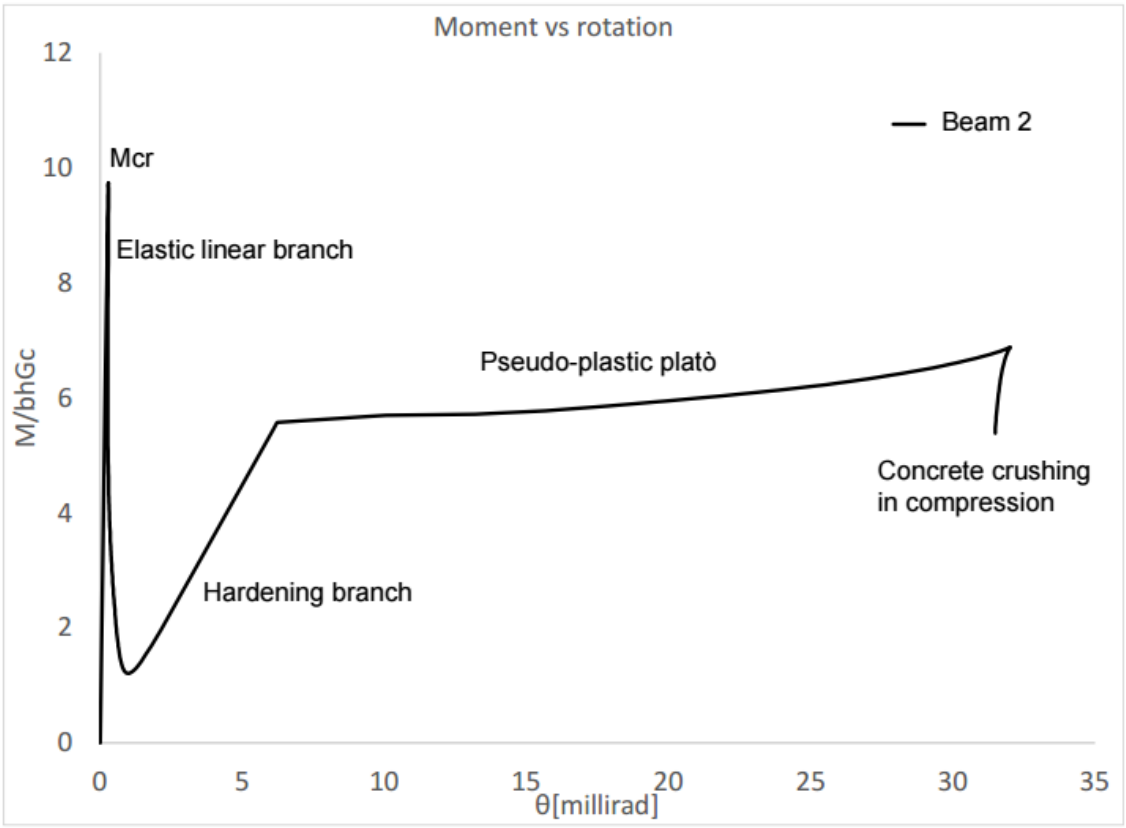

Graph 1: Moment-rotation.

The value of the moment on the vertical axis is dimensionless with the area of the cross section and the value of the fractural energy in compression in order to obtain a graph layout easily readable. The first linear part of the graph represents the linear elastic behavior of the beam. The ultimate bending value of the linear elastic behavior is the cracking bending moment M_{cr}. When this value of the moment is reached the beam will crack and the elastic behavior is ultimately. In order to obtain an easily readable, the model represent the end of the elastic linear behavior with a drop off load. Consequently, at the drop off load the hardening branch start to develop and represents the benefit of the reinforcement in the concrete beam. The third part of the graph is

represented by the pseudo-plastic plateau. Considering a parallelism with the concrete beam reinforced with the steel bars, the plastic plateau is reached when the yielding tension in the steel bars is reached. On the other hand, considering the constitutive law of the GFRP bars there are no yielding point, and this means that the plastic plateau is impossible to replace. Anyway, according to the results given by the Cohesive/Overlapping model and thanks to the intuition to reduce the bond strength between concrete and GFRP bar, it is possible to obtain a pseudo-plastic plateau thanks to small slip of the GFRP bar. The last part of the graph shows a softening/snap back branch which means the concrete crushing in compression.

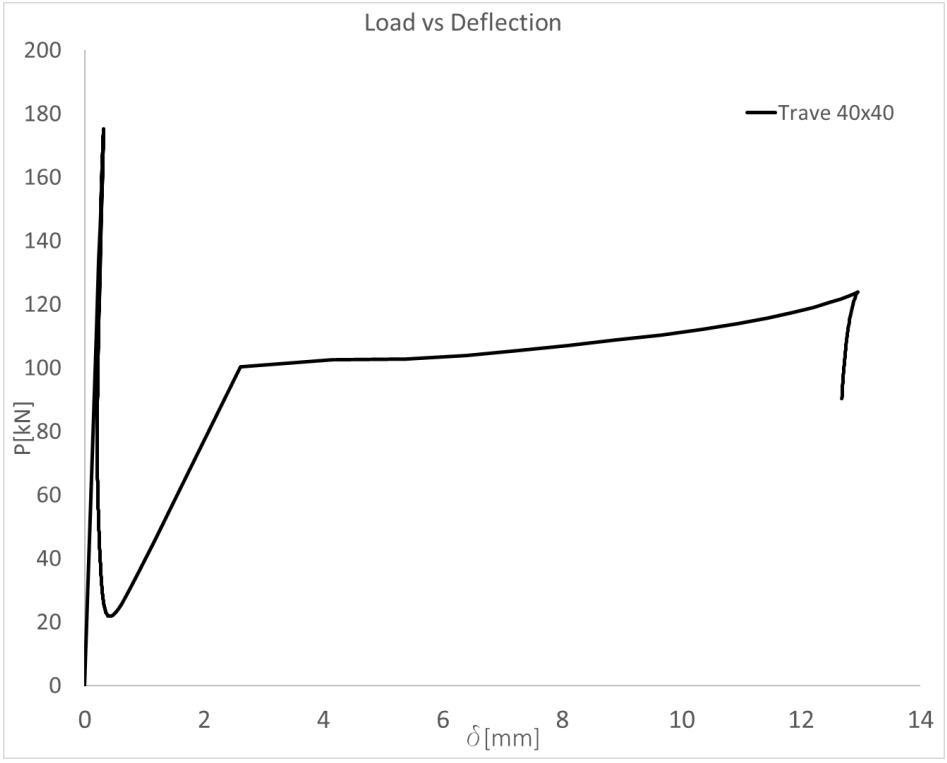

Graph 2: Load deflection

The second graph given by the Cohesive/Overlapping model is the load deflection diagram. In this case, it is possible to see the value of the load reached in the different behavior in the concrete beam. The other parameter is the deflection of the beam that it is possible to use for serviceability verification during the design process.

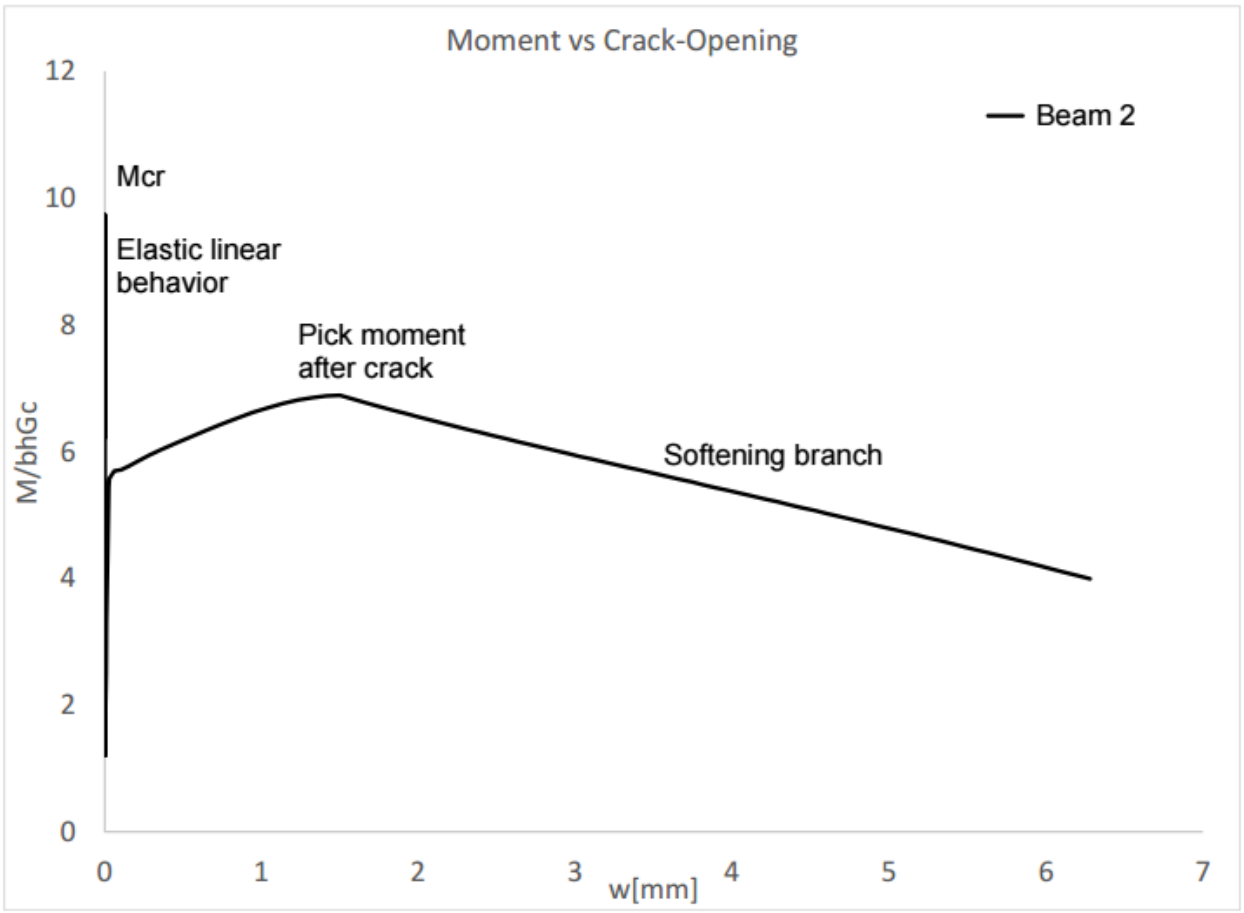

Graph 3: Moment-crack opening

The third graph is the Moment-crack opening. Even in this case the value of the crack moment is dimensionless. Anyway, the meaning of this graph is to follow the variation of the bending moment with the crack opening. The first part of the graph is a vertical line until the value of the cracking

moment correlated to the crack opening equal to 0 because this is the elastic branch. After this point, the cracking start in the section and the value of the moment increase in the first part thanks at the GFRP bars presents in the cross section until the pick moment value after crack but after a low increase the moment start to decrease following a softening branch linked to the increase of the crack opening. This graph is a graphic representation of the Cohesive/Overlapping model for its capacity to link the cohesive zone inside the crack length with the bending moment and showing the bending moment variation in this process.

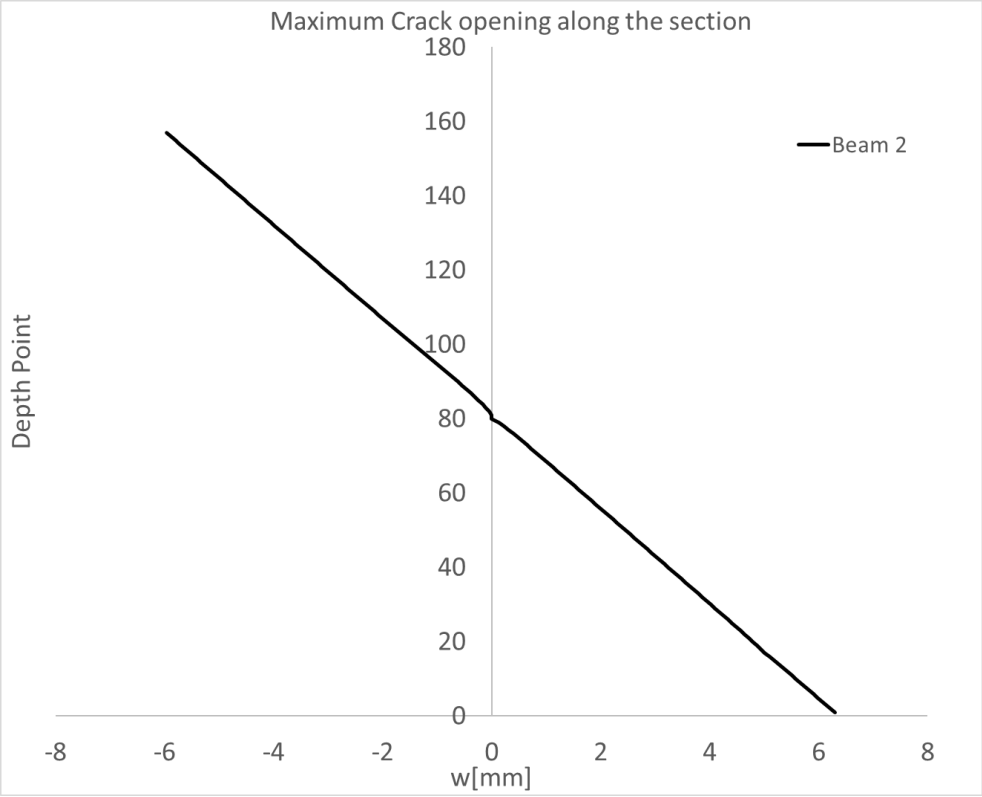

Graph 4: Maximum crack opening along the section

The last graph made by the Cohesive/Overlapping model show the crack opening along the depth of the beam section. The depth of the beam is divided into 161 points. Moreover, along the horizontal axis the value of the crack opening is positive if the crack opening is in tension and negative if the crack opening is in compression.

Chapter 3:

Experimental testing program

3.1: Introduction

The experimentation of this thesis project in collaboration with the Miami universities (UM) has a double aim. The first target is the ductile-brittle transition by the concrete beam reinforcement with Glass fiber reinforcement polymer bars. The second target is to find an innovative procedure that allows for the definition of the intrinsic parameters of a reinforced concrete beam using the smallest possible resources. In order to study the ductile-brittle transition have been investigated 2 beam scale reinforcement with 4 different reinforcement percentage. In addition, the casting has been repeated with different GFRP bars typologies. Matching all the needs as laboratory capacity, experimental research, and concreteness of the results, the two scales adopting in the thesis were:

1) Cross section: square; dimension $0.2\ x\ 0.2\ m$; length $L = 0.8m$. Called beam 1.
2) Cross section: square; dimension $0.4\ x\ 0.4\ m$; length $L = 1.6m$. Called beam 2.

The reinforcement percentage given by the ratio between the reinforcement areas and the concrete area with the following formulation:

$$\rho = \frac{A_s}{A_C}$$

Eq 26

Where:

- A_s = reinforcement area in $[mm^2]$ of the GFRP bars;
- A_C = concrete area in $[mm^2]$ of the matrix.

It has been chosen equal to: [0.2, 0.4, 0.8, 1.6]% in order to cover all the possibilities reinforcement typologies between the under reinforcement condition and over reinforcement condition.

For reinforcement the concrete beam, GFRP bars have been used considering different diameter of the same bar typologies and different bar typologies. The diameter that has been adopted are: 10 mm; 12 mm; 20 mm. The bars typologies are: helical wrapping bars with high bond strength and helical wrapping bars with low bond strength.

The entirely thesis experimentation is based on 15 beams divided into 7 beam 1 and 8 beam 2.

It is fundamental remind that, the entirely beams have been predesigned and studied with the Cohesive/Overlapping model. Changing different parameters like: cross section dimension, slenderness of the beam, concrete characteristics, bar characteristic and bond strength the parametric analysis has been developed. Anyway, these aspects are going to be investigated in the next chapters.

The experimental procedures are divided into fourth different steps:

- First of all, the formwork has been built through plywood plate with the thickness equal to 2 mm;

- secondly, the GFRP cage composite by steel stirrups and GFRP longitudinal bars has been made;
- next steps have been the cast of the specimens and of the cylinders;
- Finally, after 28 days for the concrete curing, the test on the beams has been started.

The experimental beams are divided into three different groups:

1) Four beams named 1 with helical wrapping bars with high bond strength divided in:
    - 1 GFRP reinforcement bars with the diameter of 12mm consequently ρ = 0.28%;
    - 2 GFRP reinforcement bars with the diameter of 12mm consequently ρ = 0.57%;
    - 3 GFRP reinforcement bars with the diameter of 12mm consequently ρ = 0.85%;
    - 2 GFRP reinforcement bars with the diameter of 20mm consequently ρ = 1.57%.
2) Four beams named 2 with helical wrapping bars with high bond strength divided in:
    - 1 GFRP reinforcement bars with the diameter of 20mm consequently ρ = 0.20%;
    - 2 GFRP reinforcement bars with the diameter of 20mm consequently ρ = 0.39%;
    - 4 GFRP reinforcement bars with the diameter of 20mm consequently ρ = 0.79%;
    - 8 GFRP reinforcement bars with the diameter of 20mm consequently ρ = 1.57%.
3) Three beams named 1 with helical wrapping bars with low bond strength divided in:
    - 1 GFRP reinforcement bars with the diameter of 10mm consequently ρ = 0.20%;
    - 2 GFRP reinforcement bars with the diameter of 10mm consequently ρ = 0.39%;
    - 4 GFRP reinforcement bars with the diameter of 10mm consequently ρ = 0.79%;

4) Four beams named 2 with helical wrapping bars with low bond strength bars divided in:
    - 3 GFRP reinforcement bars with the diameter of 12mm consequently r = 0.21%;
    - 6 GFRP reinforcement bars with the diameter of 12mm consequently r = 0.42%;
    - 11 GFRP reinforcement bars with the diameter of 12mm consequently r= 0.78%;
    - 17 GFRP reinforcement bars with the diameter of 12mm consequently r= 1.20%.

It also possible identify the beam with the made-up name G H 20 #10_1 S8_6 and meaning:

- G meaning GFRP bar;
- H meaning Helical wrapping;
- HS meaning Second Helical wrapping typologies;
- S meaning Smooth GFRP bar;
- 'First number' meaning the side of the cross section;
- '#second number' meaning the bar diameter;
- '_third number' meaning the number of the bars;
- 'S8' meaning the center stirrups distance;
- '_fourth number' meaning the total number of the stirrups in the beams.

The following Table 5 gives a general summary of the specimens:

Table 5: Specimens summarize.

G H 20 #20_1 S8_6
G H 20 #12_2 S8_6
G H 20 #12_4 S8_6
G H 20 #20_2 S8_6
G HS 20 #10_1 S8_6
G HS 20 #10_2 S8_6
G HS 20 #10_4 S8_6
G H 40 #20_1 S8_10
G H 40 #20_2 S8_10
G H 40 #20_4 S8_10
G H 40 #20_8 S8_10
G HS 40 #12_3 S8_10
G HS 40 #12_6 S8_10
G HS 40 #12_11 S8_10
G HS 40 #12_17 S8_10

3.2: Beam concrete composition

The experimental beams that are used in this thesis are characterized by a slenderness:

$$\lambda = \frac{L}{h} = 4$$

Eq 27

Where:

- L = length of the beam;
- h = dept of the beam.

The value of the slender equal to 4 is lower than the characteristic value for the real beam. Anyway, this value of the slender is the correct compromised between the laboratory length capacity and the possibility of considering two different specimens length. The cross-section shape choice is a square in order to have the right space for set up the number of the bars between lower and over reinforcement percentages.

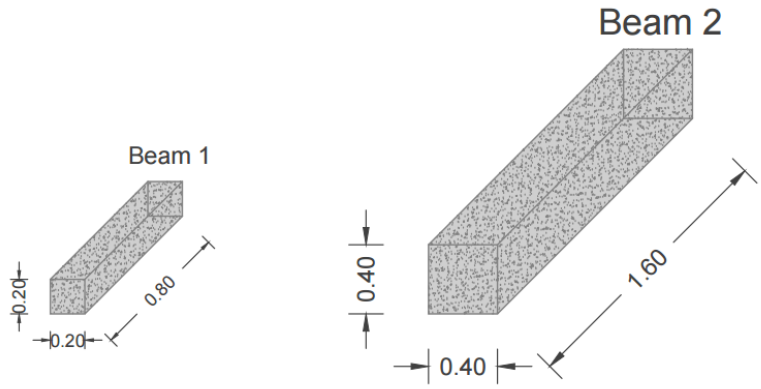

Figure 28: Experimental beams

3.3: Beam bars composition

The GFRP bars used in this thesis are fundamental for the results not only for the strength of the bars but even for their bond strength between concrete and bars.

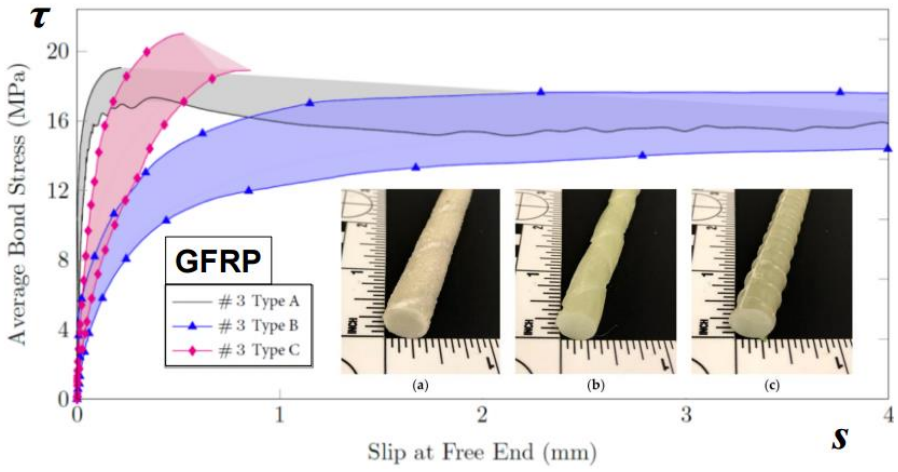

Figure 29: Bond stress

The bond stress between the concrete and the bars is function of different parameters. First of all, the most important parameters are the bar cover that influence directly on the τ value of it is possible to see in the Figure 29. On the other hand, the concrete strength and the concrete confinement are also other two important parameters that must are taking into account in this phenomenon. The bars characteristic tensile strength adopted in this thesis are the following:

$\sigma_{GFRP} = 1000\ MPa.$

The bars have been tested with the pull-out test considering 24 bars divided in three groups with 8 bars each one with:

1) Nominal diameter $d_b = 9.53mm$;
2) Effective circumference of FRP bar $C_b = 29.92mm$;
3) Bonded length $l = 47.63mm$;
4) Nominal bonded area $A_L = 1425.11mm^2$;

The test results are summarized in the Table 6.

Table 6: Pull-out test results GFRP 10 mm.

	Tensile Force F		Average Bond Stress τ	
	[kN]	[kip]	[MPa]	[ksi]
1	20.63	4.64	14.47	2.10
2	17.92	4.03	12.57	1.82
3	15.97	3.59	11.21	1.63
4	17.35	3.90	12.17	1.77
5	21.57	4.85	15.13	2.19
6	20.72	4.66	14.54	2.11
7	23.25	5.23	16.32	2.37
8	17.06	3.84	11.97	1.74
9	20.77	4.67	14.58	2.11
10	19.79	4.45	13.89	2.01
11	15.57	3.50	10.92	1.58
12	21.31	4.79	14.95	2.17
13	21.08	4.74	14.80	2.15
14	15.70	3.53	11.02	1.60
15	17.48	3.93	12.27	1.78
16	19.39	4.36	13.61	1.97
17	21.80	4.90	15.29	2.22
18	18.64	4.19	13.08	1.90
19	19.31	4.34	13.55	1.96
20	20.15	4.53	14.14	2.05
21	16.55	3.72	11.61	1.68
22	19.22	4.32	13.48	1.96
23	18.55	4.17	13.02	1.89
24	18.19	4.09	12.77	1.85
Average	**19.08**	**4.29**	***13.39***	***1.94***
S_{n-1}	2.10	0.47	1.48	0.21
CV (%)	11.0	11.0	11.02	11.02
Min	15.57	3.5	10.92	1.58
Max	23.25	5.2	16.32	2.37
Guaranteed Bond Strength			***8.96***	***1.30***

The average bond stress for every result is summarized in the graph 5. It is possible to see how the population of the results give the average bond stress in a narrow range between 10.92 MPa and 16.32 MPa. Moreover, the guaranteed bond strength for the GFRP bar with the diameter of 10mm and tested with the pull-out test is equal to 8.96 MPa.

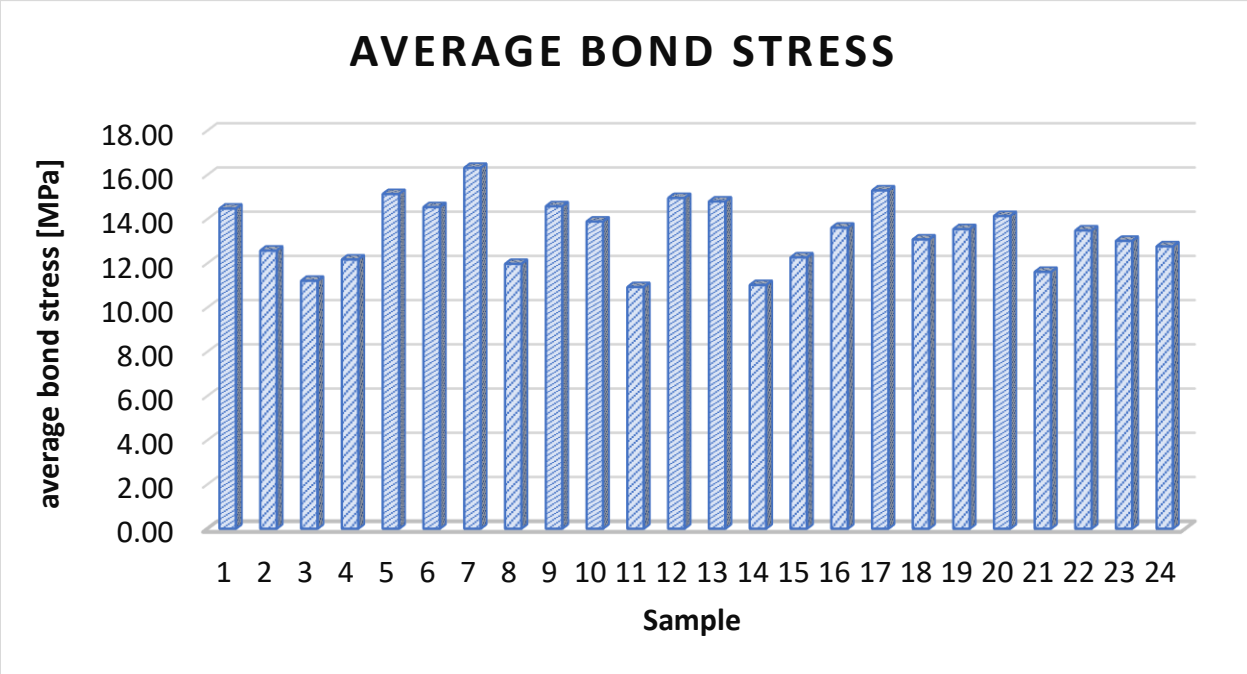

Graph 5: Average bond stress results pull-out test GFRP 10mm.

The bars diameter adopted along the thesis work has been the follows:

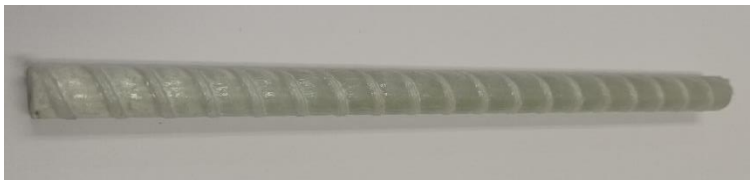

Figure 30: Helical wrapping 10 mm.

Figure 31: Helical wrapping 12 mm.

Figure 32: Figure 32: Helical wrapping 20mm.

Overall view of GFRP bars used:

Figure 33: GFRP bars overall view

. The pull-out test has been developed on the bars with the diameter equal to 10mm and the bars with the diameter of 16mm.

Pull-out test results for GFRP helical wrapping bars with diameter of 16mm is given in Table 7. In this case have been tested 24 bars divided in 3 groups composite by 8 bars each one. The results are showing an average bond stress always higher than the previous results. The average bond stress given by all the samples is equal to 13.97 MPa and the guaranteed bond strength is 10.50 MPa larger of 17.10% than the previous value (8.96MPa). These results following the dictates specified before which means that the GFRP helical wrapping with the diameter of 10 mm and 12 mm present a lower helical wrapping and a smoother finally surface than the diameter of 20 mm.

Table 7: Pull-out test results GFRP 16 mm.

	Tensile Force		Average Bond Stress	
	F		***τ***	
	[kN]	[kip]	[MPa]	[ksi]
1	57.60	12.95	14.55	2.11
2	54.97	12.36	13.89	2.01
3	63.73	14.33	16.10	2.33
4	45.19	10.16	11.41	1.66
5	60.65	13.63	15.32	2.22
6	54.41	12.23	13.74	1.99
7	59.11	13.29	14.93	2.17
8	47.04	10.58	11.88	1.72
9	55.02	12.37	13.90	2.02
10	47.95	10.78	12.11	1.76
11	57.07	12.83	14.42	2.09
12	50.31	11.31	12.71	1.84
13	56.36	12.67	14.24	2.06
14	54.31	12.21	13.72	1.99
15	55.42	12.46	14.00	2.03
16	55.38	12.45	13.99	2.03
17	57.16	12.85	14.44	2.09
18	59.74	13.43	15.09	2.19
19	48.84	10.98	12.34	1.79
20	59.21	13.31	14.96	2.17
21	59.74	13.43	15.09	2.19
22	58.05	13.05	14.66	2.13
23	54.40	12.23	13.74	1.99
24	55.51	12.48	14.02	2.03
Average	**55.30**	**12.43**	***13.97***	***2.03***
S_{n-1}	4.58	1.03	1.16	0.17
CV (%)	8.3	8.3	8.29	8.29
Min	45.19	10.2	11.41	1.66
Max	63.73	14.3	16.10	2.33
Guaranteed Bond Strength			***10.50***	***1.52***

The average bond stress for every result is summarized in the graph 2. It is possible to see how the population of the results give the average bond stress in a narrow range between 11.41 MPa and 16.10 MPa. Moreover, the guaranteed bond strength for the GFRP bar with the diameter of 10mm and tested with the pull-out test is equal to 10.50 MPa.

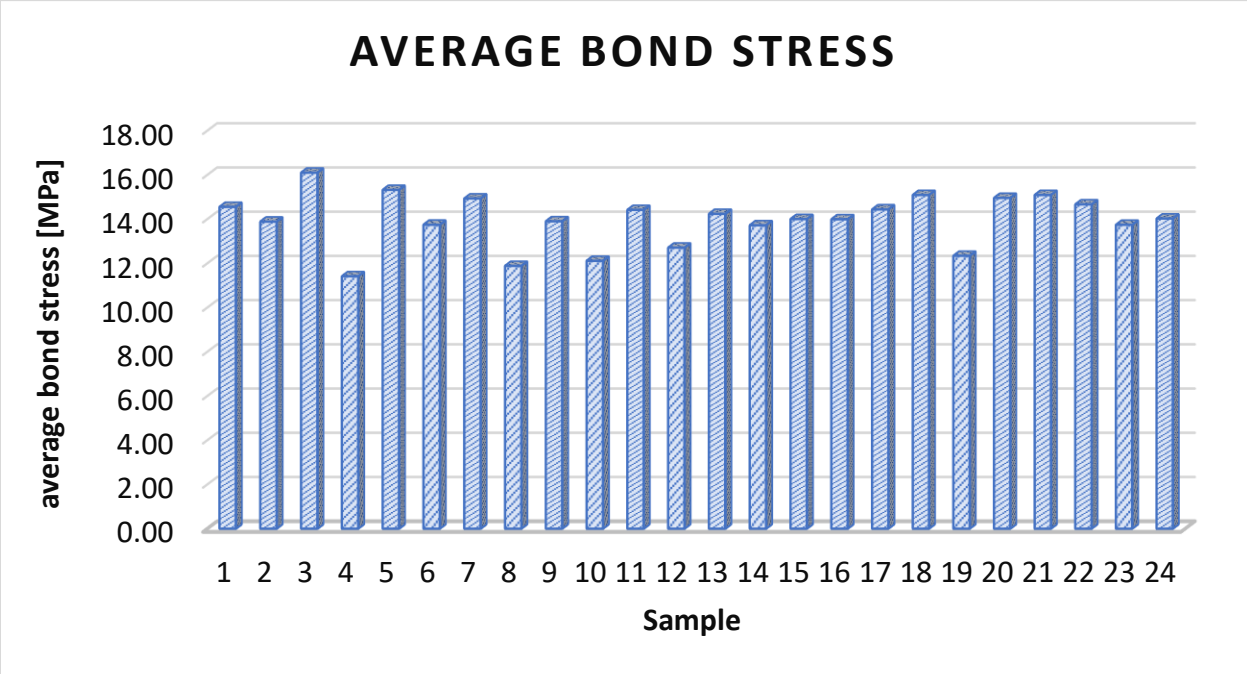

Graph 6: Average bond stress results pull-out test GFRP 16mm.

As mentioned in previous chapters, the pull-out test is not representative of the real bond conditions and moreover, it is not representative of the bending bond condition. According to the literature, it is possible to consider a correlation between the beam bond test and the pull-out test. The correlation between the results is showed how the pull-out test bond is almost the double of the beam bond test bond. Moreover, as already mentioned, even the beam bond test tends to

overestimate the bending bond. In any case, in this experimental thesis is consider a correlation factor called c given by:

$$c = \frac{\tau^1}{\tau^2}$$

Eq 28

Where:

- τ^1 = the average bond strength given by beam bond test;
- τ^2 =the average bond strength given by pull-out test.

In order to convert the Pull-out test results given by the test for the GFRP bars typologies used in this thesis, it has been calculated an average value of the factor correlation called C_{AVG}. In the Table 8 the results of the correlation factor are showed.

Table 8: Correlation value

Correlation between Pull-out test and beam bond test		
Pull-out test	Beam bond test	Correlation factor
τ[MPa]	τ[MPa]	c
24.23	10.25	2.364
16.35	9.22	1.773
12.82	7.22	1.776
21.32	10.8	1.974
22.33	12.75	1.751
13.22	8.8	1.502
8.35	7.55	1.106
Average value	C_{AVG}	1.750

Considering now the C_{AVG} that mean the average of the correlation factor, the correlation between the results of the pull-out test on the GFRP bars used in this experimentation has been made. Considering the Table 9, it is possible to see the average bond stress, the minimum and the maximum bond stress for the GFRP bars helical wrapping with the diameter of 16mm and 10mm to which has been applied the correlation factor C_{AVG} in order to consider during the analysis a value of bond stress τ close to the real one in the Cohesive/Overlapping model application.

Table 9: Bond value

Diameter 16mm			Diameter 10mm		
AVG τ[MPa]	Min τ[MPa]	Max τ[MPa]	AVG τ[MPa]	Min τ[MPa]	Max τ[MPa]
13.97	11.41	16.10	13.39	10.92	16.32

Correlated values with beam bond test

Diameter 16mm			Diameter 10mm		
AVG τ[MPa]	Min τ[MPa]	Max τ[MPa]	AVG τ[MPa]	Min τ[MPa]	Max τ[MPa]
7.985	6.524	9.202	7.654	6.244	9.326

3.4: Beam design

The beam design is divided into two different parts. Considering the Four Point Bending Test, the beam is loaded with two forces and, for this reason, the stress characteristic along the beam length is divided in two different characteristic stress:

1) In the first part of the length beam, meaning between the restrain point and the load point, the stress characteristic is given by the linear bending solicitation and the constant shear solicitation. The segment called *A* and *C* with a length of 0.325m for the *Beam 1* and 0.55m for the *Beam 2*;
2) On the other hand, in the second part of the length beam, means between the two points loads, the stress characteristic is given by the only constant bending moment solicitation without any shear interference. The segment called *B* with a length of 0.15m for the *Beam 1* and 0.30 for the *Beam 2*.

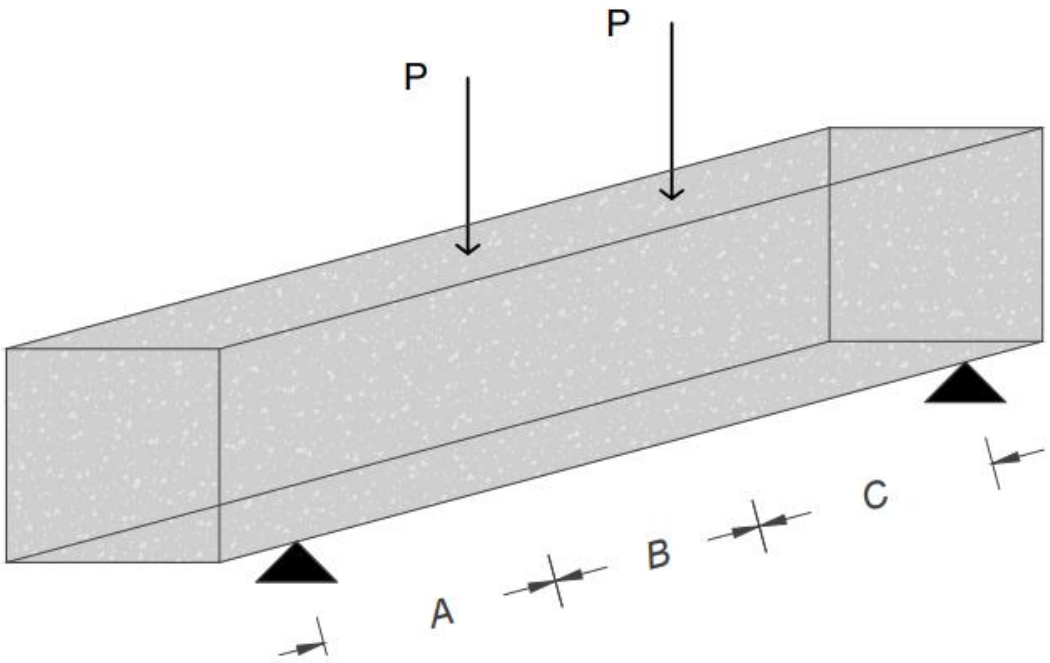

Figure 34: Bending design.

Through the Cohesive/Overlapping model has been done an analysis chanced the number of the longitudinal bars in order to obtain a different behavior of the beam. A parametric analysis has been performed through the different behavior of the beam characterized by the lower reinforcement, the medium reinforcement, and the over reinforcement. In the Graph 7 is showed three different curves representative of these three behaviors of the beam.

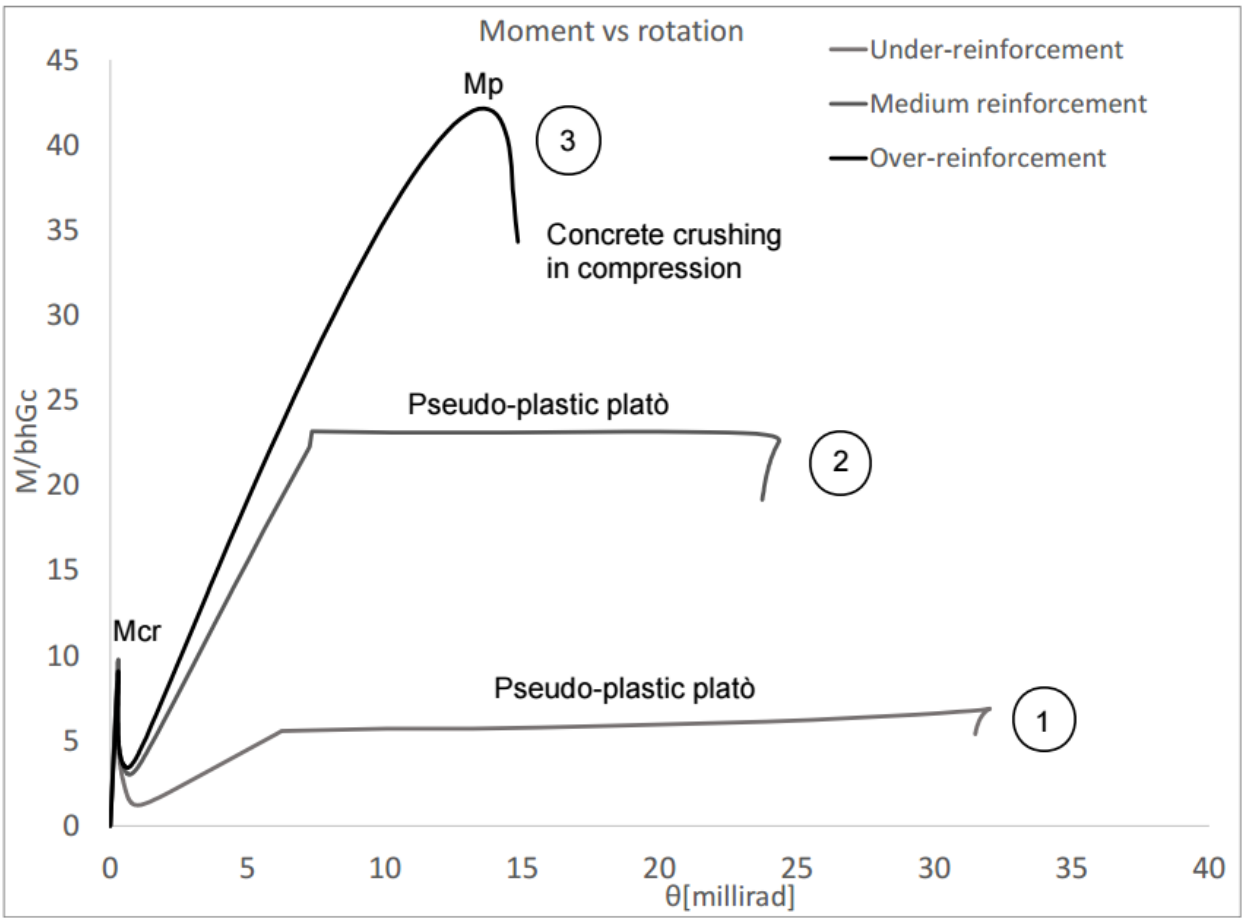

Graph 7: Under reinforcement, medium reinforcement, over reinforcement

The first curve shows the hyper resistance of the beam. This behavior is obtained when the reinforcement amount is enough low do does not express the benefit on the bending moment given by the GFRP bars. For this reason, the value of the bending moment after the M_{cr} is lower than the elastic bending moment in the section. In this case the pseudo-plastic plateau is located below the value of the cracking moment M_{cr}.

The second curve shows the medium reinforcement percentage in the concrete beam. It is possible to see the benefits in term of the increasing of the bending moment after the elastic behavior. In this case the pseudo-plastic plateau is located above the value of the cracking moment M_{cr}.

Last but not least, the third curve shows the over reinforcement percentage in the concrete beam. It is possible to see the classic and more conventional GFRP behavior. In this case after the cracking moment, the hardening branch lead the value of the bending moment until the peak value M_p with a linear branch. After the peak value M_p, the behavior of the beam is brittle, and the collapse is led by the concrete crushing in compression. The pseudo plastic plateau is not obtained in this solution because the behavior of the beam is defined as brittle behavior.

3.4.2: Shear design

The results of the analysis parametric combinate with the Cohesive/Overlapping model give the bending moment results. The set-up of the test is the Four Point Bending Test, for this reason, considering the value of the bending moment and the static scheme is possible to obtain the value of the shear. According to the static scheme of the Four Point Bending Test, the value of the shear is constant along the beam segment *A* and *C* and, moreover, it is equal to zero in the middle part

of the beam that means the segment called *B*. For this reason, the shear verification and the shear design are needed in the first and in the last segment of the beam. The shear design is divided into two different steps:

1) First of all, the shear verification for an element without any transversal reinforcement;
2) Secondly, if the step one is not satisfy the shear design for an element with transversal reinforcement is needed.

For the element without any transversal reinforcement the Italian Code CNR-DT 203/2006 given the path to follow step by step. In the CNR-DT 203/2006 at the chapter *4.8.2.1 Element without transversal reinforcement resistant to shear action* there is the equation for evaluating the shear capacity of the element:

$$V_{Rd,ct} = \left[0{,}13\left(\frac{E_f}{E_s}\right)^{1/2} \tau_{Rd}\, k\, (1.20 + 40\,\rho_l)\right] b_w d$$

Eq 29

Where:

- E_f = is the elastic modulus of the GFRP bar expressed in $[\frac{N}{mm^2}]$;
- E_s = is the elastic modulus of the steel bar expressed in $[\frac{N}{mm^2}]$;
- τ_{Rd} = is the shear collapse tension expressed in $[\frac{N}{mm^2}]$ and definite by $\tau_{Rd} = 0.25\, f_{ctd}$;
- $k = (1.6 - d) \geq 1$;
- $\rho_l = A_f/(b_w d) \leq 0.02$;

- f_{ck} = Compression strength of the concrete;
- b_w = minimum base of the cross section;
- d = useful depth of the cross section expresses in [m];

In the Table 10 there are the beam and reinforcement characteristics and the value of the shear strength compared to the shear action on the beam. The follow tables are just for the *beam 1*.

Table 10: Shear capacity

Name beam	ρ[%]	E_f[MPa]	E_s[MPa]	τ_{Rd}[MPa]	K	f_{ctd}[MPa]	b[mm]	d [mm]	σ_c[MPa]	$V_{Rd,ct}$[kN]
1	0.002066	87000	210000	0.88	1.41	3.51	200	190	40	5.04
	0.004132	87000	210000	0.88	1.41	3.51	200	190	40	5.37
	0.008263	87000	210000	0.88	1.41	3.51	200	190	40	6.02
	0.016526	87000	210000	0.88	1.41	3.51	200	190	40	7.32

The shear action on the beam, considering the results of the bending analysis, is obtained considering the distance between the restrain point and the load point through the static equation.

Table 11: Shear verification

Name beam	ρ[%]	V_{ed}[kN]	$V_{Rd,ct}$[kN]	Verify
1	0.2	18.73	5.04	FALSO
	0.4	30.09	5.37	FALSO
	0.8	42.32	6.02	FALSO
	1.6	51.97	7.32	FALSO

Considering the Table 11, the entirely stock of the beam is not verified. A design with transversal shear reinforcement is requirement. The transversal reinforcement is composite by the simplest stirrups (with two arms) with a diameter of 10mm and considering the center to center distance between two consecutive stirrups equal to 80mm. The procedure for the evaluation of the shear

strength with the transversal reinforcement element is obtained by the *Italian Code CNR-DT 203/2006 chapter 4.8.2.2 Element with the transversal reinforcement resistant at the shear.* The design shear resistance v_{rd} of structural elements with specific shear reinforcement shall be assessed on the basis of the contribution given by the concrete section and the contribution given by the transversal shear reinforcement. The transversal shear reinforcement contribution is given by:

$$V_{Rd,f} = \frac{A_{fw} \cdot f_{fr} \cdot d}{s}$$

Eq 30

Where:

- A_{fw} is the area of the transversal reinforcement;
- s is the centre distance of the two consecutive transversal reinforcement (in this case only the stirrups have been used);
- f_{fr} is the reduced design resistance, definite by $f_{fd}/\gamma_{f,\varphi}$;
- $\gamma_{f,\varphi}$ is the partial coefficient, which further penalizes the value of the characteristic resistance to Bar pull to account for the effects of bending shall be attributed:
    1. a standard value of 2, free from the obligation to carry out specific experimental tests, provided that the radii of curvature are greater than or equal to six times the equivalent diameter of the bar, d_b;

2. a value equal to the ratio of the resistance of the straight and bent bars in all other cases.

- d = useful depth of the cross section expresses in [m].

The design shear strength of the beam is the lower of the two defined above:

$$V_{Rd} = min\{V_{Rd,ct} + V_{Rd,f}\ , V_{Rd,max}\}$$

Eq 31

Table 12: Shear strength with transversal reinforcement

Name beam	ρ[%]	A_{fw}	f_{fr}	d [mm]	s[mm]	$V_{Rd,ct}$[kN]
1	0.2	157	225	190	80	83.90
	0.4	157	225	190	80	83.90
	0.8	157	225	190	80	83.90
	1.6	157	225	190	80	83.90

Name beam	ρ[%]	V_{ed}[kN]	$V_{Rd,ct}$[kN]	Verify
1	0.2	18.73	88.94	VERO
	0.4	30.09	89.27	VERO
	0.8	42.32	89.92	VERO
	1.6	51.97	91.22	VERO

The Table 12 show the shear strength of the concrete beam with the transversal reinforcement.

The same process has been developed for the *Beam 2* and the results is summarize in the following tables. The first step was the shear verification for the beam without the transversal reinforcement. The results are summarized in the Table 13 and Table 14.

Table 13: Shear capacity

Name beam	ρ[%]	E_f[MPa]	E_s[MPa]	τ_{Rd}[MPa]	K	f_{ctd}[MPa]	b[mm]	d [mm]	σ_c[MPa]	$V_{Rd,ct}$[kN]
2	0.002066	67000	210000	0.72	1.24	2.90	400	360	30	12.18
	0.004132	67000	210000	0.72	1.24	2.90	400	360	30	12.96
	0.008263	67000	210000	0.72	1.24	2.90	400	360	30	14.53
	0.016526	67000	210000	0.72	1.24	2.90	400	360	30	17.67

Table 14: Shear verification

Name beam	ρ[%]	V_{ed}[kN]	$V_{Rd,ct}$[kN]	Verify
2	0.2	60.11	12.18	FALSO
	0.4	107.15	12.96	FALSO
	0.8	202.27	14.53	FALSO
	1.6	392.02	17.67	FALSO

For the second beam stock, the value of the shear action is larger than the value of the shear capacity. The shear design with the transversal reinforcement is needed. Even in this case, the stirrups typologies are the same of the stirrup's typologies for the *Beam 1* but with a center to center distance equal to 50mm. In the Table 15 are summarized the shear capacity of the beam.

Table 15: Shear strength with transversal reinforcement

Name beam	ρ[%]	A_{fw}	f_{fr}	d [mm]	s[mm]	$V_{Rd,ct}$[kN]
2	0.2	157	225	360	50	254.34
	0.4	157	225	360	50	254.34
	0.8	157	225	360	50	254.34
	1.6	157	225	360	50	254.34

Name beam	ρ[%]	V_{ed}[kN]	$V_{Rd,ct}$[kN]	Verify
2	0.2	60.11	266.52	VERO
	0.4	107.15	267.30	VERO
	0.8	202.27	268.87	VERO
	1.6	392.02	272.01	FALSO

Even though the stirrups present in the beam, for the last beam with the largest reinforcement percentage, the shear verification is not satisfied. Anyway, the beam has been left with this transversal reinforcement percentage because the test machine present in the laboratory do not allow to reach value of the vertical load P larger than 500 kN so the maximum vertical shear in the beam is less than $V_{ed} \leq 250\ kN$.

3.4.3: Step load

The test on the beam has been development in Four Point Bending test. The beams have reached the collapse considering a load cycles. The load cycles are characterized by two different steps:

1) First of all, the load is increased until the cracking load, after this point the load decrease until the value of 0;
2) Secondly, the load start to increase again until the ultimate load and collapse of the beam is reached.

The beams are notched in the middle in order to fix the position of the first crack. Notched the beams is important because, considering the FPBT, the length span between the two points load is characterized by only the bending moment. The position of the first crack located in the middle of the beam guarantee that the second consecutive crack is also located between the two points loads. In this way, it is possible to study stress exchange between concrete and GFRP bars in an area in which the shear tension does not exist and, for this reason, there are not interference of the shear effects on this phenomenon. Considering the distance between the two consecutive cracks, it is possible to evaluate the value of the average bond strength τ_{avg} considering the simple scheme:

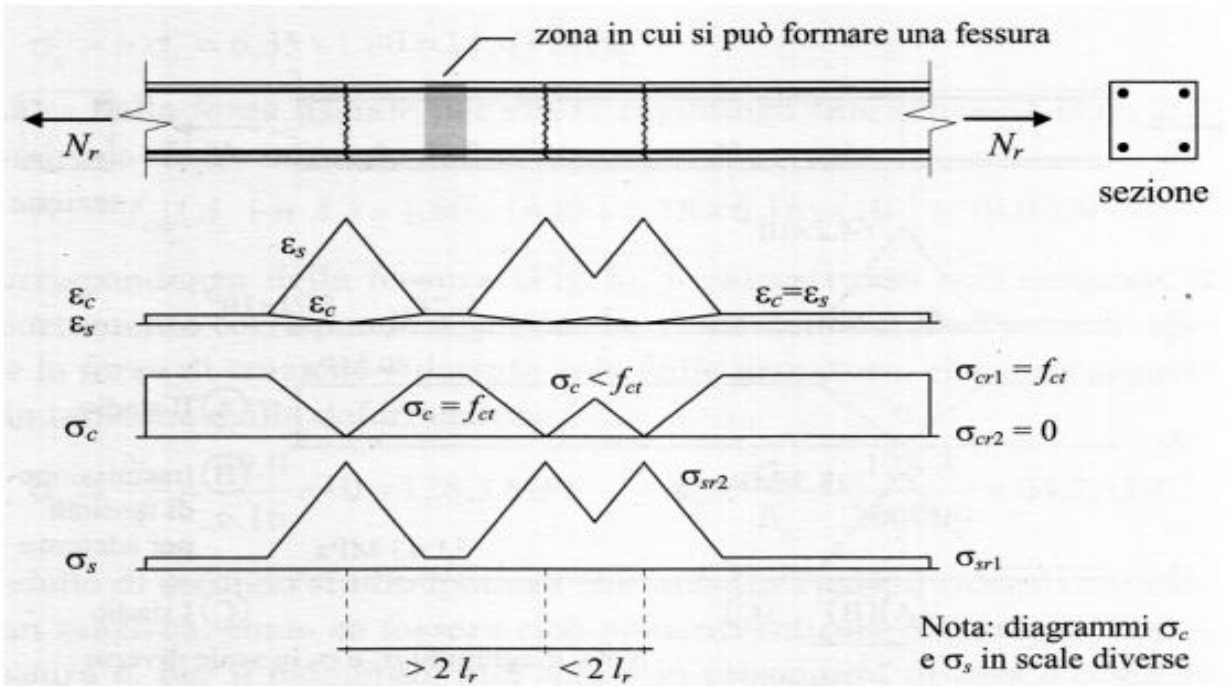

Figure 35: The average bond strength τ_{avg}

The Figure 36 show the tension exchange between the concrete and the bar. Starting with the strain values, in the crack the value of the stain in concrete is equal to 0 because there is no concrete in this section; consequently, the value of strain in the bar is the maximum possible. Considering now that, concrete in the tension field is characterized by the linear constitutive law in which the form of the strain is equal at the form of the tension but consider the Hook equation:

$$\sigma = E\,\varepsilon$$

Eq 32

For this reason, it is possible to conclude that the value of the tension in the concrete is equal to 0 in the crack.

Moreover, consider the strain in the GFRP bar in the crack, this is the maximum possible in this section and, consequently, the value of the tension is maximum. The path of the tension between two consecutive crack is linear and, for this reason, it is possible to write an equilibrium equation in order to obtain the value of the τ_{avg}:

$$\frac{\sigma_s \pi \varphi^2}{4} = \pi\, \varphi \cdot l_r \cdot \tau_{avg}$$

Eq 33

Where:

1) σ_s is the value of the tension in the GFRP bar;
2) φ is the diameter of the GFRP bar;
3) l_r is the distance between two consecutive cracks;
4) τ_{avg} is the average bond strength between concrete and GFRP bar.

Definitely, the value of the τ_{avg} is obtain through the following equation:

$$\tau_{avg} = \frac{\sigma_s \varphi}{4\, l_r}$$

Eq 34

Summarized the process, with the notched on the beam the position of the first crack is fixed, and it is reached on the first cycle load; with the second cycle load the consecutive crack is reached and it is possible to study the bond strength between the two materials.

Chapter 4:

Identification method with three parameters

The input in the Cohesive Overlapping model it is possible to summarize in a tern input in which the first two define the matrix characteristics and the last one defines the reinforced characteristic. The matrix parameters, following the fractural mechanics procedure, are the fractural energy parameters G_f and G_c. These two are enough to describe the entirely matrix characteristics because:

1) Inside the G_f there are the tensile strength and the maximum crack opening w_{ct};
2) Inside the G_c there are the compression strength and the maximum crack compenetration w_{cc}.

After the matrix descriptors, in order to define correctly the heterogeneous material as reinforced concrete, the GFRP parameters are needed. The GFRP parameters are composite by the elastic modulus E_G , the tensile strength σ_t and the bond strength. The elastic modulus and the tensile strength is given by the company that produce the bars, on the other hand, the value of the bond strength τ is the finally parameter that describe the reinforcement.

4.1: Inadequacy of existing tests

The matrix parameters are possible to hypothesize in certain range considering the experimental formulation presented in the chapter §2.4 Overlapping model. In particular:

1. The eq 16 define the value of G_f in function of σ_c;
2. The eq 17 define the value of G_c in function of k_b;

It is even possible to consider the §Table 3: Concrete stress and fractural energy and §Table 4: Concrete characteristics in order to define the first range for these parameters. Anyway, the range definition is not satisfied to define the input parameters. Obviously, there are different tests used to define them:

1. compressive test on a cylinder concrete for the σ_c;
2. three-point bending test for the G_f;
3. different experimental tests for the G_c;

The reinforced parameter that the input data required is the bond strength τ. The value of the bond strength as defined in the chapters §1.3: Bond test is difficult to define with the existing tests. The entirely stock of the existing tests are going to overestimate the value of the bond strength given in this way a wrong and dangerous input.

With the Cohesive Overlapping model all the previous parameters and all the previous tests are possible to summarize in just one test that in one shot give us the entirely parameters stock. This is possible considering a four-point bending test and considering an identification procedure for the parameters. Using the range presented in the Table 3: Concrete stress and fractural energy and Table 4: Concrete characteristics is possible to start the code and consequently the identification procedure.

4.2: Identification procedure

The identification procedure is based on the Four Point Bending Test (FPBT) results. Considering the force displacement graph that is possible to obtain by a FPBT as the follow:

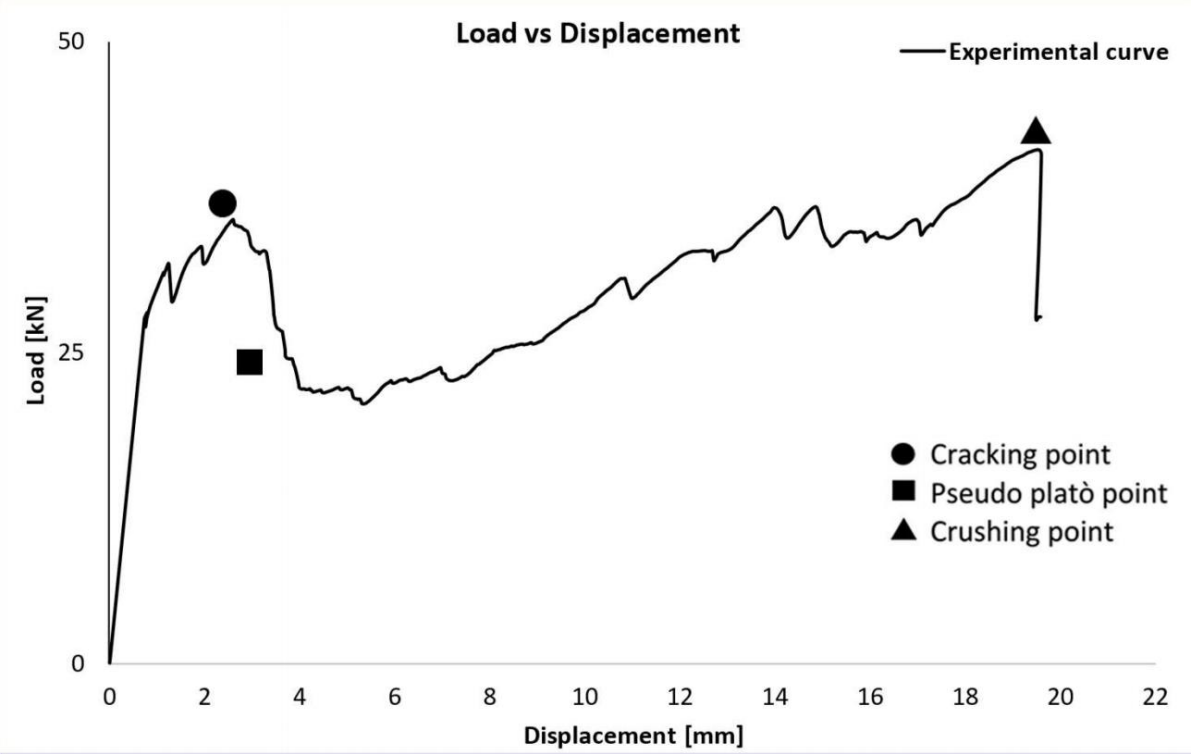

Graph 8: Four Point Bending Test result

This graph represents the load deflection variation for a GFRP reinforced concrete beam in a four-point bending test. In this graph is possible to identify 3 different point that represent the matrix and the reinforcement parameters expressed in the previous chapter. The first point named $Cracking\ point$ is the combination of *Load* and *Deflection* that represents the moment in which along the beam appears the first crack. This point is function by the fractur energy G_f that is

function by the tensile strength f_t and the maximum tensile crack opening w_{ct}. The identification procedure between the experimental and theoretical curves will be through the ordinate value of the cracking point. The second point named *Crushing point* is the combination of *Load* and *Deflection* that represents the moment in which the beam collapse. This point is function by the fractur energy G_c that is function by the tensile strength f_c and the maximum tensile crack opening w_{cc}. The identification procedure between the experimental and theoretical curves will be through the abscissa value of the crushing point.

The third point named *Pseudo plastic plateau* is the combination of *Load* and *Deflection* that represents the moment in which the GFRP reinforced bars start to have same slipping movement inside the concrete matrix. This point is function by the bond strength τ and, in a second way, by the tensile strength f_c. The identification procedure between the experimental and theoretical curves will be through the ordinate value of the pseudo plastic plateau point.

The realization of a theoretical curve, used to compared with the experimental, is managing in the follow steps:

1. considering a value of G_f and G_c given by the §Table 3: Concrete stress and fractural energy and §Table 4: Concrete characteristics to define the first approach;
2. considering the value of bond strength given by §Table 9: Bond value considering the minimum values;
3. run the cohesive overlapping model with these parameters and obtain a theoretical curve to be compared with the experimental curve;

The results of this first procedure give a couple of curves that are not comparable to each other. This means that an identification procedure is needed because the input data are not close enough to real.

The identification procedure of the tern parameters is managing in the follow steps:

1. considering the $Cracking\ point$, the cracking point in the experimental curve and the cracking point of the theoretical curve has to be in reached at the same value of *Load.* This point is influenced by G_f and for this reason, chancing the value of the fractural energy is possible to fix the correlation between the points as shown in the follow graph:

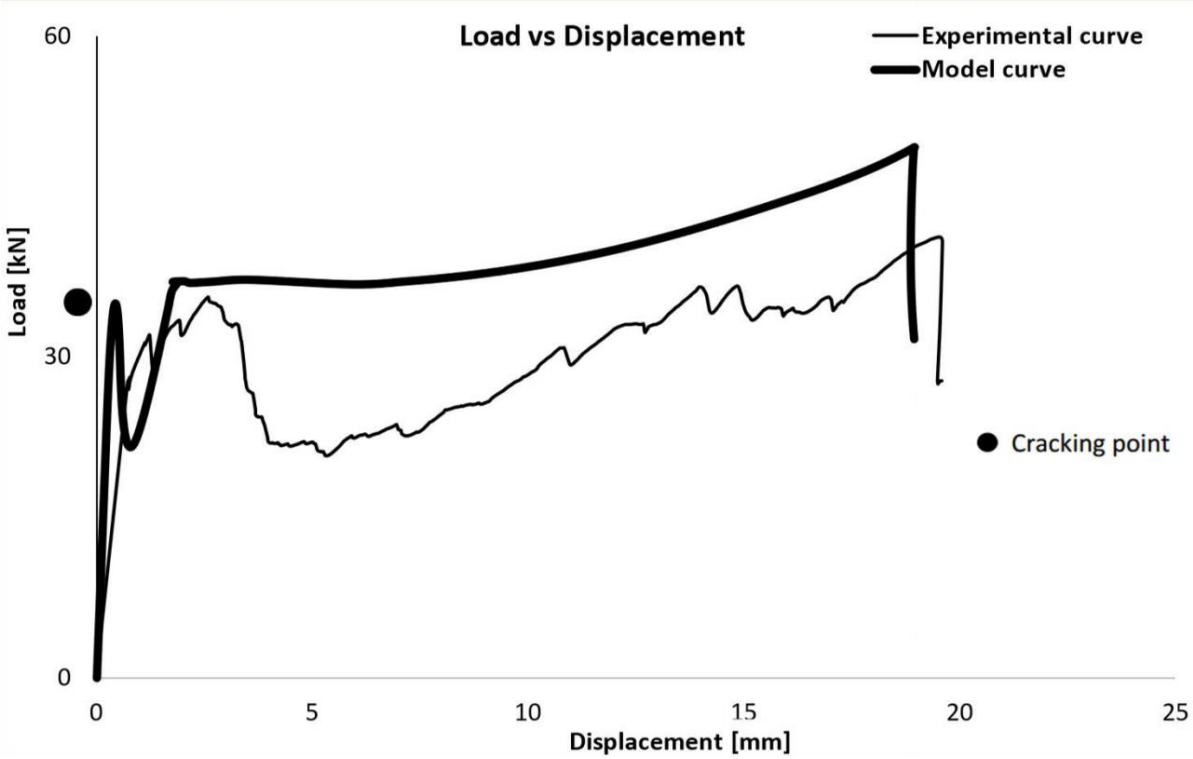

Graph 9: Cracking point identification

2. Considering the *Crushing point,* the crushing point in the experimental curve and the crushing point of the theoretical curve has to be in reached at the same value of *Deflection.* This point is influenced by G_c and for this reason, chancing the value of the fractural energy is possible to fix the correlation between the points as shown in the follow graph:

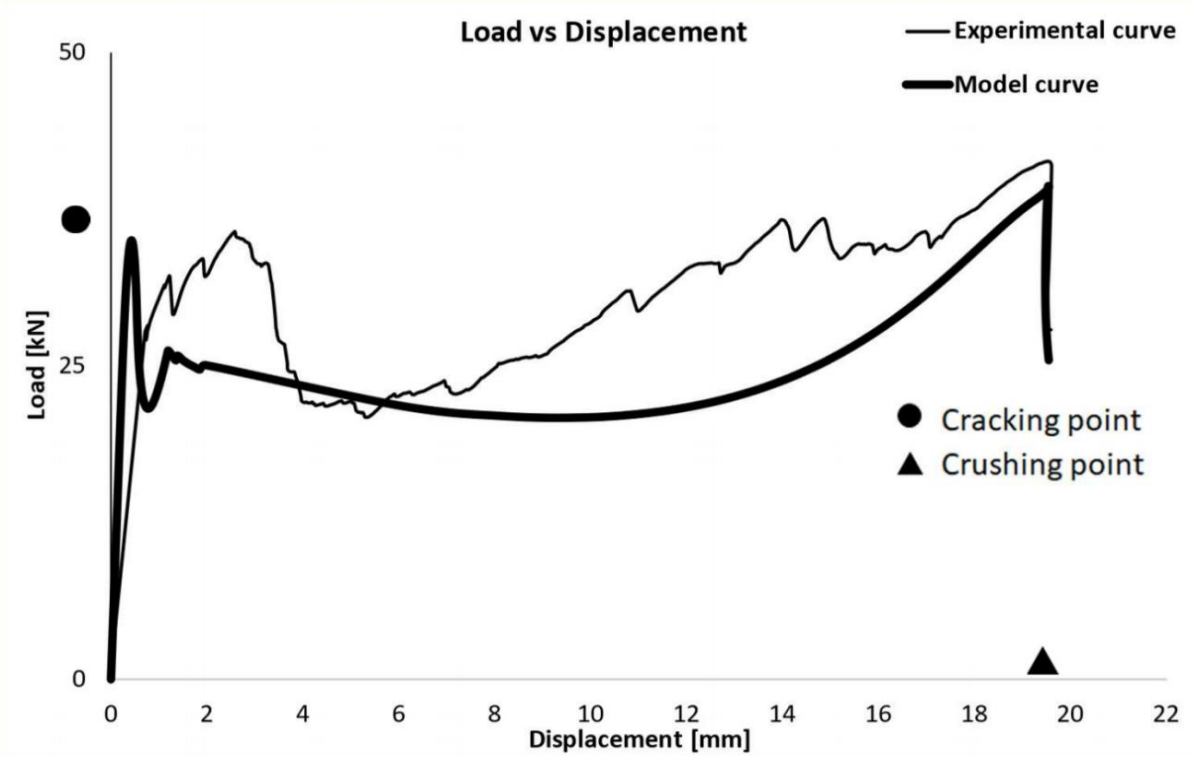

Graph 10: crushing point identification

3. Considering the *Pseudo plastic plateau point,* the pseudo plastic plateau in the experimental curve and the pseudo plastic plateau of the theoretical curve has to be started at the same value of *Load.* This point is influenced by the bond strength τ and for this reason, chancing the value of the bond strength is possible to fix the correlation between the points as shown in the follow graph:

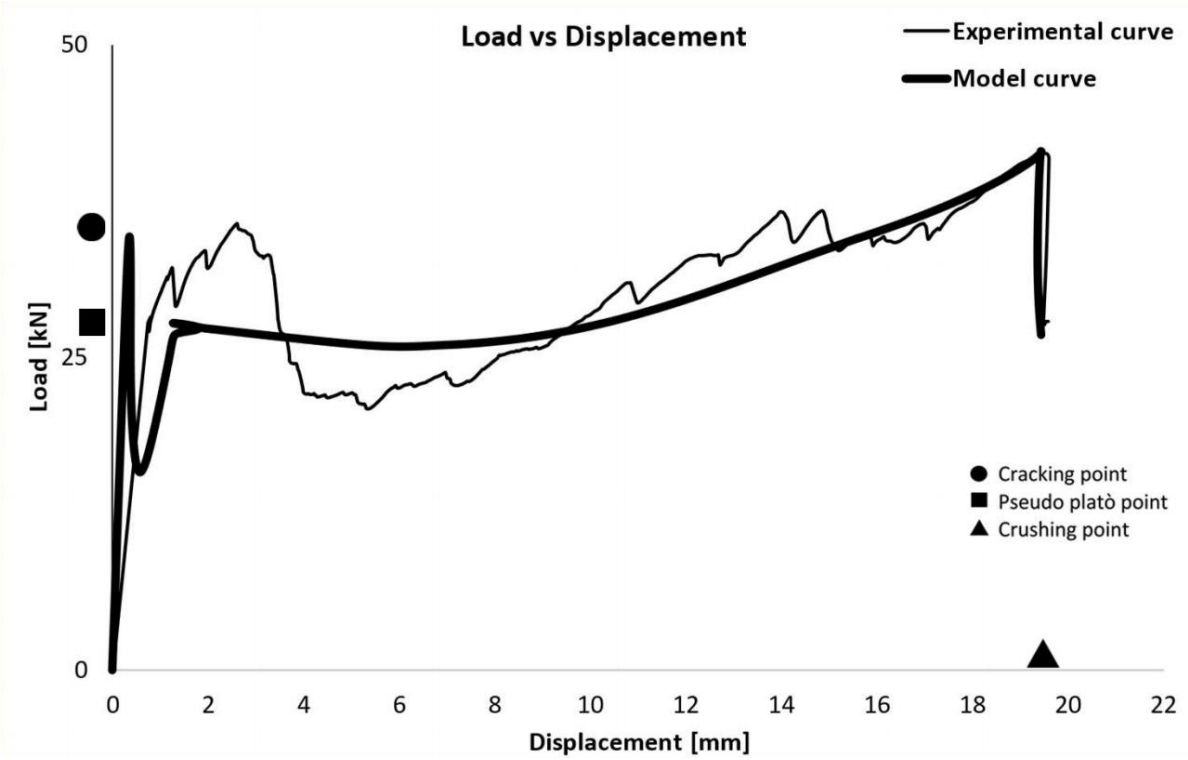

Graph 11: pseudo plateau point identification.

After the different steps is possible to see a global movement of the curve. After the identification procedure the experimental and theoretical curve is comparable.

4.3: The worth of an innovative approach

This innovative approach shows how is possible to obtain an identification of three parameters just considering a single test and the Cohesive Overlapping model. The gain of this approach is to avoid the million and million pull-out tests that any day is done in the laboratory of the world. The pull-out test is a very old and obsolete test that supposes to show a value of bond but, thankful at the intrinsic limitation, gives a value of the bond completely overestimated and useless. Moreover,

the test used to obtain the value of the G_f is the Three Point Bending Test (TPBT) is useless too. The TPBT, for the test set-up, is an obsolete test because the value of the factorial energy parameter is highly influenced by the shear effects in the bending zone. Finally, there is no test validation to the G_c that is an important parameter in the fractural mechanic's approach. All these problems are possible to solve in one shot, with one test and reducing the cost and the time needed to arrive at the results. The Cohesive Overlapping model unit with the FPBT give a new and fully advanced road to obtain in the smartest, most practical, and correct way the fundamental parameters necessary in a reinforced GFRP concrete beam.

Chapter 5:

Experimental results

The following graphs will be used to show the test results and the identification procedure for each beam. There will be 4 different group identification divided for scale and bond strength expressed by the GFRP reinforcement bars. After each single group identification, a statistics analysis will be performed, and the graphs will be run considering the mean parameters. The aim of this procedure is to obtain a mean parameter representing the concrete matrix characteristic and the GFRP bar characteristic.

5.1: The first scale: h = 0.2 m

The scale h = 0.2m is divided into two different subgroups that represent the smooth bar and the rough bar. This distinction is fundamental because the value of the bond strength between the two different bars is not comparable and, for this reason, a different τ identification is needed.

5.1.1: Identification procedure beam H = 20cm smooth bar

The beam H =20 cm with GFRP smooth bar and a geometric reinforcement percentage equal to ρ=0,4%.

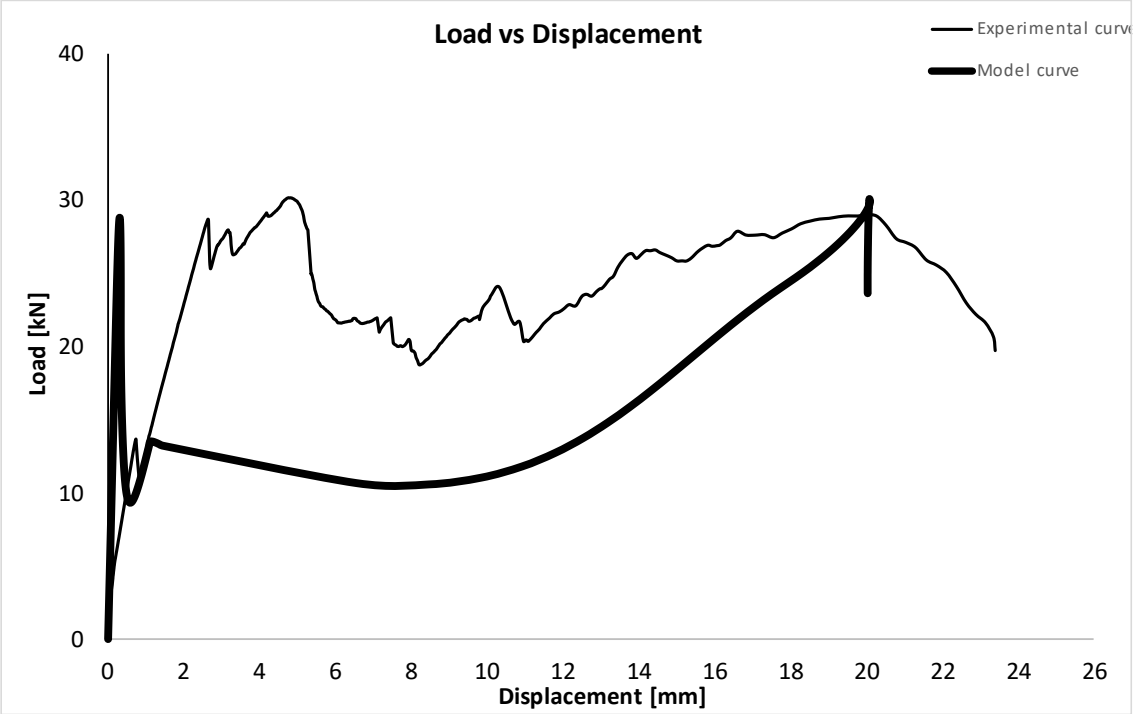

Graph 12: cracking identification.

Table 16: Parameters

Beam name			**Ec**	**21000**	**MPa**
h	**0.2**	**[m]**	**Wcc**	**3.00**	**mm**
N. Bars	**1**	**[N]**	**Wct**	**0.1**	**mm**
Φ	**12**	**[mm]**	**Gc**	**67.5**	**N/mm**
σ_c	**45**	**MPa**	**Gf**	**0.15**	**N/mm**
σ_t	**3.00**	**MPa**	**t**	**1.1**	**MPa**

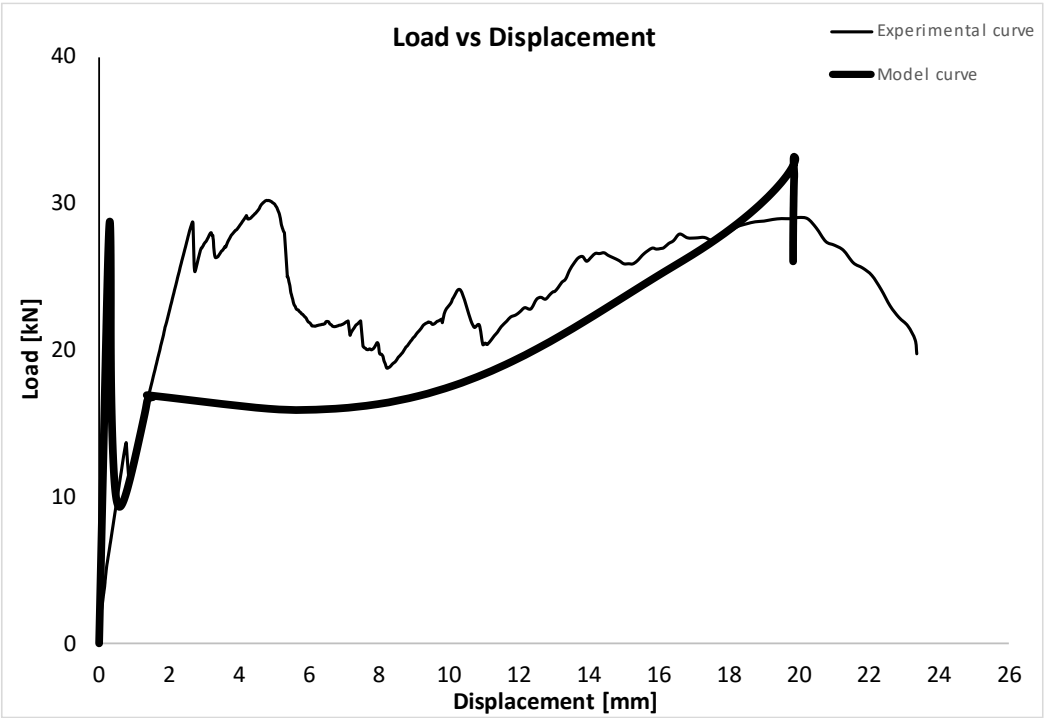

Graph 13: crushing identification.

Table 17: parameters

Beam name			**Ec**	**21000**	**MPa**
h	**0.2**	**[m]**	**Wcc**	**3**	**mm**
N. Bars	**1**	**[N]**	**Wct**	**0.1**	**mm**
Φ	**12**	**[mm]**	**Gc**	**67.5**	**N/mm**
σc	**45**	**MPa**	**Gf**	**0.15**	**N/mm**
σt	**3**	**MPa**	**t**	**1.2**	**MPa**

The graph 13 shows a high correlation between the experimental curve and the theoretical curve. The three most important points that describe the 3 most important moments during a beam test are perfectly obtained. These points are represented by the cracking moment, the crushing moment, and the starting of the slippage phase during a beam test. The Cohesive Overlapping model not only express a significant correlation among these points, but also the structure of the branches are highly comparable giving us an important result.

The beam H =20 cm with GFRP smooth bar and a geometric reinforcement percentage equal to ρ=0,8%.

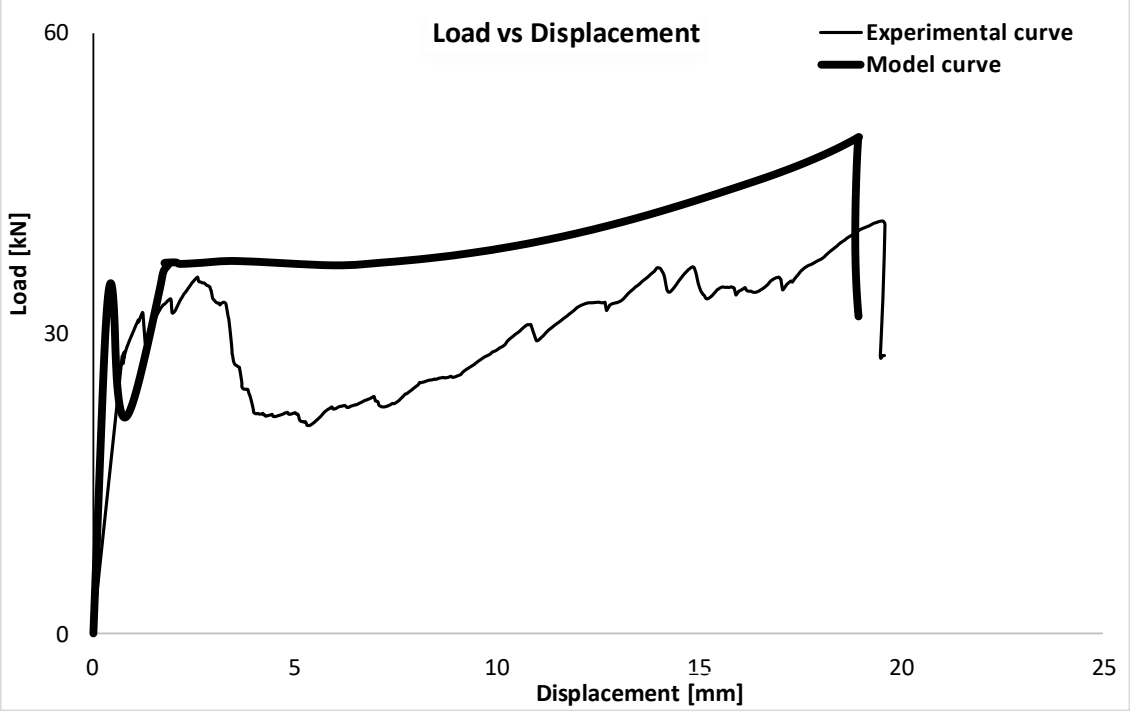

Graph 14: cracking identification.

Table 18: Parameters

Beam name			Ec	21000	MPa
h	0.2	[m]	Wcc	3.00	mm
N. Bars	2	[N]	Wct	0.1	mm
Φ	12	[mm]	Gc	60	N/mm
σ_c	40	MPa	Gf	0.1575	N/mm
σ_t	3.15	MPa	t	1.5	MPa

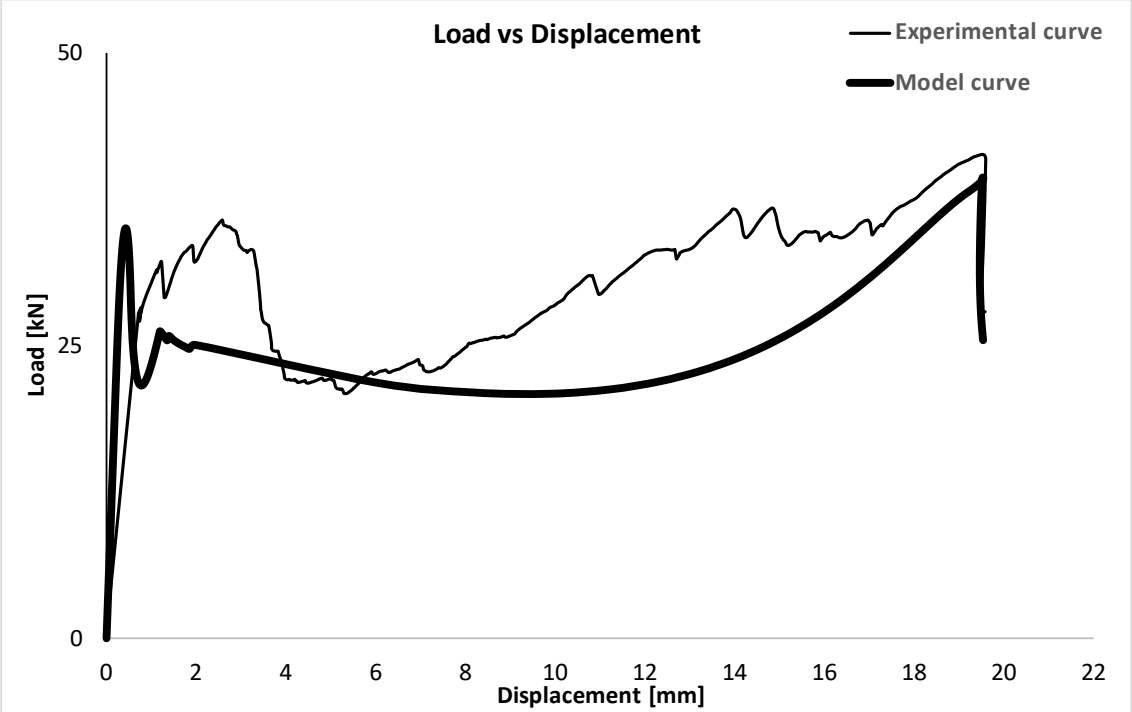

Graph 15: crushing identification.

Table 19: parameters

Beam name			**Ec**	**21000**	**MPa**
h	**0.2**	**[m]**	**Wcc**	**3**	**mm**
N. Bars	**2**	**[N]**	**Wct**	**0.1**	**mm**
Φ	**12**	**[mm]**	**Gc**	**67.5**	**N/mm**
σ_c	**45**	**MPa**	**Gf**	**0.158**	**N/mm**
σ_t	**3.15**	**MPa**	**t**	**1**	**MPa**

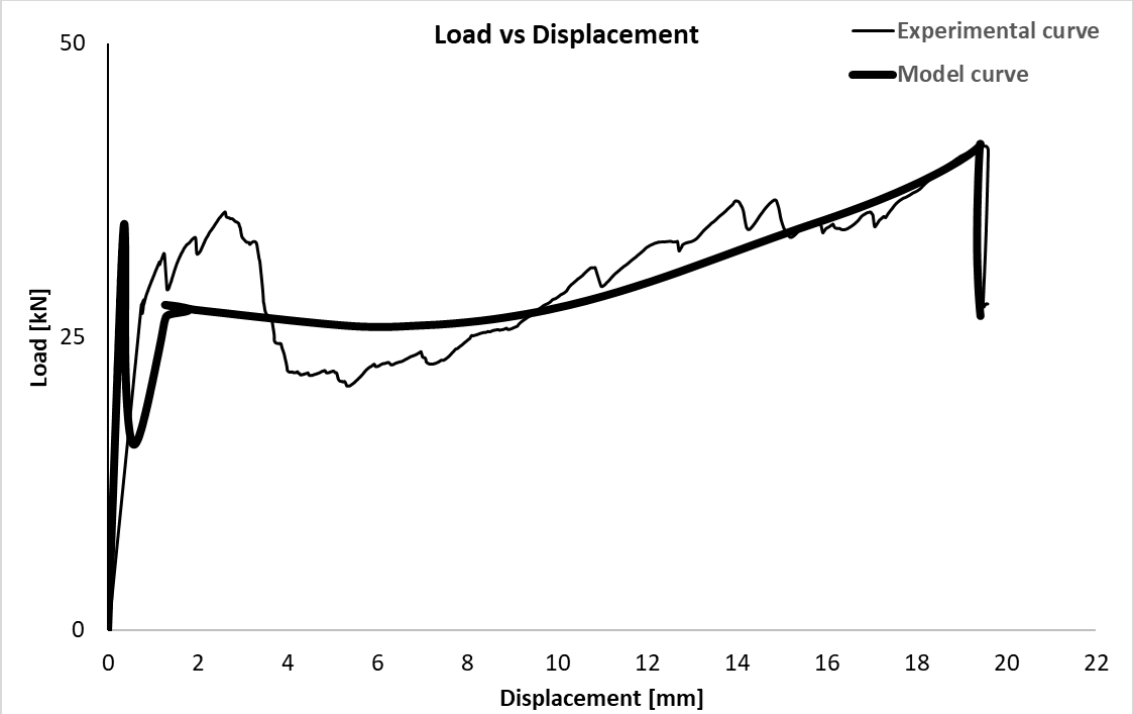

Graph 16: pseudo plastic plateau identification.

Table 20: parameters

Beam name			Ec	21000	MPa
h	0.2	[m]	Wcc	3	mm
N. Bars	2	[N]	Wct	0.1	mm
Φ	12	[mm]	Gc	67.5	N/mm
σc	45	MPa	Gf	0.175	N/mm
σt	3.5	MPa	t	1.1	MPa

The graph 16 shows a high correlation between the experimental curve and the theoretical curve. In this case the identification procedure is composite by 2 different steps. This happen because the input parameters, used to this curve, are the parameters that take into account the previous identification procedure, just two small variation is needed to match the experimental and theoretical curves again. Also in this case, the three most important points that describe the 3 most important moments during a beam test are perfectly obtained. The Cohesive Overlapping model not only express a significant correlation among these points, but also the structure of the branches are highly comparable giving us an important result.

The beam H =20 cm with GFRP smooth bar and a geometric reinforcement percentage equal to ρ=1.6%.

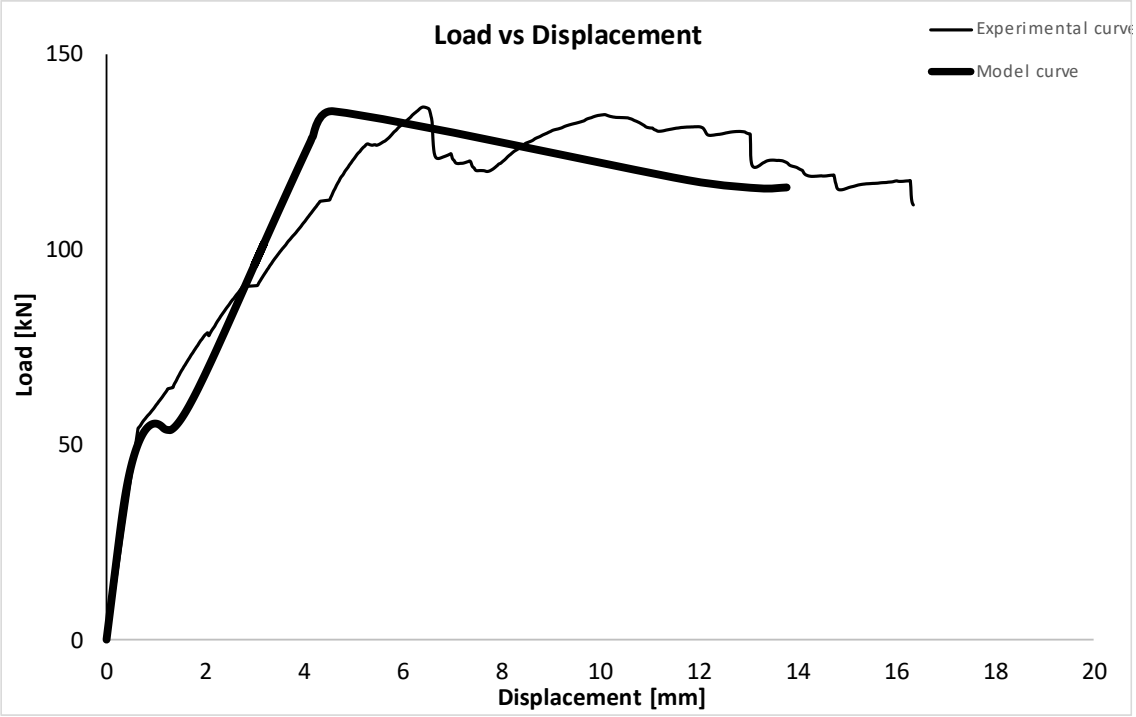

Graph 17: cracking identification.

Table 21: Parameters

Beam name			**Ec**	**21000**	**MPa**
h	**0.2**	**[m]**	**Wcc**	**3.00**	**mm**
N. Bars	**4**	**[N]**	**Wct**	**0.12**	**mm**
Φ	**12**	**[mm]**	**Gc**	**60**	**N/mm**
σ_c	**40**	**MPa**	**Gf**	**0.129**	**N/mm**
σ_t	**2.15**	**MPa**	**t**	**2.85**	**MPa**

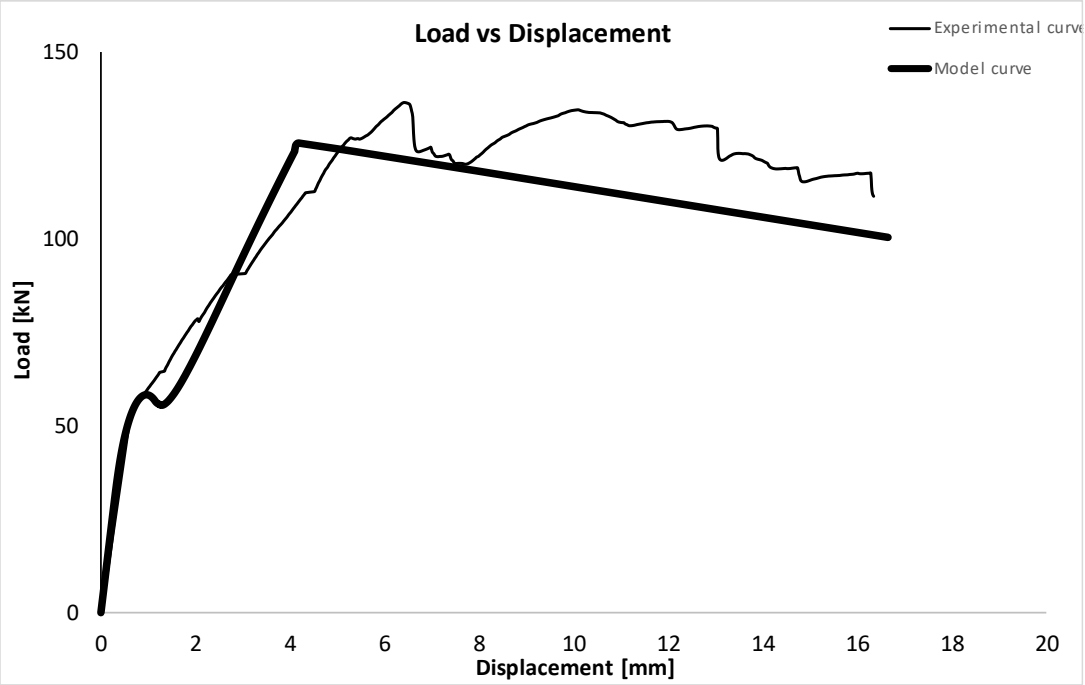

Graph 18: crushing identification.

Table 22: parameters

Beam name			**Ec**	**21000**	**MPa**
h	**0.2**	**[m]**	**Wcc**	**4.5**	**mm**
N. Bars	**4**	**[N]**	**Wct**	**0.12**	**mm**
Φ	**12**	**[mm]**	**Gc**	**90**	**N/mm**
σ_c	**40**	**MPa**	**Gf**	**0.129**	**N/mm**
σ_t	**2.15**	**MPa**	**t**	**2.85**	**MPa**

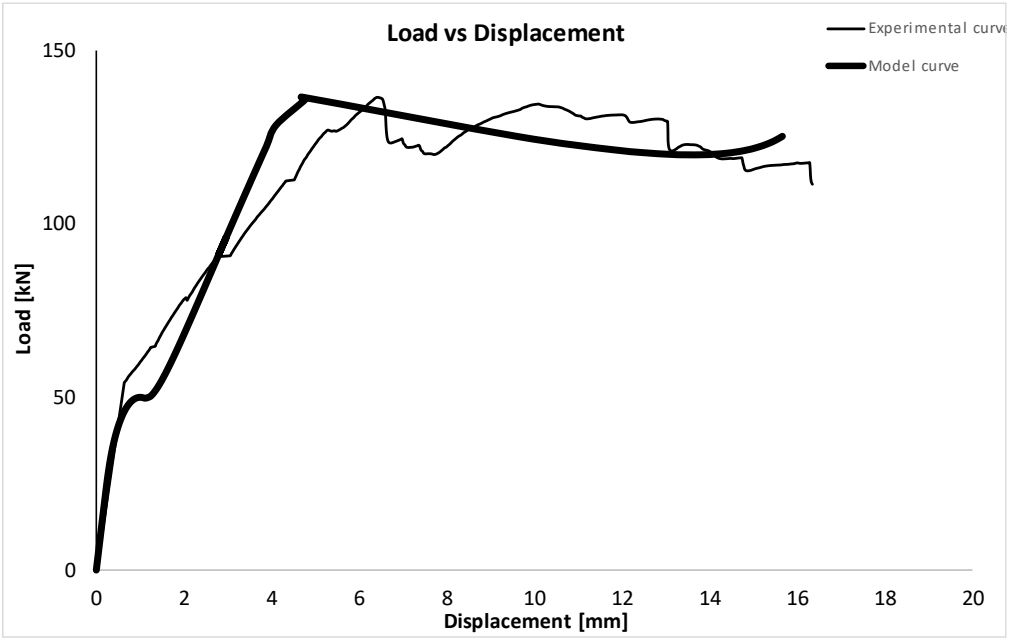

Graph 19: pseudo plastic plateau identification.

Table 23: parameters

Beam name			**Ec**	**21000**	**MPa**
h	**0.2**	**[m]**	**Wcc**	**4.5**	**mm**
N. Bars	**4**	**[N]**	**Wct**	**0.12**	**mm**
Φ	**12**	**[mm]**	**Gc**	**90**	**N/mm^2**
σ_c	**40**	**MPa**	**Gf**	**0.129**	**N/mm^2**
σ_t	**2.15**	**MPa**	**t**	**1.9**	**MPa**

The graph 19 shows a high correlation between the experimental curve and the theoretical curve. The three most important points that describe the 3 most important moments during a beam test are perfectly obtained. These points are represented by the cracking moment, the crushing moment,

and the starting of the slippage phase during a beam test. The Cohesive Overlapping model not only express a significant correlation among these points, but also the structure of the branches are highly comparable giving us an important result.

A statical analysis is performed for this first group of concrete beams the *beam H =20 cm smooth bar group*. The statical analysis consist of evaluation the mean value of the three parameters identifies and considering the range variation of $\pm 20\%$ of the mean value.

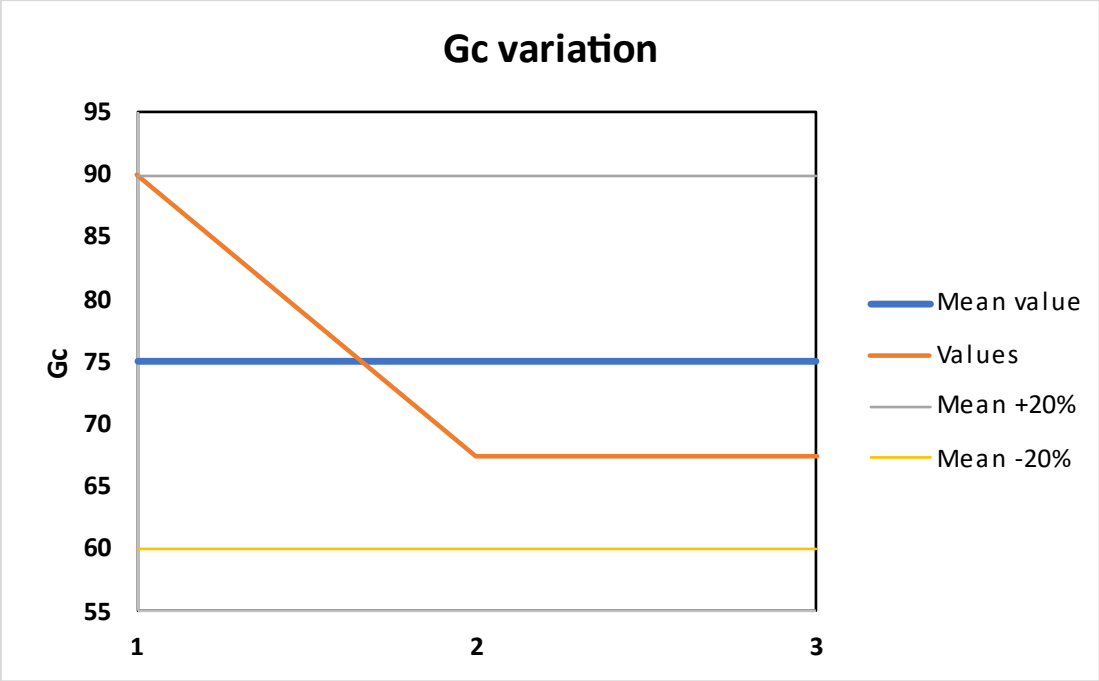

Graph 20: Gc variation.

The G_c values are in the between the minimum and maximum value of showing by the graph 20.

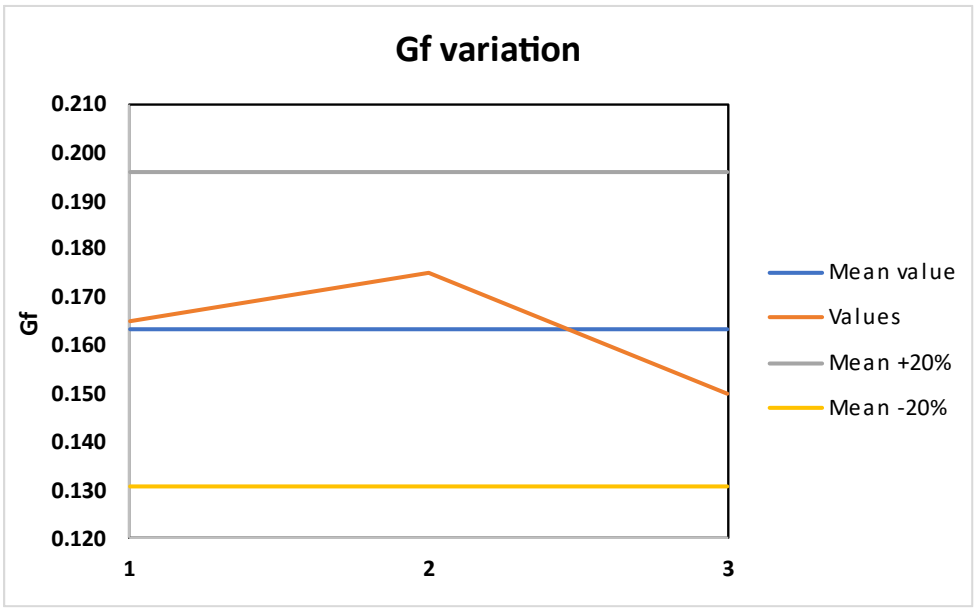

Graph 21: Gf variation.

The G_f values are in the between the minimum and maximum value of showing by the graph 21.

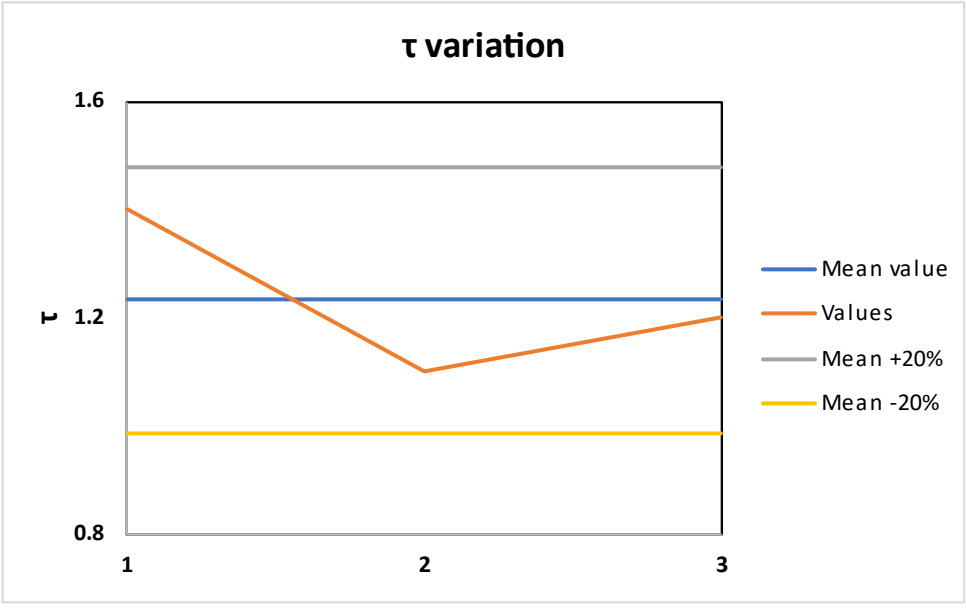

Graph 22: t variation.

The τ values are in the between the minimum and maximum value of showing by the graph 22 except than the first value that is in the range of 23%.

The table 24 shows the mean parameters and in the table 25 is possible to see the value of the variation among them.

Table 24: Mean parameters

Beam H=20cm smooth bar	
Parameters	**Mean**
Gc	**75.00**
Gf	**0.16**
t	**1.23**

Table 25: Parameters variation

Variation			
Beam	**1**	**2**	**3**
Gc	**120.00**	**90.00**	**90.00**
Gf	**101.02**	**107.14**	**91.84**
τ	**113.51**	**89.19**	**97.30**

The variation is in a small range and that express the power of the identification given by the cohesive overlapping model.

The *beam H =20 cm smooth bar group* graphs considering the mean parameter obtained by the identification procedure are shown in the following graphs.

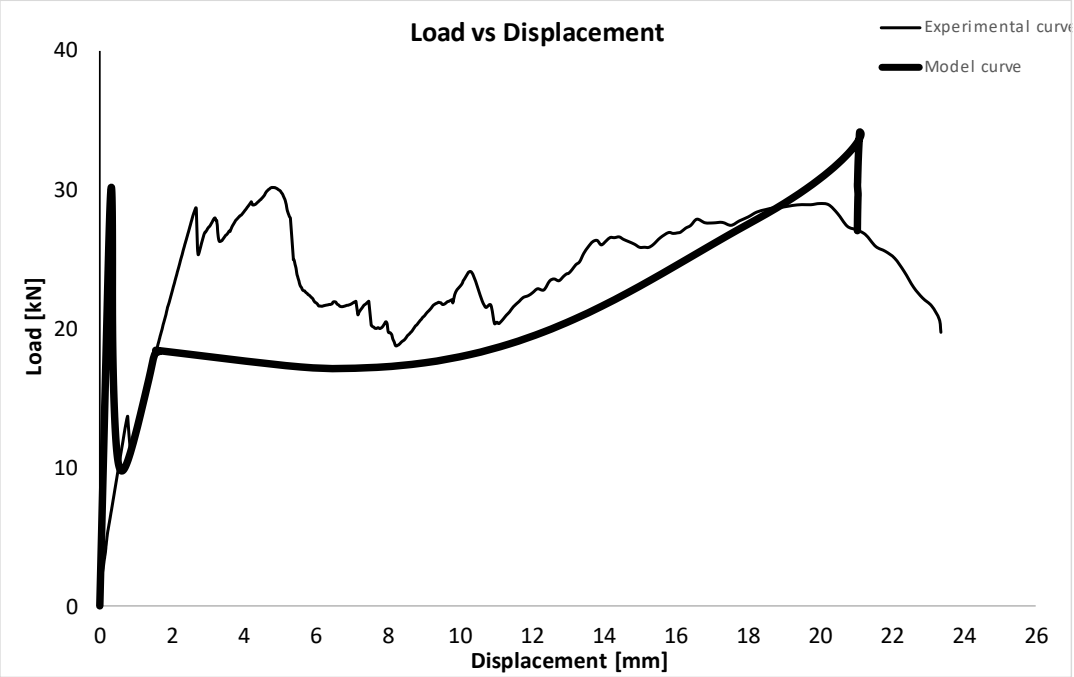
Load vs Displacement
Experimental curve
Model curve
Load [kN]
Displacement [mm]
0
10
20
30
40
0
2
4
6
8
10
12
14
16
18
20
22
24
26

Graph 23: ρ=0,4%.

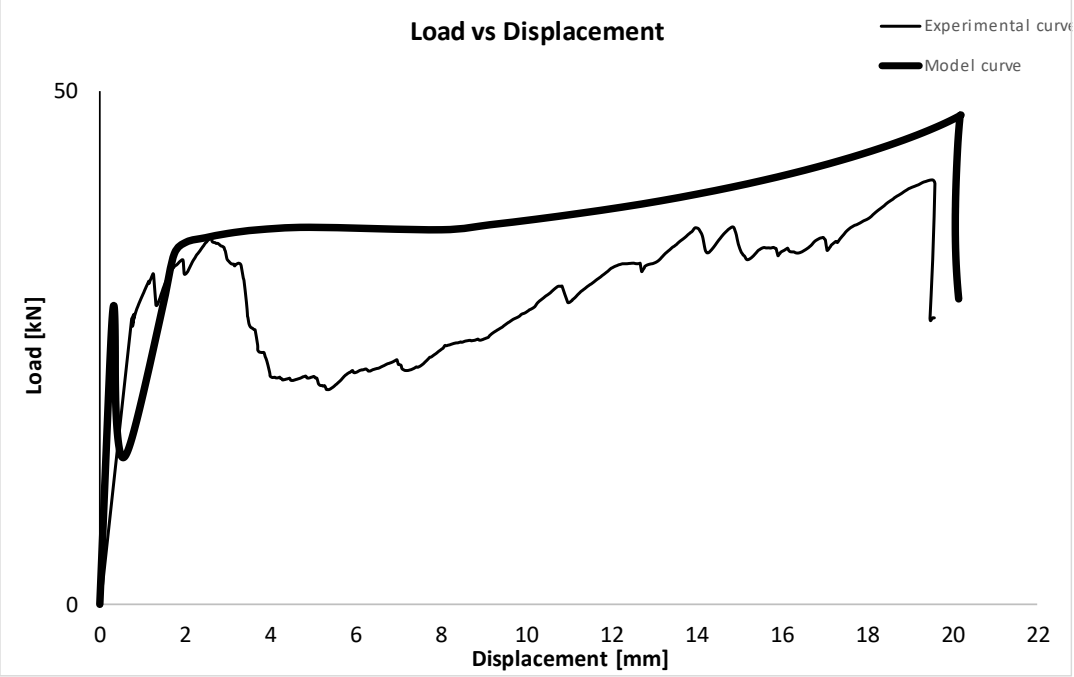
Load vs Displacement
Experimental curve
Model curve
Load [kN]
Displacement [mm]
0
50
0
2
4
6
8
10
12
14
16
18
20
22

Graph 24: ρ=0,8%.

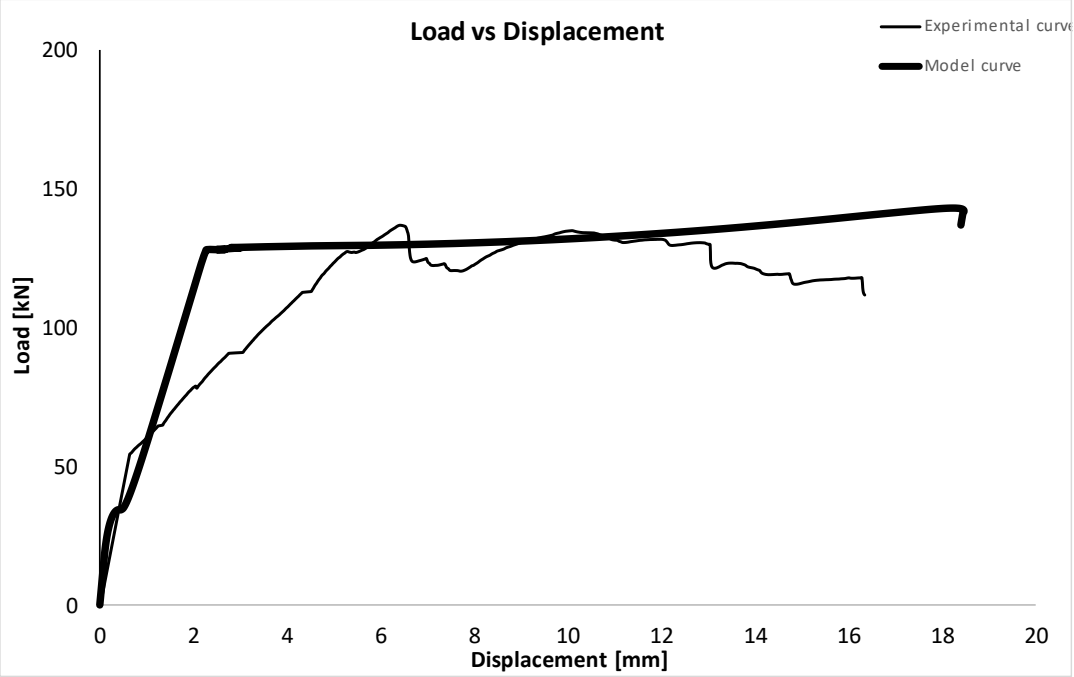

Graph 25: ρ=1,6%.

The using of the mean parameters for the group beam modifies the curves. The perfect correlation among the three most important points is not guaranteed, anyway, a good approximation in the range of $\pm 20\%$ is obtained. The theoretical curves shape is remaining highly comparable. The using of the mean parameters has an incredible power because through the using of them it is possible to estimate the missing data in an experimental campaign. Moreover, in the present thesis, the mean parameters are using in order to prove the power of the identification given by the cohesive overlapping model. The power of this procedure allows to identify the matrix material and reinforcement material of any experimental campaign even without any preliminary dates on the matrix material and reinforcement material. This method deletes the necessity to do the pull-

out test, the TPBT and the entirely different tests before analyzing the data results. The other tests through this procedure are not mandatory but they are just a starting point and for this reason, there is no benefit in making high number of them.

5.1.2: Brittle-ductile transition for the beam H =20 cm smooth bar group

The previous graphs show how the ductility of the beam is going to reduce considering an increasing of ρ. Having the same beam geometry and the same bond strength for each beam the only factor that change is the ρ value and for this reason it is possible to define that the ductility of the beam is inversely proportional with the increasing to the ρ percentage.

5.1.3: Identification procedure beam H = 20cm rough bar

The beam H =20 cm with GFRP rough bar and a geometric reinforcement percentage equal to ρ=0,4%.

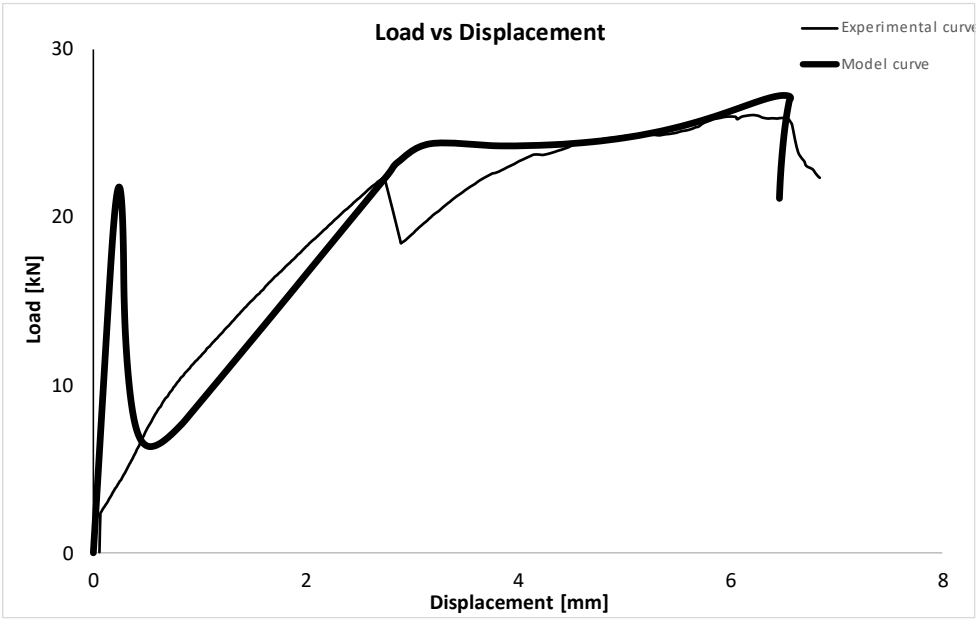

Graph 26: identification graph.

Table 26: Parameters

Beam name			**Ec**	**21000**	**MPa**
h	**0.2**	**[m]**	**Wcc**	**1.80**	**mm**
N. Bars	**1**	**[N]**	**Wct**	**0.1**	**mm**
Φ	**10**	**[mm]**	**Gc**	**36**	**N/mm²**
σ_c	**40**	**MPa**	**Gf**	**0.1075**	**N/mm²**
σ_t	**2.15**	**MPa**	**t**	**2.5**	**MPa**

The graph 26 shows a high correlation between the experimental curve and the theoretical curve. The three most important points that describe the 3 most important moments during a beam test are perfectly obtained. These points are represented by the cracking moment, the crushing moment, and the starting of the slippage phase during a beam test. The Cohesive Overlapping model not only express a significant correlation among these points, but also the structure of the branches are highly comparable giving us an important result.

The beam H =20 cm with GFRP rough bar and a geometric reinforcement percentage equal to ρ=0,8%.

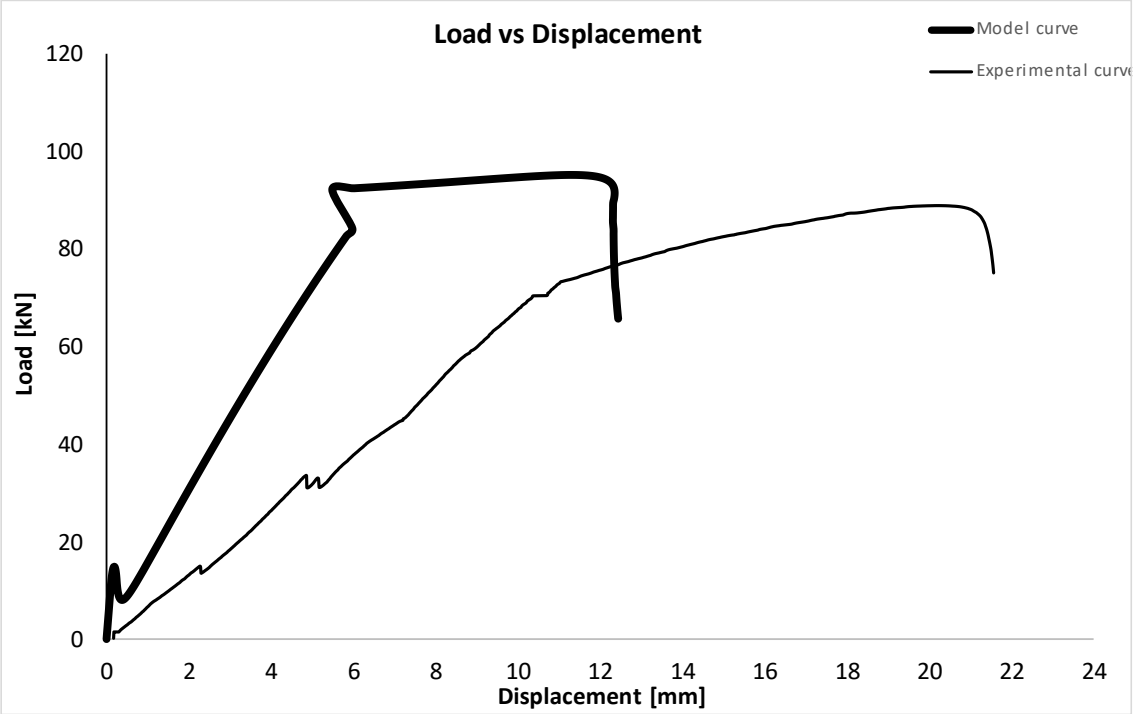

Graph 27: cracking identification.

Table 27: Parameters

Beam name			**Ec**	**21000**	**MPa**
h	**0.2**	**[m]**	**Wcc**	**3.00**	**mm**
N. Bars	**2**	**[N]**	**Wct**	**0.1**	**mm**
Φ	**10**	**[mm]**	**Gc**	**45**	**N/mm**
σ_c	**30**	**MPa**	**Gf**	**0.115**	**N/mm**
σ_t	**2.30**	**MPa**	**t**	**4.5**	**MPa**

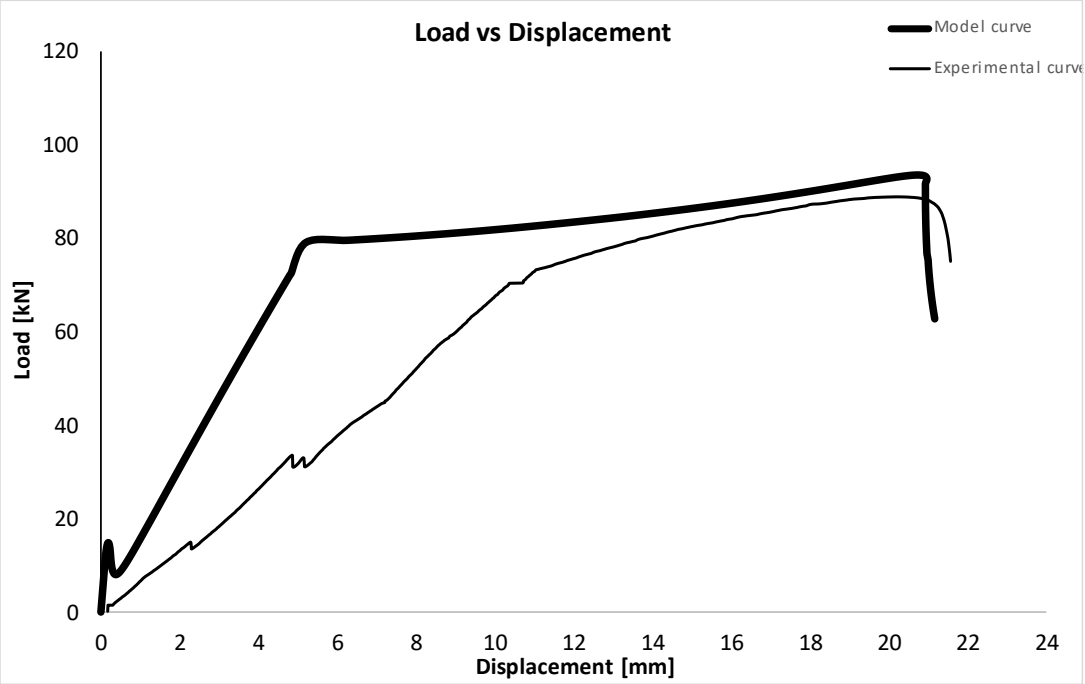

Graph 28: crushing identification.

Table 28: parameters

Beam name			**Ec**	**21000**	**MPa**
h	**0.2**	**[m]**	**Wcc**	**2.30**	**mm**
N. Bars	**2**	**[N]**	**Wct**	**0.1**	**mm**
Φ	**10**	**[mm]**	**Gc**	**46**	**N/mm**
σ_c	**40**	**MPa**	**Gf**	**0.115**	**N/mm**
σ_t	**2.30**	**MPa**	**t**	**3.8**	**MPa**

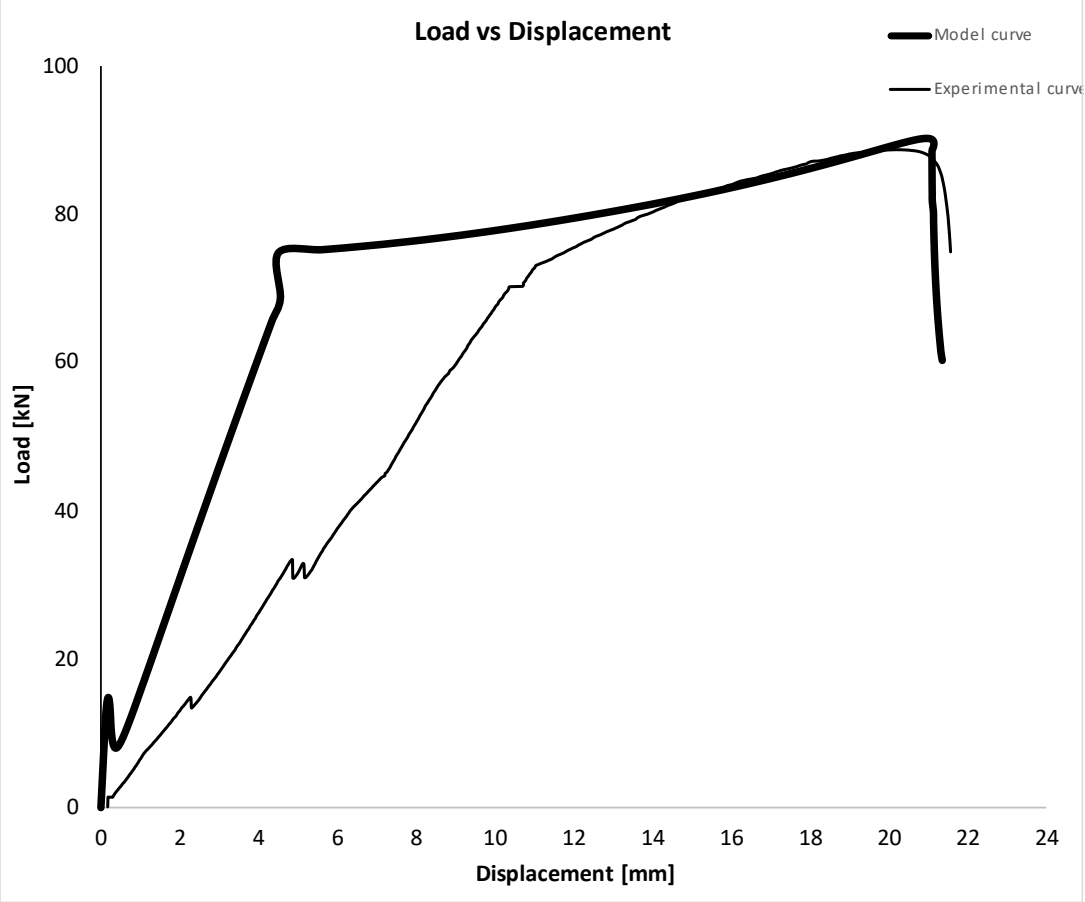

Graph 29: pseudo plastic plateau identification.

Table 29: parameters

Beam name			**Ec**	**21000**	**MPa**
h	**0.2**	**[m]**	**Wcc**	**2.3**	**mm**
N. Bars	**2**	**[N]**	**Wct**	**0.1**	**mm**
Φ	**10**	**[mm]**	**Gc**	**46**	**N/mm^2**
σ_c	**40**	**MPa**	**Gf**	**0.115**	**N/mm^2**
σ_t	**2.3**	**MPa**	**t**	**3.6**	**MPa**

The graph 29 shows a high correlation between the experimental curve Also in this case, the three most important points that describe the 3 most important moments during a beam test are perfectly obtained. The Cohesive Overlapping model not only express a significant correlation among these points, but also the structure of the branches is highly comparable giving us an important result. The beam H =20 cm with GFRP rough bar and a geometric reinforcement percentage equal to ρ=1.6%.

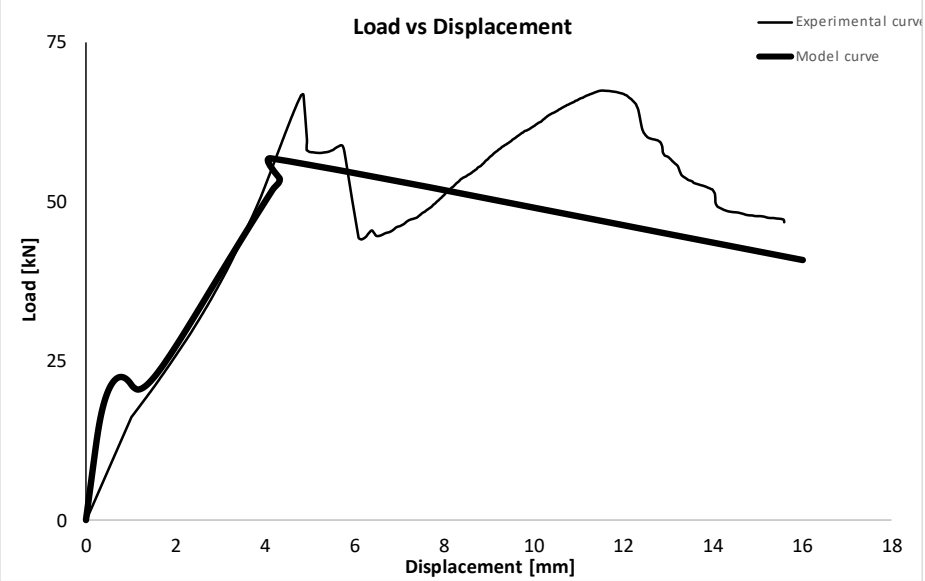

Graph 30: cracking identification.

Table 30: Parameters

Beam name			**Ec**	**21000**	**MPa**
h	**0.2**	**[m]**	**Wcc**	**3.00**	**mm**
N. Bars	**4**	**[N]**	**Wct**	**0.15**	**mm**

Φ	**10**	**[mm]**	**Gc**	**60**	**N/mm**
σ_c	**40**	**MPa**	**Gf**	**0.165**	**N/mm**
σ_t	**2.20**	**MPa**	**t**	**2.85**	**MPa**

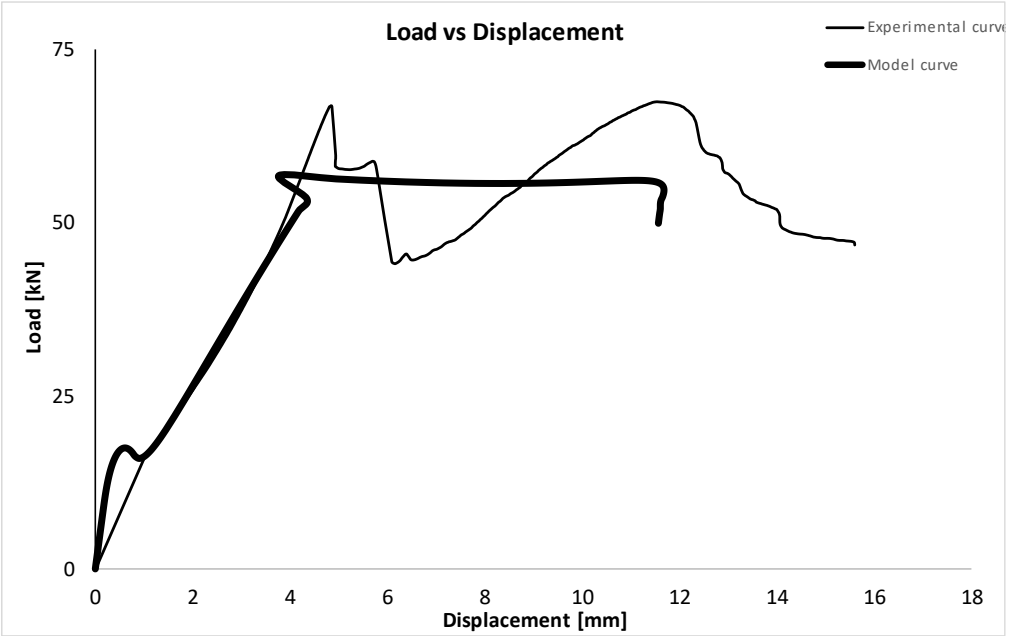

Graph 31: crushing identification.

Table 31: parameters

Beam name			**Ec**	**21000**	**MPa**
h	**0.2**	**[m]**	**Wcc**	**3**	**mm**
N. Bars	**4**	**[N]**	**Wct**	**0.35**	**mm**
Φ	**10**	**[mm]**	**Gc**	**60**	**N/mm**
σ_c	**40**	**MPa**	**Gf**	**0.42**	**N/mm**
σ_t	**2.4**	**MPa**	**t**	**2.85**	**MPa**

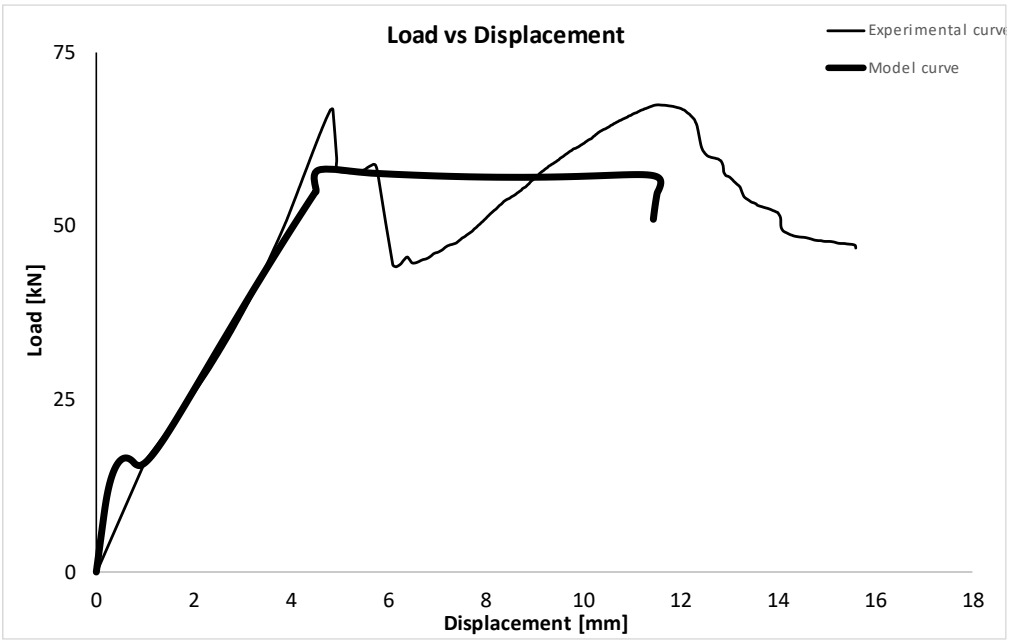

Graph 32: pseudo plastic plateau identification.

Table 32: parameters

Beam name			**Ec**	**21000**	**MPa**
h	**0.2**	**[m]**	**Wcc**	**2.00**	**mm**
N. Bars	**4**	**[N]**	**Wct**	**0.15**	**mm**
Φ	**10**	**[mm]**	**Gc**	**37**	**N/mm**
σ_c	**37**	**MPa**	**Gf**	**0.165**	**N/mm**
σ_t	**2.2**	**MPa**	**τ**	**2.85**	**MPa**

The graph 32 shows a high correlation between the experimental curve and the theoretical curve. The three most important points that describe the 3 most important moments during a beam test are perfectly obtained. These points are represented by the cracking moment, the crushing moment,

and the starting of the slippage phase during a beam test. The Cohesive Overlapping model not only express a significant correlation among these points, but also the structure of the branches are highly comparable giving us an important result.

A statical analysis is performed for this first group of concrete beams the *beam H =20 cm rough bar group*. The statical analysis consist of evaluation the mean value of the three parameters identifies and considering the range variation of $\pm 20\%$ of the mean value.

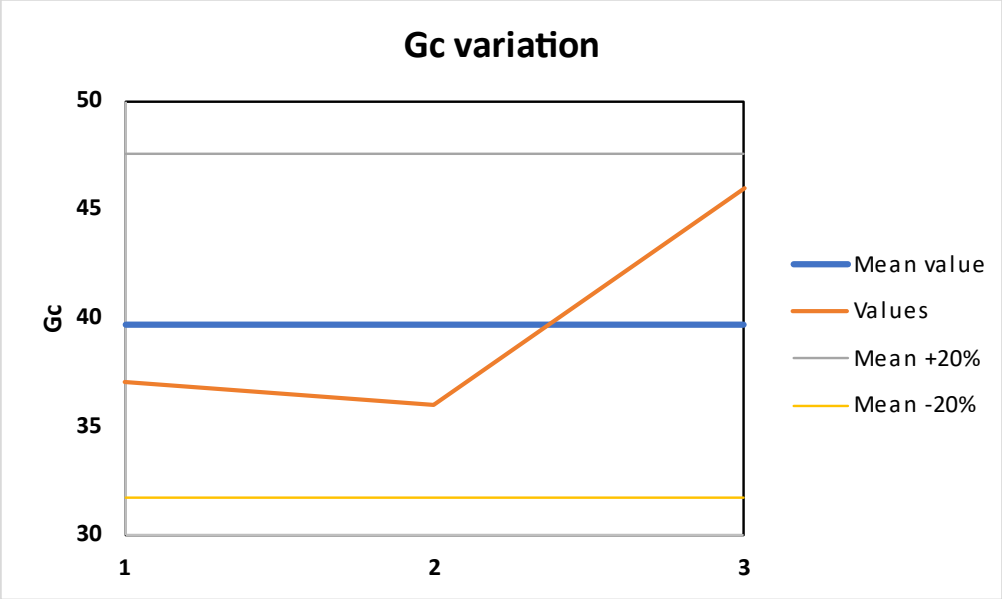

Graph 33: Gc variation.

The G_c values are in the between the minimum and maximum value of showing by the graph 33.

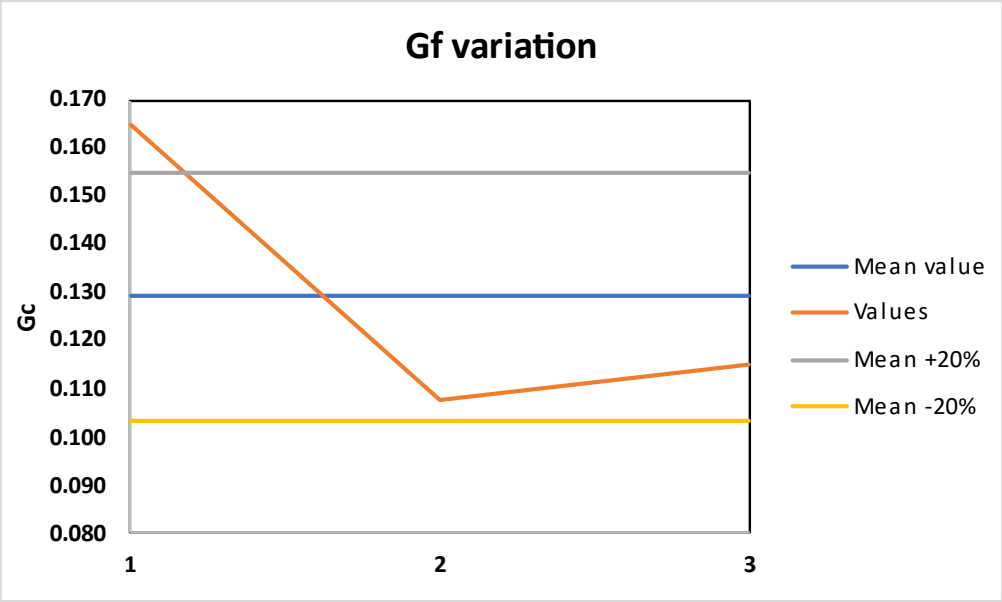

Graph 34: Gf variation.

The G_f values are in the between the minimum and maximum value of showing by the graph 34.

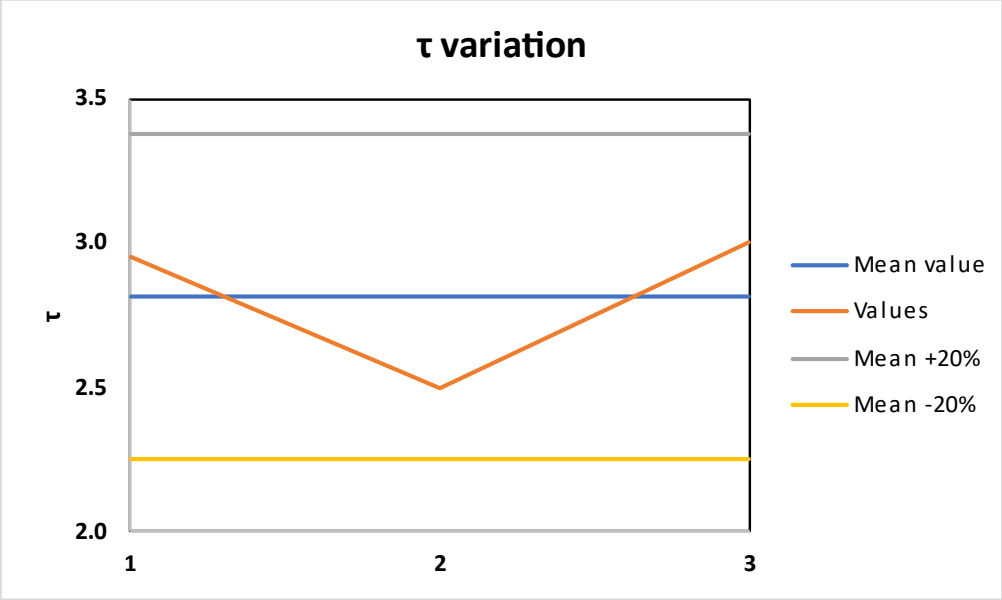

Graph 35: t variation.

The τ values are in the between the minimum and maximum value of showing by the graph 36.

The table 33 shows the mean parameters and in the table 34 is possible to see the value of the variation among them.

Table 33: Mean parameters

Beam H=20cm rough bar	
Parameters	**Mean**
Gc	**39.67**
Gf	**0.13**
t	**2.82**

Table 34: Parameters variation

Variation			
Beam	**1**	**2**	**3**
Gc	**93.28**	**90.76**	**115.97**
Gf	**127.74**	**83.23**	**89.03**
τ	**104.73**	**88.76**	**106.51**

The variation is in a small range and that express the power of the identification given by the cohesive overlapping model.

The *beam H =20 cm rough bar group* graphs considering the mean parameter obtained by the identification procedure are shown in the following graphs.

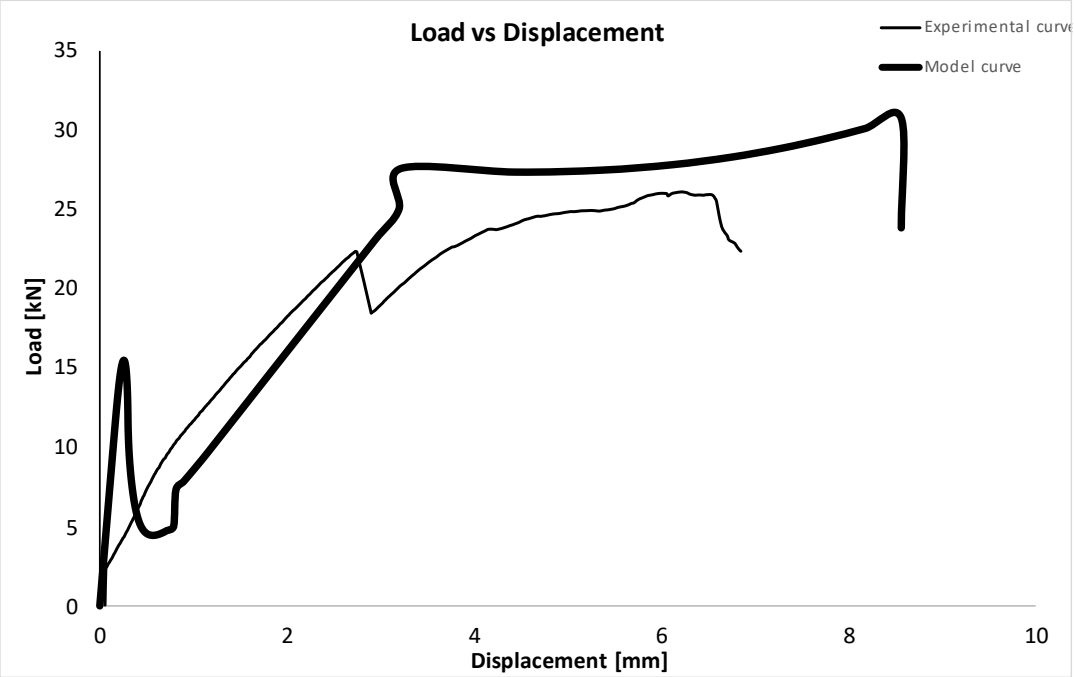
Load vs Displacement
Experimental curve
Model curve
Load [kN]
35
30
25
20
15
10
5
0
0
2
4
6
8
10
Displacement [mm]

Graph 36: ρ=0,4%.

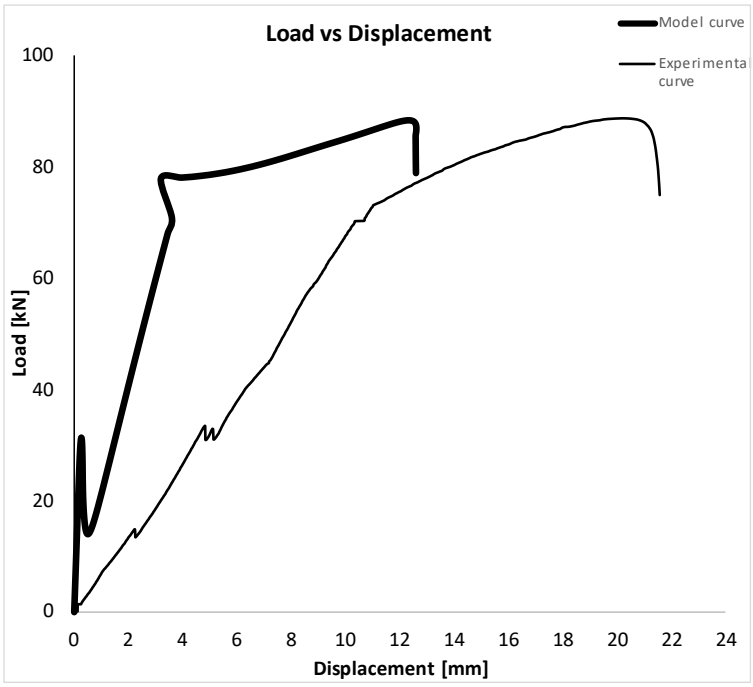

Graph 37: ρ=0,8%.

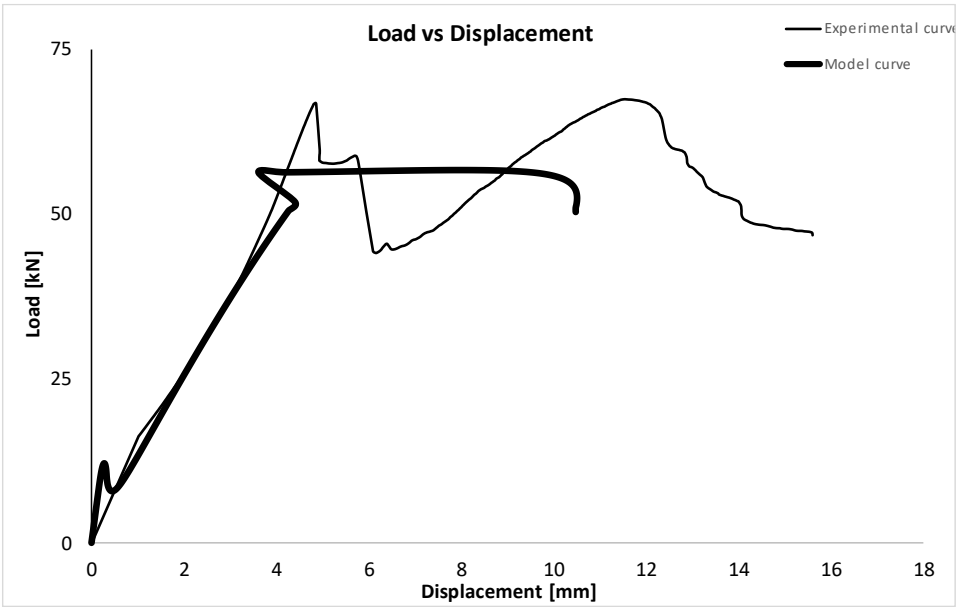

Graph 38: ρ=1,6%.

The using of the mean parameters for the group beam modifies the curves. The perfect correlation among the three most important points is not guaranteed, anyway, a good approximation in the range of $\pm 20\%$ is obtained. The theoretical curves shape is remaining highly comparable. The using of the mean parameters has an incredible power because through the using of them it is possible to estimate the missing data in an experimental campaign. Moreover, in the present thesis, the mean parameters are using in order to prove the power of the identification given by the cohesive overlapping model. The power of this procedure allows to identify the matrix material and reinforcement material of any experimental campaign even without any preliminary dates on the matrix material and reinforcement material. This method deletes the necessity to do the pull-out test, the TPBT and the entirely different tests before analyzing the data results. The other tests through this procedure are not mandatory but they are just a starting point and for this reason, there is no benefit in making high number of them.

5.1.4: Brittle-ductile transition for the beam H =20 cm rough bar group

The previous graphs show how the ductility of the beam is going to reduce considering an increasing of ρ. Having the same beam geometry and the same bond strength for each beam the only factor that change is the ρ value and for this reason it is possible to define that the ductility of the beam is inversely proportional with the increasing to the ρ percentage. Moreover, considering the value of the ductility between the previous group and the new group it is possible to see how the global value of the ductile is reducing between the two groups. The two groups have the same scale geometry, and the only difference is the bond strength. Considering the

evidence, it is possible to assess that the increasing of the bond strength reducing the value of the ductility of the group.

5.2: The second scale: h = 0.4 m

5.2.1: Identification procedure beam H = 40cm smooth bar

The beam H =40 cm with GFRP smooth bar and a geometric reinforcement percentage equal to ρ=0,2%.

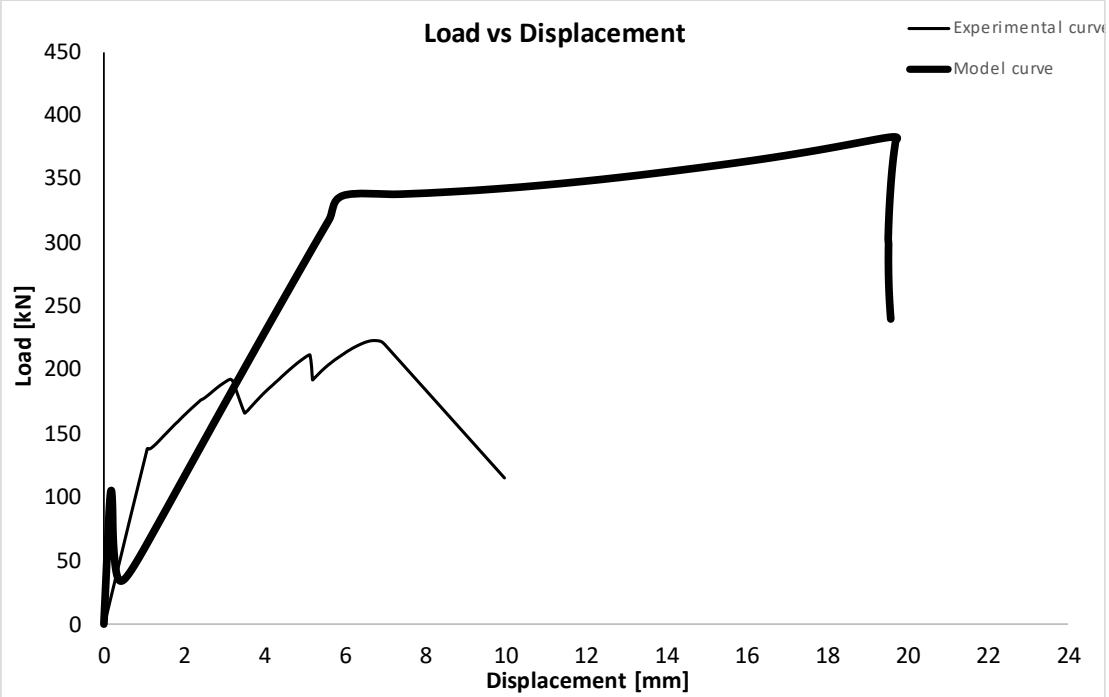

Graph 39:cracking point identification.

Table 35: Parameters

Beam name			**Ec**	**21000**	**MPa**
h	**0.4**	**[m]**	**Wcc**	**3.50**	**mm**
N. Bars	**1**	**[N]**	**Wct**	**0.1**	**mm**
Φ	**20**	**[mm]**	**Gc**	**61.25**	**N/mm**
σ_c	**35**	**MPa**	**Gf**	**0.06**	**N/mm**
σ_t	**1.20**	**MPa**	**t**	**4.75**	**MPa**

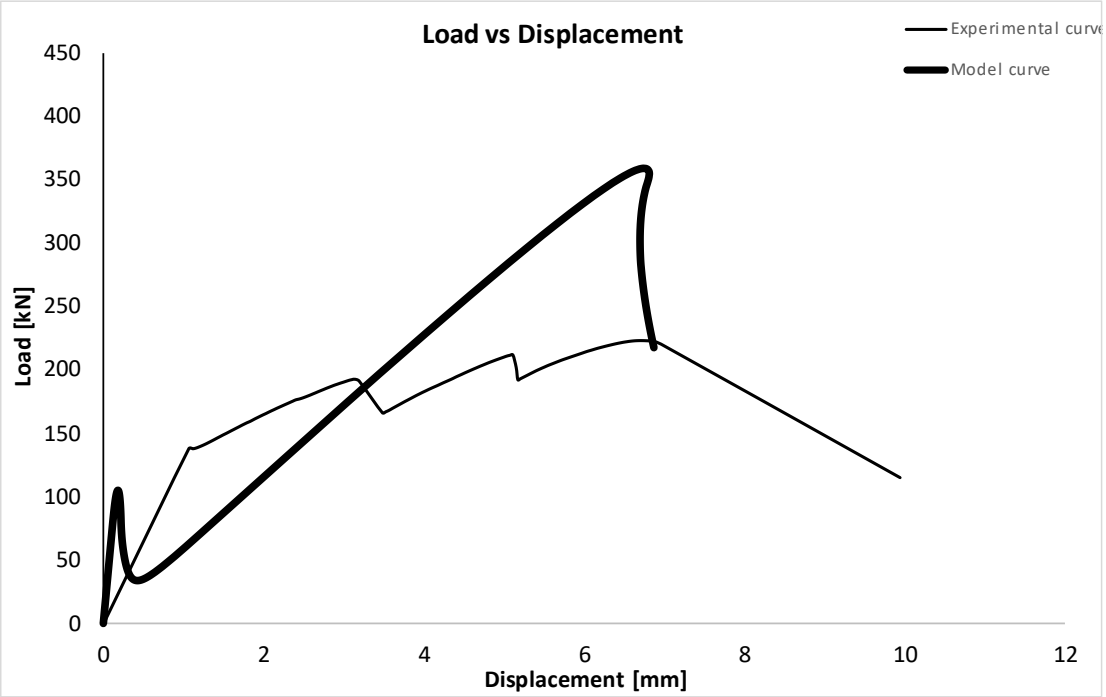

Graph 40:crushing point identification.

Table 36: Parameters

Beam name			**Ec**	**21000**	**MPa**
h	**0.4**	**[m]**	**Wcc**	**0.40**	**mm**
N. Bars	**1**	**[N]**	**Wct**	**0.1**	**mm**
Φ	**20**	**[mm]**	**Gc**	**6**	**N/mm**
σ_c	**30**	**MPa**	**Gf**	**0.06**	**N/mm**
σ_t	**1.20**	**MPa**	**t**	**6.75**	**MPa**

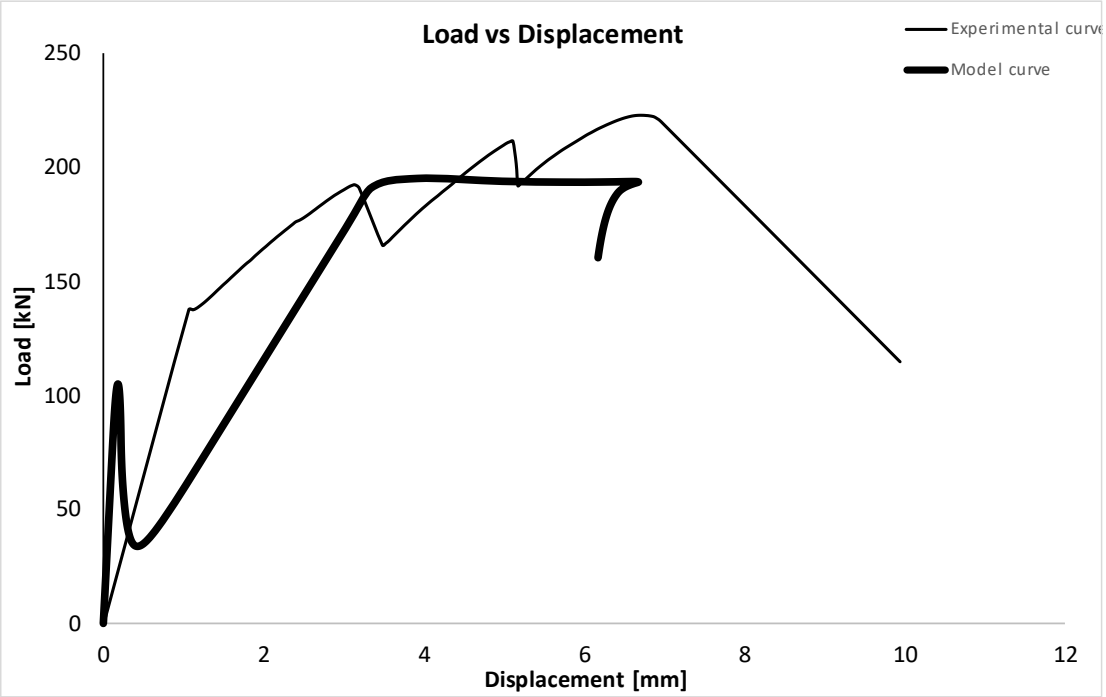

Graph 41:pseudo plastic plateau point identification.

Table 37: Parameters

Beam name			**Ec**	**21000**	**MPa**
h	**0.4**	**[m]**	**Wcc**	**0.40**	**mm**
N. Bars	**4**	**[N]**	**Wct**	**0.1**	**mm**
Φ	**12**	**[mm]**	**Gc**	**6**	**N/mm**
σ_c	**30**	**MPa**	**Gf**	**0.06**	**N/mm**
σ_t	**1.20**	**MPa**	**t**	**2.85**	**MPa**

The graph 41 shows a high correlation between the experimental curve and the theoretical curve. The three most important points that describe the 3 most important moments during a beam test are perfectly obtained. These points are represented by the cracking moment, the crushing moment, and the starting of the slippage phase during a beam test. The Cohesive Overlapping model not only express a significant correlation among these points, but also the structure of the branches are highly comparable giving us an important result.

The beam H =40 cm with GFRP rough bar and a geometric reinforcement percentage equal to ρ=0,4%.

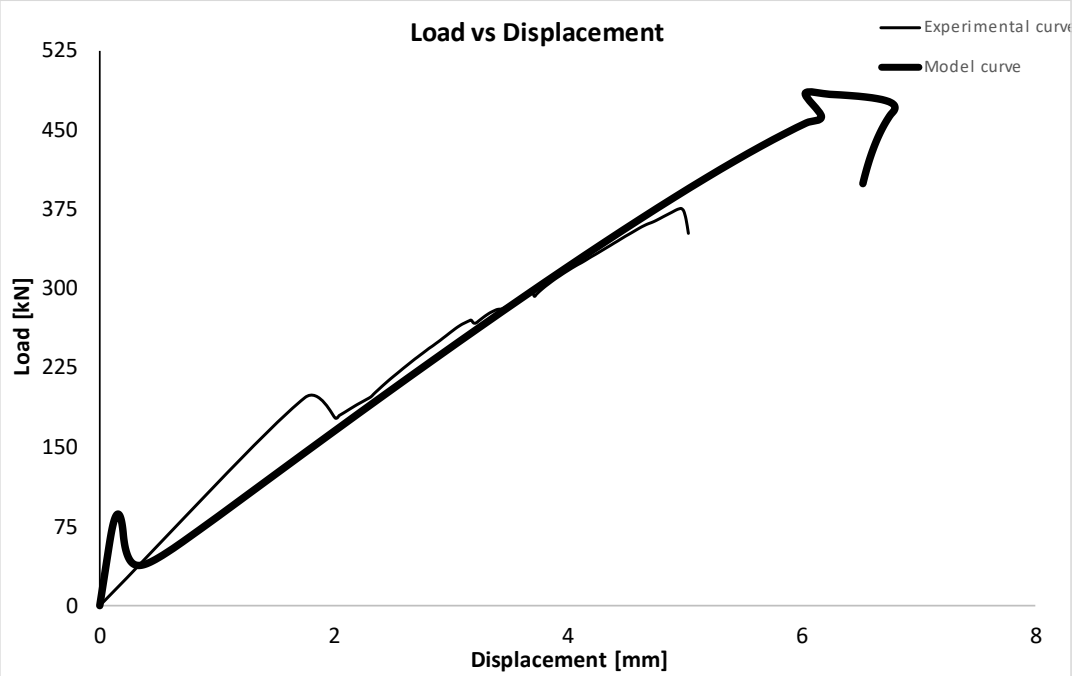

Graph 42: cracking identification.

Table 38: Parameters

Beam name			**Ec**	**35000**	**MPa**
h	**0.4**	**[m]**	**Wcc**	**1.00**	**mm**
N. Bars	**2**	**[N]**	**Wct**	**0.1**	**mm**
Φ	**20**	**[mm]**	**Gc**	**17.5**	**N/mm**
σ_c	**35**	**MPa**	**Gf**	**0.06**	**N/mm**
σ_t	**1.20**	**MPa**	**t**	**4.75**	**MPa**

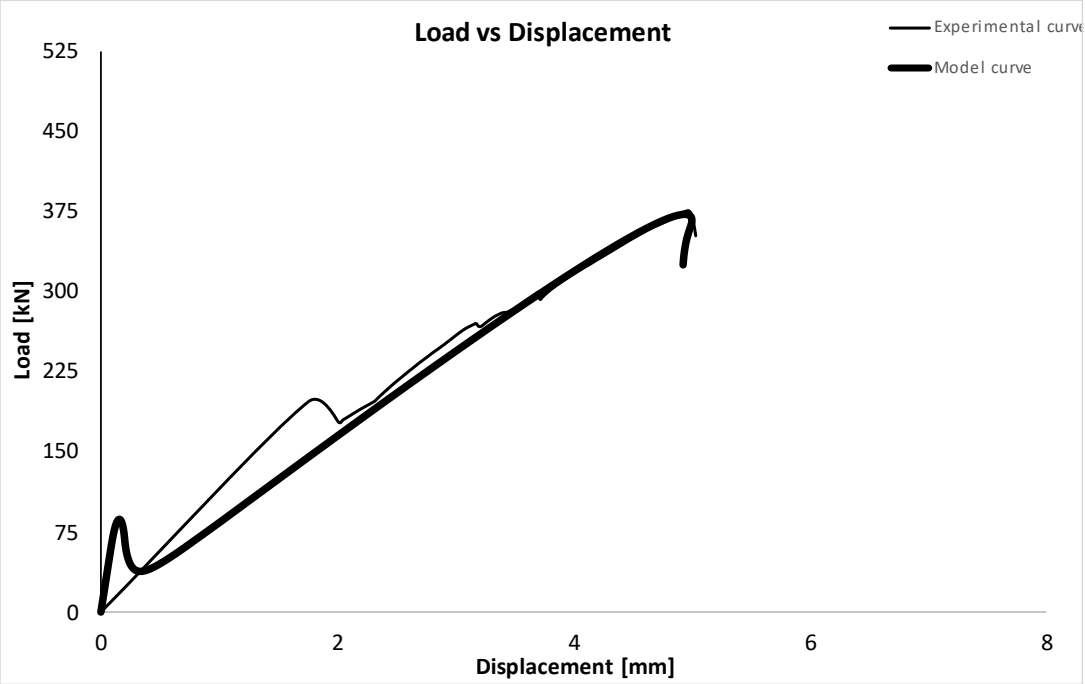

Graph 43: crushing identification.

Table 39: parameters

Beam name			**Ec**	**35000**	**MPa**
h	**0.4**	**[m]**	**Wcc**	**0.50**	**mm**
N. Bars	**2**	**[N]**	**Wct**	**0.1**	**mm**
Φ	**20**	**[mm]**	**Gc**	**8.75**	**N/mm**
σ_c	**35**	**MPa**	**Gf**	**0.06**	**N/mm**
σ_t	**1.20**	**MPa**	**t**	**4.75**	**MPa**

The graph 43 shows a high correlation between the experimental curve Also in this case, considering as a starting point the identification parameters obtained by the previous identification, just two small modification is done to obtain a really high correlation of the most important points

that describe the 3 most important moments during a beam test are perfectly obtained. The Cohesive Overlapping model not only express a significant correlation among these points, but also the structure of the branches is highly comparable giving us an important result.

A statical analysis is performed for this first group of concrete beams the *beam H =40 cm rough bar group*. The statical analysis consist of evaluation the mean value of the three parameters identifies and considering the range variation of $\pm 20\%$ of the mean value.

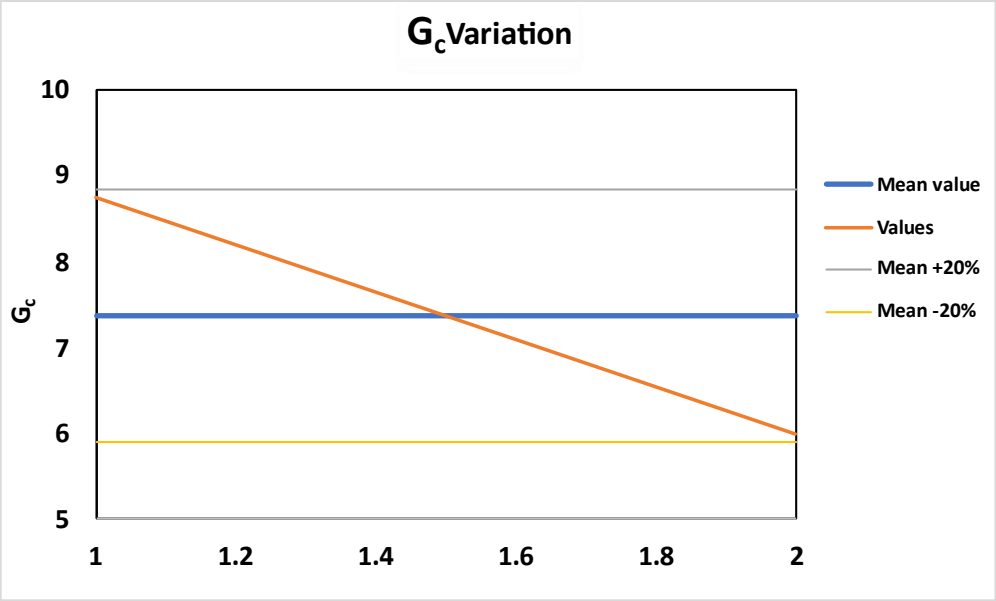

Graph 44: Gc variation.

The G_c values are in the between the minimum and maximum value of showing by the graph 44.

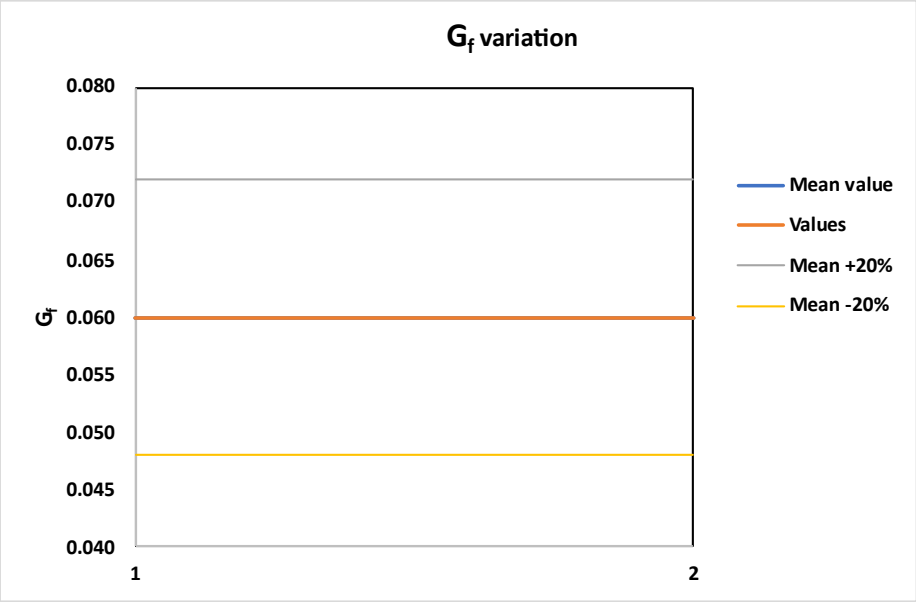

Graph 45: Gf variation.

The G_f values are in the between the minimum and maximum value of showing by the graph 45.

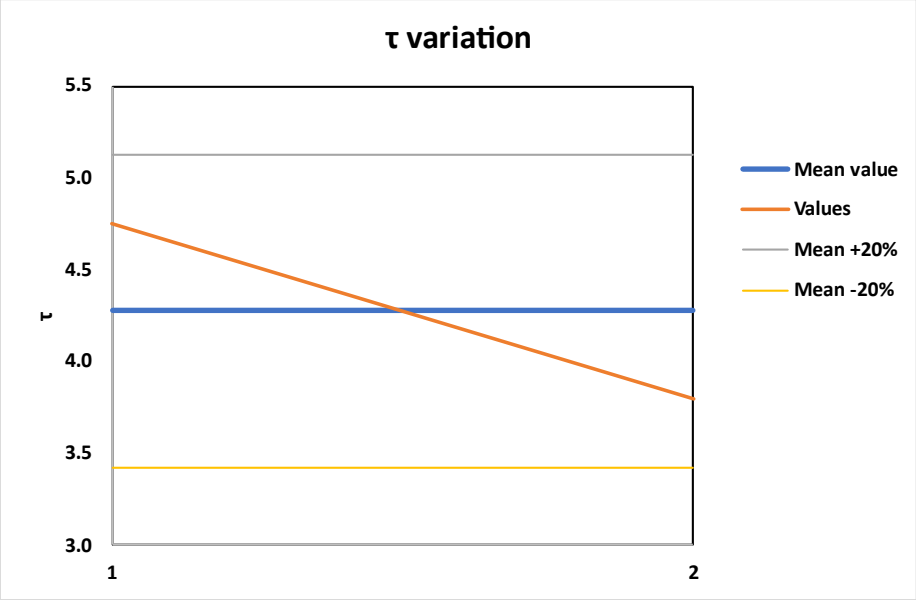

Graph 46: t variation.

The τ values are in the between the minimum and maximum value of showing by the graph 46.

The table 40 shows the mean parameters and in the table 41 is possible to see the value of the variation among them.

Table 40: Mean parameters

Beam H=40cm smooth bar	
Parameters	**Mean**
Gc	**7.38**
Gf	**0.06**
t	**4.28**

Table 41: Parameters variation

Variation		
Beam	**1**	**2**
Gc	**118.64**	**81.36**
Gf	**100.00**	**100.00**
τ	**111.11**	**88.89**

The variation is in a small range and that express the power of the identification given by the cohesive overlapping model.

The *beam H =40 cm smooth bar group* graphs considering the mean parameter obtained by the identification procedure are shown in the following graphs.

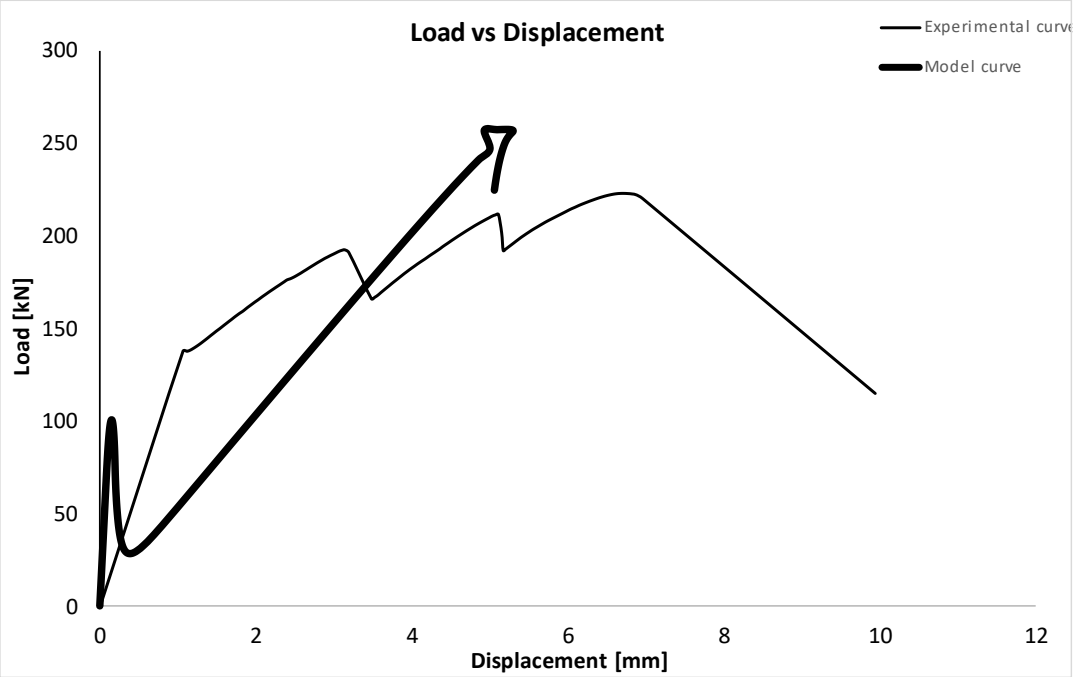
Load vs Displacement
Experimental curve
Model curve
Load [kN]
300
250
200
150
100
50
0
0
2
4
6
8
10
12
Displacement [mm]

Graph 47: ρ=0,2%.

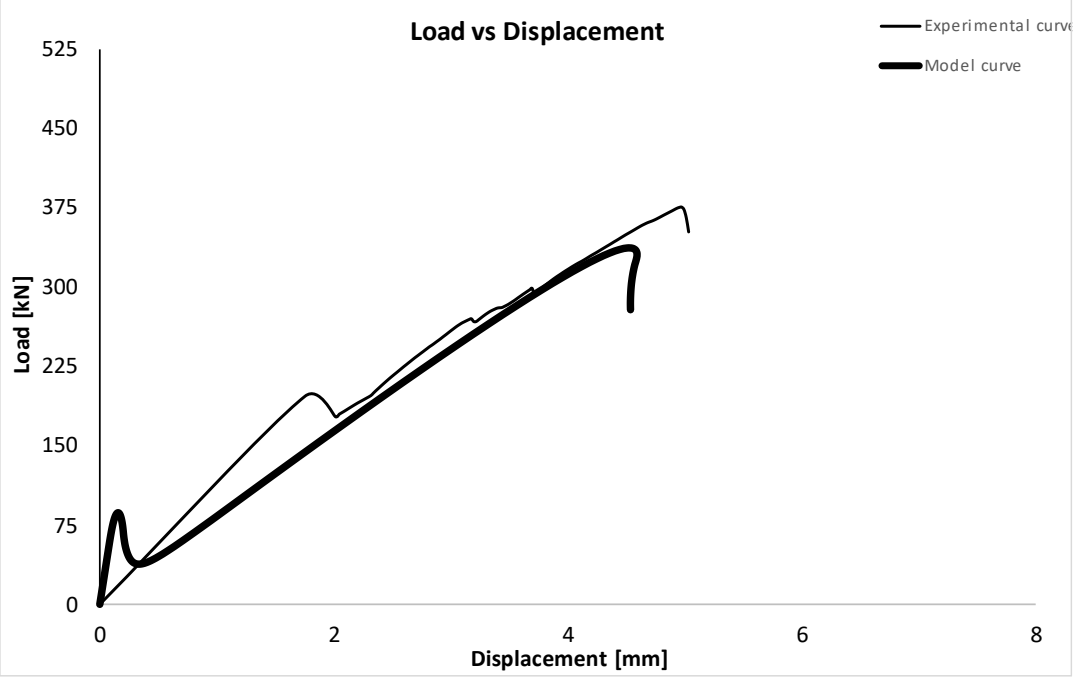
Load vs Displacement
Experimental curve
Model curve
Load [kN]
525
450
375
300
225
150
75
0
0
2
4
6
8
Displacement [mm]

Graph 48: ρ=0,4%.

The using of the mean parameters for the group beam modifies the curves. The perfect correlation among the three most important points is not guaranteed, anyway, a good approximation in the range of $\pm 20\%$ is obtained. The theoretical curves shape are remaining highly comparable. The using of the mean parameters have an incredible power because through the using of them it is possible to estimate the missing data in an experimental campaign. Moreover, in the present thesis, the mean parameters are using in order to prove the power of the identification given by the cohesive overlapping model. The power of this procedure allows to identify the matrix material and reinforcement material of any experimental campaign even without any preliminary dates on the matrix material and reinforcement material. This method deletes the necessity to do the pull-out test, the TPBT and the entirely different tests before analyzing the data results. The other tests through this procedure are not mandatory but they are just a starting point and for this reason, there is no benefit in making high number of them.

5.2.2: Identification procedure beam H = 40cm rough bar

The beam H =40 cm with GFRP rough bar and a geometric reinforcement percentage equal to ρ=0,8%.

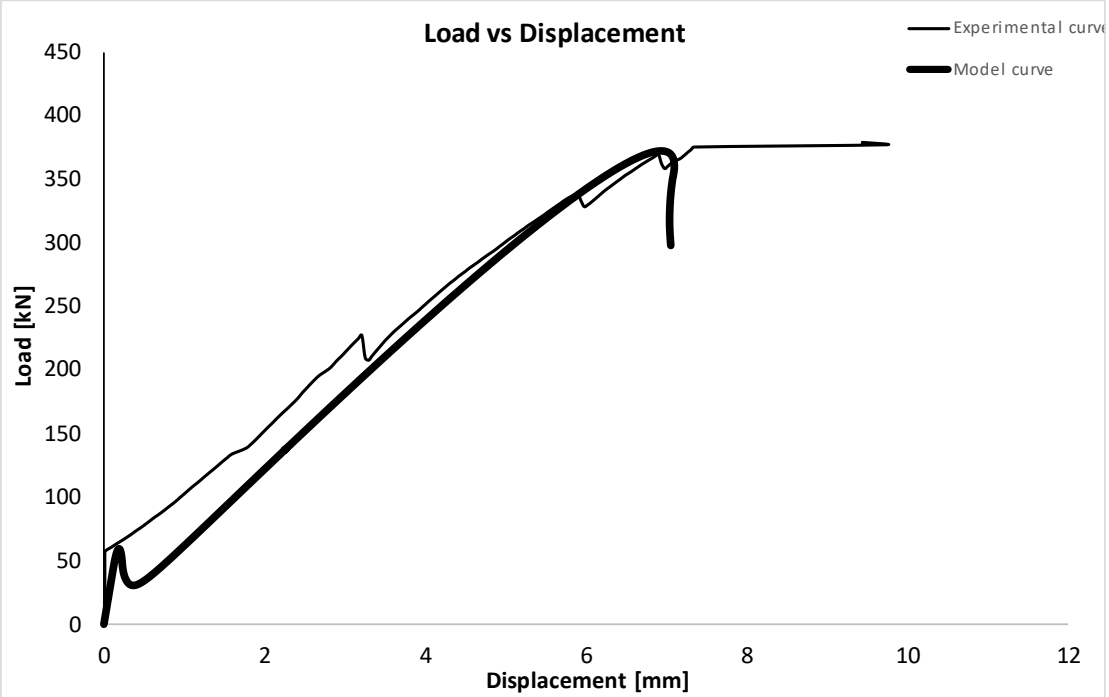

Graph 49:cracking point identification.

Table 42: Parameters

Beam name			**Ec**	**21000**	**MPa**
h	**0.4**	**[m]**	**Wcc**	**1.02**	**mm**
N. Bars	**6**	**[N]**	**Wct**	**0.1**	**mm**
Φ	**12**	**[mm]**	**Gc**	**15.3**	**N/mm**
σ_c	**30**	**MPa**	**Gf**	**0.06**	**N/mm**
σ_t	**1.20**	**MPa**	**t**	**4.5**	**MPa**

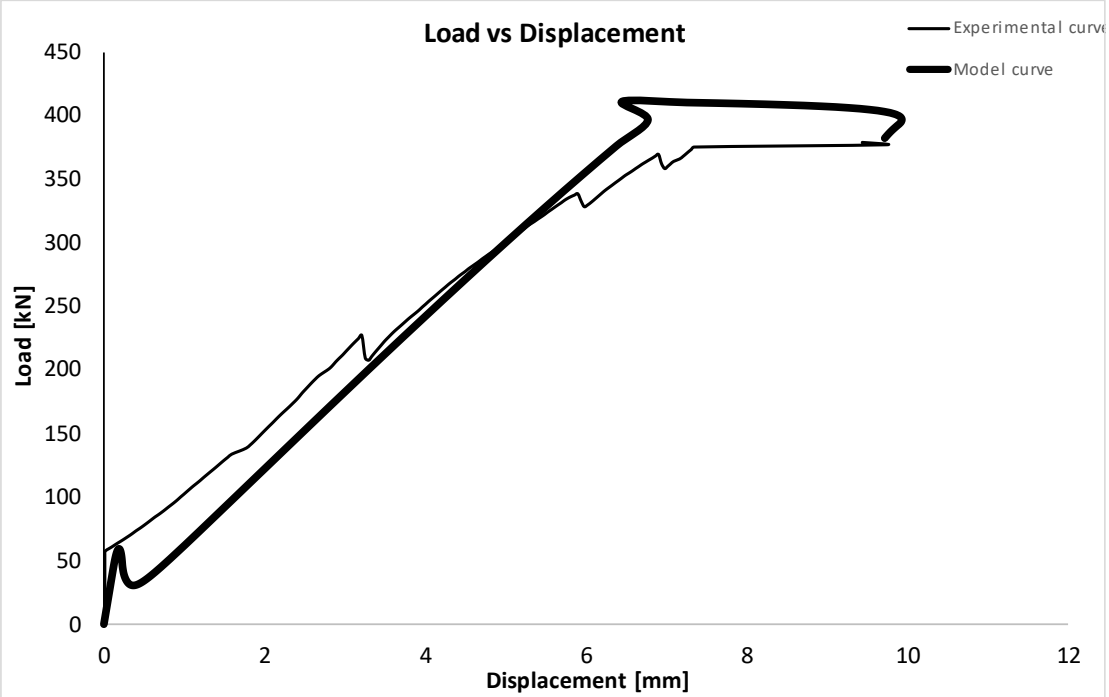

Graph 50:crushing point identification.

Table 43: Parameters

Beam name			**Ec**	**21000**	**MPa**
h	**0.4**	**[m]**	**Wcc**	**1.15**	**mm**
N. Bars	**6**	**[N]**	**Wct**	**0.1**	**mm**
Φ	**12**	**[mm]**	**Gc**	**23**	**N/mm**
σ_c	**40**	**MPa**	**Gf**	**0.06**	**N/mm**
σ_t	**1.20**	**MPa**	**τ**	**3**	**MPa**

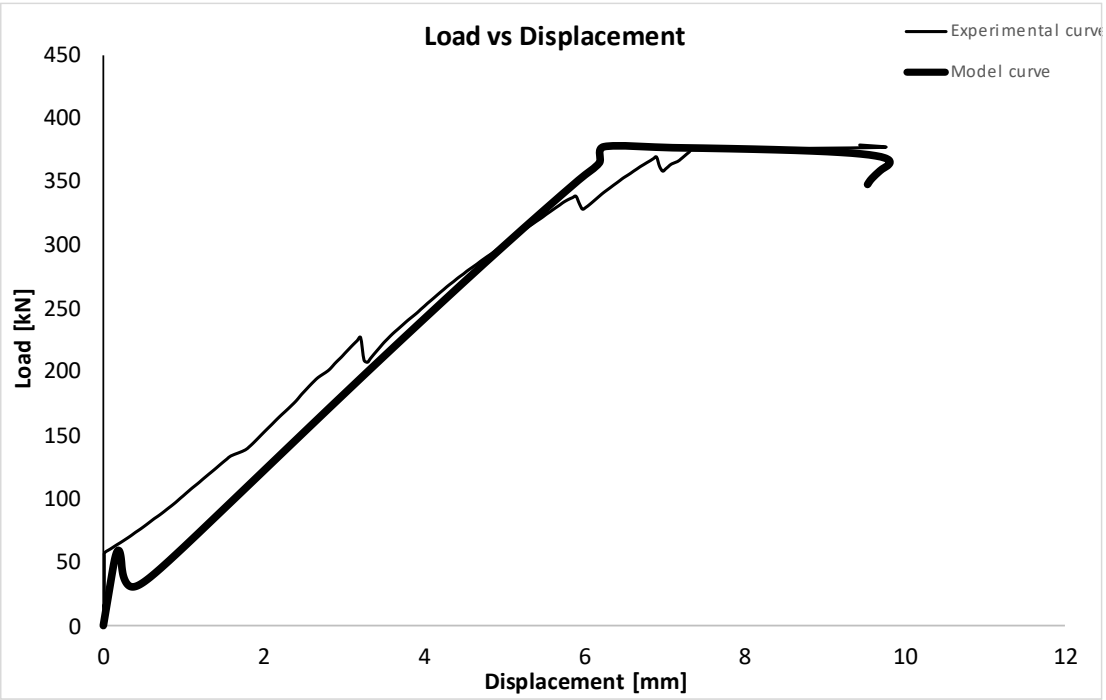

Graph 51:pseudo plastic plateau point identification.

Table 44: Parameters

Beam name			**Ec**	**21000**	**MPa**
h	**0.4**	**[m]**	**Wcc**	**1.15**	**mm**
N. Bars	**6**	**[N]**	**Wct**	**0.1**	**mm**
Φ	**12**	**[mm]**	**Gc**	**23**	**N/mm**
σ_c	**40**	**MPa**	**Gf**	**0.06**	**N/mm**
σ_t	**1.20**	**MPa**	**τ**	**2.75**	**MPa**

The graph 51 shows a high correlation between the experimental curve and the theoretical curve. The three most important points that describe the 3 most important moments during a beam test are perfectly obtained. These points are represented by the cracking moment, the crushing moment,

and the starting of the slippage phase during a beam test. The Cohesive Overlapping model not only express a significant correlation among these points, but also the structure of the branches is highly comparable giving us an important result.

The beam H =40 cm with GFRP rough bar and a geometric reinforcement percentage equal to ρ=1.6%.

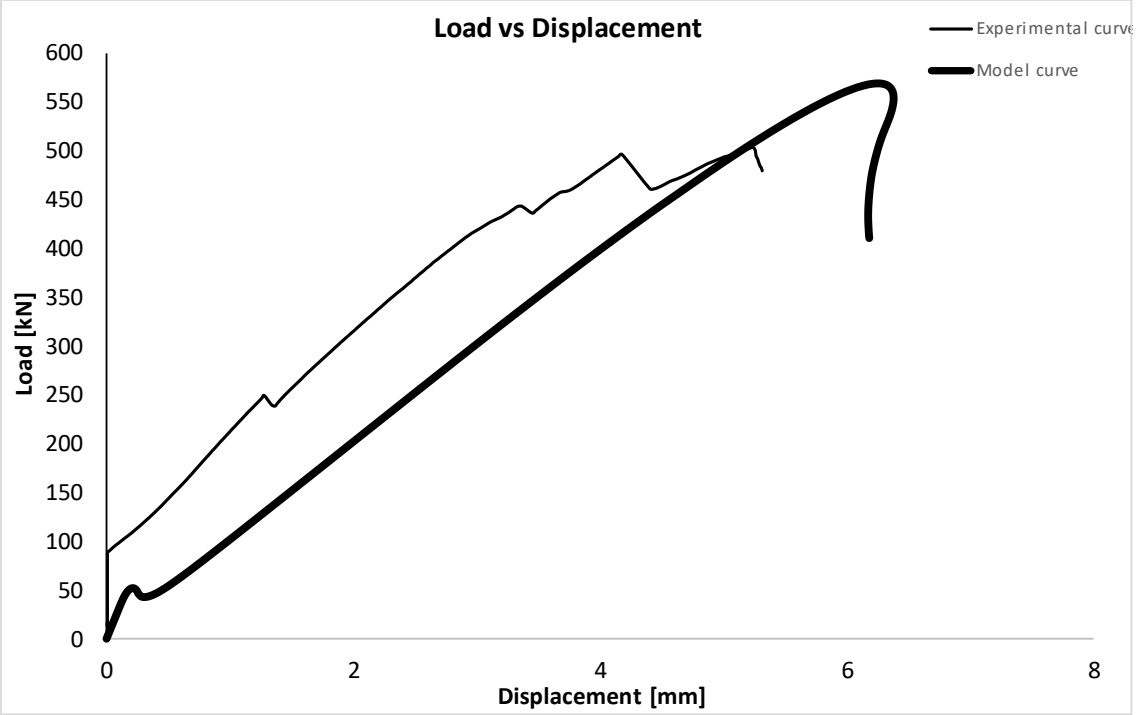

Graph 52: cracking identification.

Table 45: Parameters

Beam name			**Ec**	**21000**	**MPa**
h	**0.4**	**[m]**	**Wcc**	**1.00**	**mm**
N. Bars	**17**	**[N]**	**Wct**	**0.1**	**mm**
Φ	**12**	**[mm]**	**Gc**	**20**	**N/mm**

σ_c	40	MPa	Gf	0.06	N/mm
σ_t	1.20	MPa	t	2.75	MPa

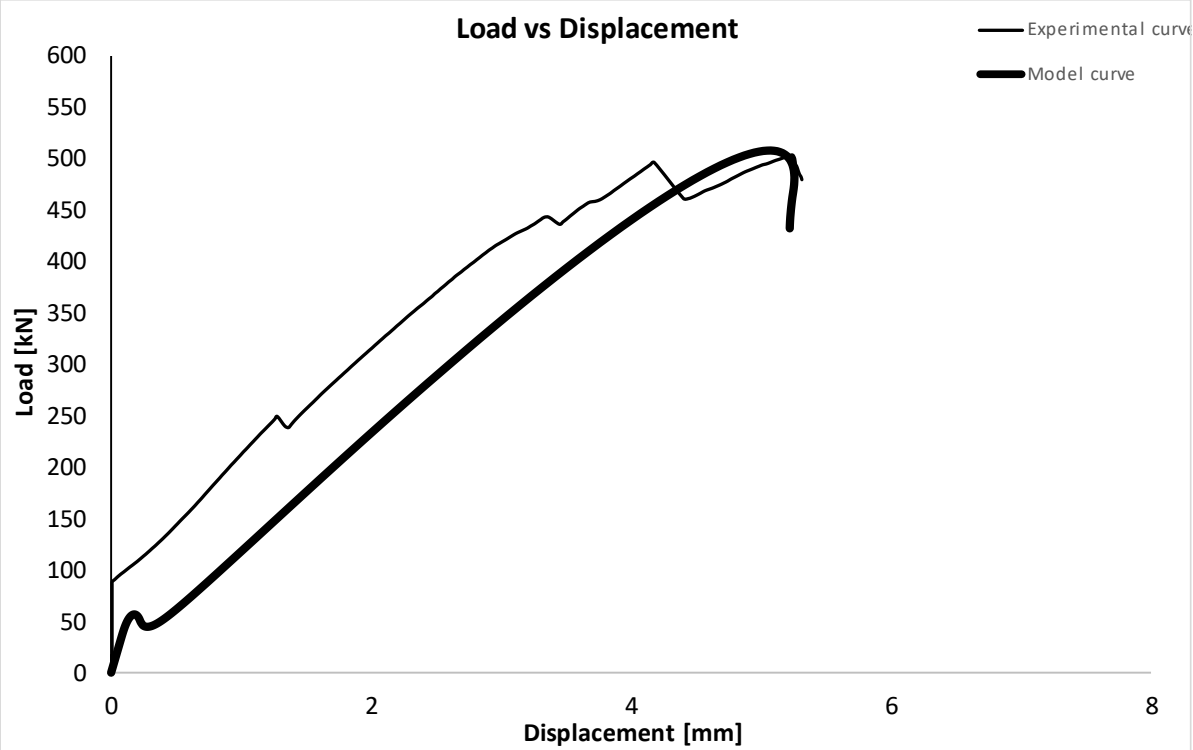

Graph 53: crushing identification.

Table 46: parameters

Beam name			Ec	35000	MPa
h	0.4	[m]	Wcc	1.00	mm
N. Bars	17	[N]	Wct	0.1	mm
Φ	12	[mm]	Gc	17.5	N/mm
σ_c	35	MPa	Gf	0.06	N/mm
σ_t	1.20	MPa	t	4.75	MPa

The graph 53 shows a high correlation between the experimental curve Also in this case, considering as a starting point the identification parameters obtained by the previous identification, just two small modification is done to obtain a really high correlation of the most important points that describe the 3 most important moments during a beam test are perfectly obtained. The Cohesive Overlapping model not only express a significant correlation among these points, but also the structure of the branches are highly comparable giving us an important result.

A statical analysis is performed for this first group of concrete beams the *beam H =40 cm rough bar group*. The statical analysis consist of evaluation the mean value of the three parameters identifies and considering the range variation of $\pm 20\%$ of the mean value.

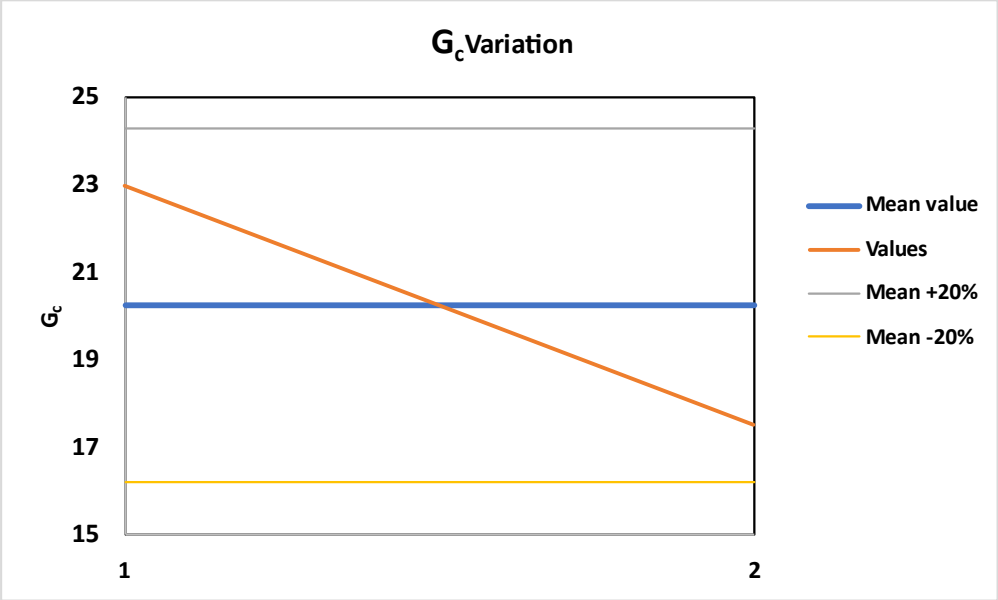

Graph 54: Gc variation.

The G_c values are in the between the minimum and maximum value of showing by the graph 54.

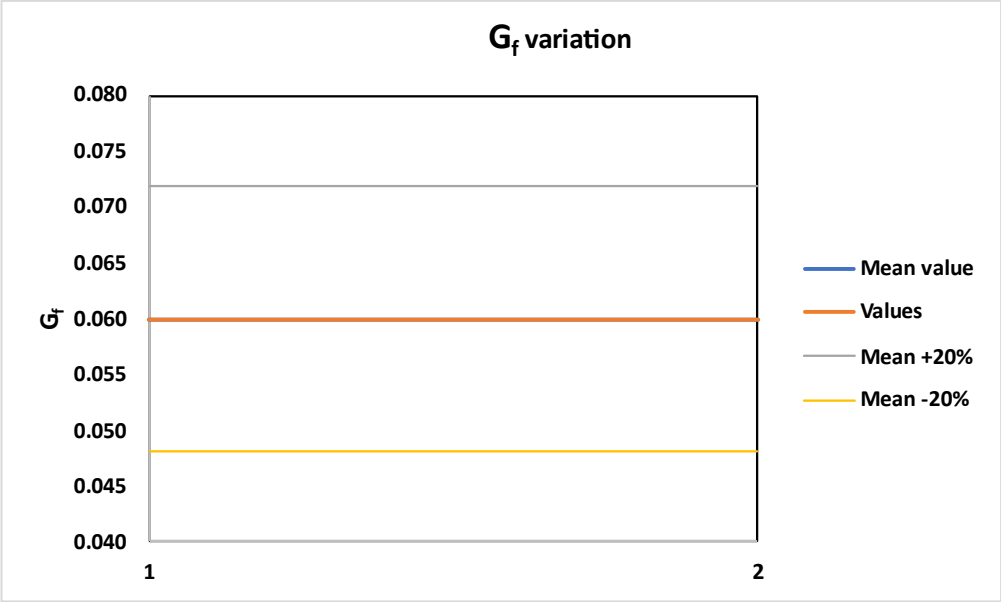

Graph 55: Gf variation.

The G_f values are in the between the minimum and maximum value of showing by the graph 55.

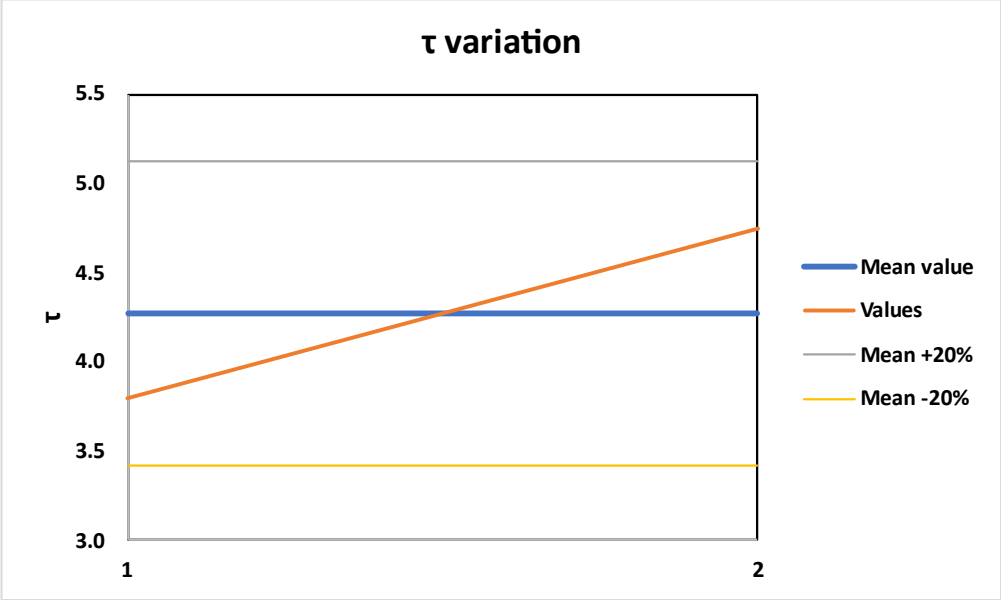

Graph 56: t variation.

The τ values are in the between the minimum and maximum value of showing by the graph 56.

The table 47 shows the mean parameters and in the table 48 is possible to see the value of the variation among them.

Table 47: Mean parameters

Beam H=40cm rough bar	
Parameters	**Mean**
Gc	**20.25**
Gf	**0.06**
t	**4.28**

Table 48: Parameters variation

Variation		
Beam	**1**	**2**
Gc	**113.58**	**86.42**
Gf	**100.00**	**100.00**
τ	**88.89**	**111.11**

The variation is in a small range and that express the power of the identification given by the cohesive overlapping model.

The *beam H =40 cm rough bar group* graphs considering the mean parameter obtained by the identification procedure are shown in the following graphs.

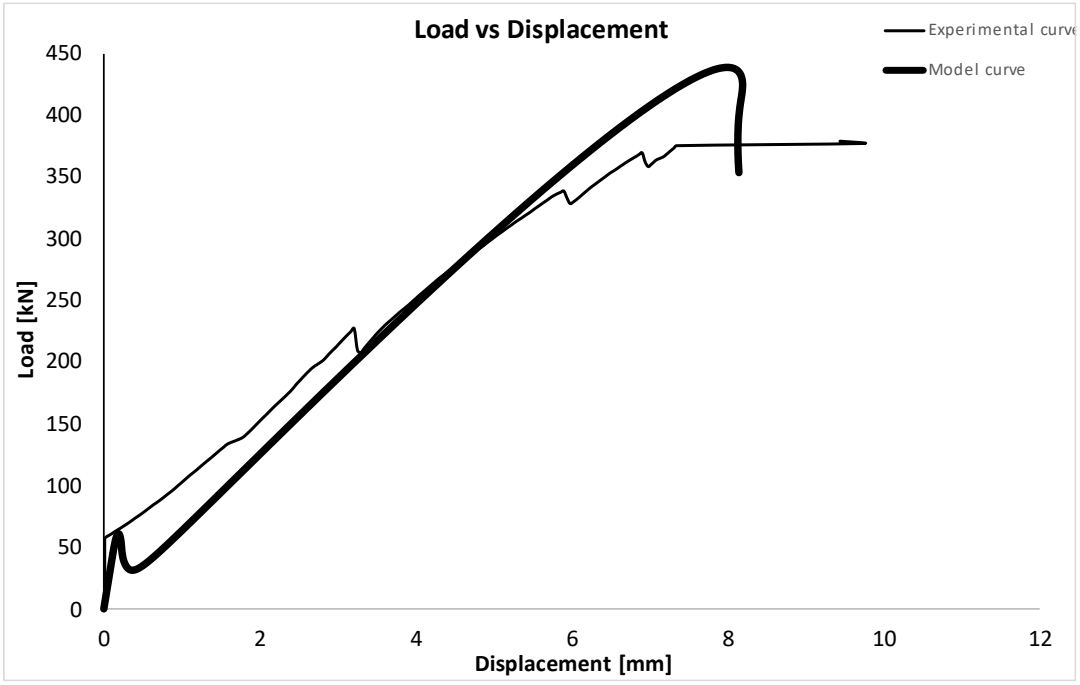
Load vs Displacement
Experimental curve
Model curve
Load [kN]
Displacement [mm]
0
50
100
150
200
250
300
350
400
450
0
2
4
6
8
10
12

Graph 57: ρ=0,8%.

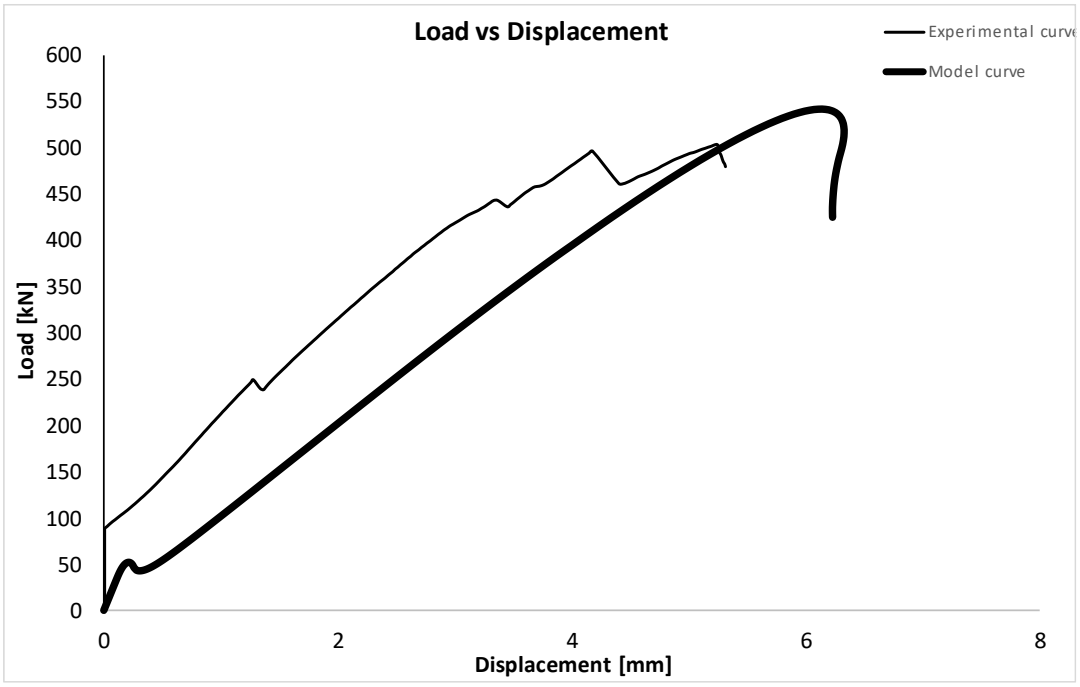
Load vs Displacement
Experimental curve
Model curve
Load [kN]
Displacement [mm]
0
50
100
150
200
250
300
350
400
450
500
550
600
0
2
4
6
8

Graph 58: ρ=1,6%.

The using of the mean parameters for the group beam modifies the curves. The perfect correlation among the three most important points is not guaranteed, anyway, a good approximation in the range of $\pm 20\%$ is obtained. The theoretical curves shape is remaining highly comparable. The using of the mean parameters has an incredible power because through the using of them it is possible to estimate the missing data in an experimental campaign. Moreover, in the present thesis, the mean parameters are using in order to prove the power of the identification given by the cohesive overlapping model. The power of this procedure allows to identify the matrix material and reinforcement material of any experimental campaign even without any preliminary dates on the matrix material and reinforcement material. This method deletes the necessity to do the pull-out test, the TPBT and the entirely different tests before analyzing the data results. The other tests through this procedure are not mandatory but they are just a starting point and for this reason, there is no benefit in making high number of them.

5.2.3: Brittle-ductile transition for the group beam H =20 cm and group beam H = 40cm

The previous graphs (for both the groups) show how the ductility of the beam is going to reduce considering an increasing of ρ. Having the same beam geometry and the same bond strength for each beam the only factor that change is the ρ value and for this reason it is possible to define that the ductility of the beam is inversely proportional with the increasing to the ρ percentage. Moreover, considering the value of the ductility between the group beam H = 20 cm and the group

beam H = 40 cm it is possible to see how the global value of the ductile is reducing between the two groups. The two groups have the different scale geometry, but same reinforcement percentage between them. Considering the evidence, it is possible to assess that the scale increasing is going to reduce the value of the ductility of the group.

Chapter 6:

Conclusions

The experimental study protagonist of the thesis is based on the substitution of steel bars with GFRP bars inside the concrete matrix. The experimental campaign was composed of 2 different dimensional scales, 2 different bond strength represented by the GFRP bars and 4 different geometric reinforcement percentages for each subdivision group for a total of 16 beams. The purpose of the experiment was to investigate the ductile brittle transition. To accomplish this, it is necessary the process of identifying the parameters of fracture mechanics such as G_F and G_C, as well as the bond strength τ of the GFRP bars. The possibility of obtaining these parameters through the tests currently in use has immediately proved to be in vain as the existing tests do not produce results sufficiently precise. A new identification process was then used for material characterization. The identification process is based on 3 fundamental points: the first cracking point that represent the fractural energy G_F, the crushing point that represent the fractural energy G_c, and the starting point of the pseudo-plastic plateau that represent τ. The identification of the fracture energy values G_F and G_c are directly correlate to the concrete matrix characteristics. On the other hand, the identification of the bond strength τ is directly correlated to the bar cover surface. This information complements the framework of geometric and mechanical characteristics representative of the reinforcing bar provided by the manufacturer such as the tensile strength σ_t, the elastic modulus E, and nominal diameter D. The identification process is based on the COCM

and the results of experimental tests such as FPBT. For the 4 groups in which the different beams were divided, the values identified were within the limits of $\pm 20\%$ of the mean, thus giving consistency of the results obtained. Ultimately, this new method of identification replaces the other previous and inaccurate tests. As regards the brittle ductile transition, this has been shown to be a function of the scale of the element, the geometric reinforced percentage, and the bond strength of the bar. More precisely, the possibility of obtaining a pseudo-plastic plateau is inversely proportional to the scale of the element. This result is consistent with the existing dimensional theory of fracture mechanics. Regarding the geometric reinforced percentage, this parameter turns out to be inversely proportional with the ductility expressed by the beam. This statement is in contrast with current technical regulations which do not place an upper limit of reinforcement inside the beams in function of the scale. Regarding the bond strength of the GFRP bar, this parameter has several impacts within the matrix. Despite its reduced value increases the ductility of the beams, it strongly penalizes the load capacity. It is also shown to be of strong impact on the resistance ductility balance even with small percentage variation of it. The current producers greatly overestimate the value of the bond strength that their bars can reach and, moreover, every producer company has its coating methodology. This variation does not guarantee a standardization of the τ thus giving ambiguity in the forecast of the obtainable results. Research has free rein because the technical regulations in place do not provide enough guidance on how to cover GFRP bars. In conclusion, the use of GFRP bars opens a door to the future of sustainable engineering. In order to continue in this direction, current technologies and test procedures must be innovated. The identification process employed in this thesis utilizes COCM and FPBT, which

is a valid replacement for all previous canonic tests used to identify mechanical properties. Through more precise studies, it is possible to guide the development of GFRP bars by increasing the resistance of the bars and balancing the bond strength, thus giving equal importance to the strength and ductility of the final composite. The future of engineering is to find new solutions and new materials that lead the structures towards greater sustainability, durability, and safety over time.

Ringraziamenti

I miei ringraziamenti non possono che non iniziare dal Politecnico di Torino e dall'Università di Miami, due istituti dove l'innovazione e le sfide verso il futuro vengono messi al primo posto accogliendo sempre più studenti a farne parte.

Questo progetto di tesi non sarebbe stato possibile senza i miei due relatori il Professore Alberto Carpinteri e il Professore e presidente dell'ACI Antonio Nanni. Ringrazio il Professore Alberto Carpinteri per aver accettato la mia proposta di tesi estera ed avermi affiancato in questo percorso con spunti e idee sempre innovative. Con profonda stima e ammirazione per uno dei più grandi Professori mai incontrati nel mio percorso accademico. Al mio secondo relatore, il Professor Antonio Nanni, la ringrazio per avermi accolto all'interno dell'Università di Miami e avermi reso partecipe delle infinite sfide che affronta con il suo gruppo di ricerca. La stimo non solo come il grande Professore quale è ma soprattutto per come si rende disponibili con noi ragazzi, sempre pronto ad ascoltarci e darci consigli in materia universitaria e non solo.

Alla mia famiglia alla quale devo tutto per il supporto morale che mi hanno dato, gli incoraggiamenti, i confronti sull'intraprendere questa sfida di tesi e i diversi punti di riflessione, per il supporto economico senza mai farmi pesare niente e senza il quale questa esperienza sarebbe stata impossibile da portare avanti. Alle mie sorelle per gli scontri incoraggianti che abbiamo, gli scleri e gli scherzi, vi voglio bene.

A Sara, sei senza dubbio la persona che più di tutte conosce i miei alti, i miei tanti bassi, i miei momenti no, eppure nonostante questo sei sempre al mio fianco. Se la persona che più di tutte sa starmi vicino anche a distanza. La mia compagna, la mia amica, la mia spalla, se sono riuscito a portare a termine questo percorso di laurea è sicuramente anche grazie a te. Siamo un duo bello che funziona alla grande, invincibili insieme.

A Vit, Leo e Roby, al gruppo di giù, si dice spesso che il percorso conta più della meta, più del suo inizio e del suo traguardo e sicuramente voi siete parte di questo percorso e di questa mia crescita. Grazie per i momenti di supporto, i momenti leggeri, le risate e le nostre litigate, è un mix del quale non potrei fare a meno. Siamo la media delle persone della quale ci circondiamo e per questo, non avrei mai potuto desiderare amici migliori.

A Chiara, Dori e Rafa, siete stati senza dubbio i protagonisti di questa esperienza a Miami. Mi avete visto in tanti momenti e probabilmente anche nel più brutto di sempre. Grazie per essermi stati vicini e avermi supportato. Senza di voi l'esperienza a Miami sarebbe stata sicuramente meno significativa e importante.

Bene, siamo arrivati alla fine, ringrazio il mio alter ego Gianfrancesco per non aver mollato. In questo percorso abbiamo affrontato tante sfide e qualche difficoltà. Ci siamo fatti qualche pianto, abbiamo pensato di non potercela fare e di non essere abbastanza ma alla fine, in un modo o nell'altro, ci siamo sempre buttati con la testa sui libri e ne siamo usciti vincitori. Perseveranti, ossessionati dalla meta e dall'obiettivo siamo riusciti a concludere tutte le sfide prefissate. Riusciremo a raggiungere anche i prossimi obiettivi spostando di giorno in giorno l'asticella

sempre più in alto, sapendo di non poterci arrivare facilmente, sapendo di dover faticare e sbatterci la testa e ricordandoci che:

if it's simple, it means it's not enough, it means it's stupid.

References

1) *Scienza delle costruzioni 2. Alberto Carpinteri*
2) *Scienza delle costruzioni 1. Alberto Carpinteri*
3) *Bond behavior of GRFP bars to concrete in beam test Renata Kotyniaa,*, Damian Szczecha, Monika Kaszubskaa. International Conference on Analytical Models and New Concepts in Concrete and Masonry Structures AMCM'2017.*
4) *Bond-slip behavior of self-compacting concrete and vibrated concrete using pull-out and beam tests. Fernando Menezes de Almeida Filho Æ Mounir K. El Debs Æ Ana Lucia H. C. El Debs*
5) *Bond behavior of reinforcing bars in self-compacting concrete: experimental determination by using beam tests. Pieter Desnerck • Geert De Schutter • Luc Taerwe*
6) *Cohesive crack model description of ductile to brittle size-scale transition: dimensional analysis vs. renormalization group theory. A. Carpinteri *, P. Cornetti, F. Barpi, S. Valente. Dipartimento di Ingegneria Strutturale e Geotecnica, Politecnico de Torino, Corso Duca degli Abruzzi 24, Torino 10129, Italy*
7) *Scale-dependent maximum reinforcement percentage in reinforced concrete beams. Alberto Carpinteri | Federico Accornero | Renato Cafarelli. Politecnico di Torino, Department of Structural, Geotechnical, and Building Engineering, 24, C.so Duca degli Abruzzi, Turin, Italy*
8) *Cracking and Crushing in Prestressed Concrete Beams by Federico Accornero, Renato Cafarelli, and Alberto Carpinteri. ACI STRUCTURAL JOURNAL TECHNICAL PAPER Title No. 118-S32.*

9) *The cohesive/overlapping crack model for plain and RC beams: scale effects on cracking and crushing failures.* *Cite this article Accornero F, Cafarelli R and Carpinteri A The cohesive/overlapping crack model for plain and RC beams: scale effects on cracking* and crushing *failures. Magazine of Concrete Research,*

10) *Reinforcement bond strength, beam bond test vs pull-out test.* *Lan, Li, Weng, Wang, Journal of materials in Civil Engineering*

Web bibliography

1) Glass Fiber Reinforced Polymer (GFRP) Rebar - Aslan ™ 100 series FIBERGLASS REBAR: Aslan100 (alb-rebar.com).
2) Fiberglass Rebar: Aslan 100 GFRP rebar FLYER (sefindia.org).
3) Standard Test Method for Bond Strength of Fiber-Reinforced Polymer Matrix Composite Bars to Concrete by Pullout Testing1: https://compass.astm.org/document/?contentCode=ASTM%7CD7913_D7913M-14R20%7Cen-US